



Long & low; or short & high; photoperiods and light differentially influence growth and potential niches of PhycoCyanin and PhycoErythrin-rich picocyanobacteria

Journal:	<i>Limnology and Oceanography</i>
Manuscript ID	LO-24-0249.R2
Wiley - Manuscript type:	Research Article
Date Submitted by the Author:	n/a
Complete List of Authors:	Śliwińska-Wilczewska, Sylwia; Mount Allison University Department of Biology; University of Gdańsk, Department of Marine Ecosystems Functioning, Faculty of Oceanography and Geography Konik, Marta; University of Victoria, Department of Geography; Polish Academy of Sciences, Institute of Oceanology Savoie, Mireille; Mount Allison University Department of Biology Aguilera, Anabella; Linnaeus University, Department of Biology and Environmental Science, Centre for Ecology and Evolution in Microbial Model Systems (EEMiS); Swedish University of Agricultural Sciences, Department of Aquatic Sciences and Assessment Omar, Naaman M; Mount Allison University Department of Biology Campbell, Douglas; Mount Allison University Department of Biology
Keywords:	Cumulative diel photon dose, Light-capture, PAR, Photic regime, Phase of growth, Photoperiod, Picocyanobacteria, PUR
Abstract:	Strains from the picocyanobacteria genus <i>Synechococcus</i> are currently found across a wide range of photoperiods and photosynthetically active radiation. Future scenarios now forecast range expansions of marine <i>Synechococcus</i> into new photic regimes. We found that strains of temperate, coastal PhycoCyanin(PC)-rich and PhycoErythrin(PE)-rich <i>Synechococcus</i> grew fastest under moderate photosynthetically active radiation, and a 24-hour photoperiod, despite a cumulative diel photon dose equivalent to conditions where growth was slower, under higher light and shorter photoperiods. Under optimal conditions, a PE-rich <i>Synechococcus</i> strain achieved a highest recorded cyanobacterial chlorophyll-specific exponential growth rate (μ) of 4.5 d^{-1} . Two PE-rich strains demonstrated wider ability to modulate light capture capacity, whereas two PC-rich strains showed less change in light capture across increasing cumulative diel photon dose. All four coastal strains showed a decrease of effective absorption cross section for PSII photochemistry, versus increasing cumulative diel PAR doses. Within each strain, μ showed consistent, saturating responses to increasing cumulative diel PSII electron flux, with more variations in responses of μ to cumulative Photosynthetically Usable Radiation. As photoperiod opportunists, coastal picocyanobacteria show potential to expand into longer photic regimes as higher latitudes warm.



SCHOLARONE™
Manuscripts

Scientific Significance Statement Topic

In PhycoCyanin(PC)-rich, and particularly in PhycoErythrin(PE)-rich phenotypes of *Synechococcus*, photoperiod alters the responses of growth rates to cumulative diel photons, with both 8 and 24 h photoperiods provoking increased photoinhibition of growth. In contrast, growth rates show simpler saturating responses to cumulative diel reductant generation, accessed through a chlorophyll fluorescence measure of electron flux, across a matrix of photoperiods and photosynthetically active radiation levels.

Under optimal conditions of 24 h photoperiod and moderate photosynthetically active radiation, a PE-rich *Synechococcus* sp. reached a chlorophyll-specific exponential growth rate of 4.5 d^{-1} , a record for cyanobacteria, comparable with genetically-modified industrial strains.

As photoperiod opportunitists, with capacity to grow rapidly under 24 h photoperiod, coastal *Synechococcus* sp. show potential to emerge as phytoplankton components during summer in future, warmed, polar regions.

Scientific Significance Statement Outlet

Dear Editor-in-Chief

K. David Hambright,

Our work indicating that picocyanobacteria have the potential to expand into new photic regimes while PE-rich picocyanobacteria may emerge as the dominant phytoplankton.

The findings of this study are helpful for further research on picocyanobacteria ecophysiology, and should be of interest to readers of Limnology and Oceanography, which has previously published articles on similar topics.

1 **Long & low; or short & high; photoperiods and light**
2 **differentially influence growth and potential niches of**
3 **PhycoCyanin and PhycoErythrin-rich picocyanobacteria**

4

5 **Sylwia Śliwińska-Wilczewska^{1,2}, Marta Konik^{3,4}, Mireille Savoie¹, Anabella**
6 **Aguilera^{5,6}, Naaman M. Omar¹, and Douglas A. Campbell^{1,✉}**

7

8 ¹ Department of Biology, Mount Allison University, 53 York St., Sackville, NB, E4L 1C9,
9 Canada

10 ² Institute of Oceanography, University of Gdańsk, 46 Piłsudskiego St, 81-378, Gdynia, Poland

11 ³ Department of Geography, University of Victoria, Victoria, BC, V8P 5C2, Canada

12 ⁴ Institute of Oceanology, Polish Academy of Sciences, 81-712 Sopot, Poland

13 ⁵ Department of Biology and Environmental Science, Centre for Ecology and Evolution in
14 Microbial Model Systems (EEMiS), Linnaeus University, Kalmar, Sweden

15 ⁶ Department of Aquatic Sciences and Assessment, Swedish University of Agricultural Sciences,
16 Uppsala, Sweden (present address)

17 ✉ Correspondence: Douglas A. Campbell <dubhglascambeuil@gmail.com>

18

19 **Running head:** *Picocyanobacteria across photic regimes*

20 **Keywords:** Cumulative diel photon dose; Light-capture, PAR; Photic regime; Phase of growth;
21 Photoperiod; Picocyanobacteria; PUR

22 **Abstract**

23 Strains from the picocyanobacteria genus *Synechococcus* are currently found across a wide
24 range of photoperiods and photosynthetically active radiation. Future scenarios now forecast
25 range expansions of marine *Synechococcus* into new photic regimes. We found that strains of
26 temperate, coastal PhycoCyanin(PC)-rich and PhycoErythrin(PE)-rich *Synechococcus* grew
27 fastest under moderate photosynthetically active radiation, and a 24-hour photoperiod, despite a
28 cumulative diel photon dose equivalent to conditions where growth was slower, under higher
29 light and shorter photoperiods. Under optimal conditions, a PE-rich *Synechococcus* strain
30 achieved a highest recorded cyanobacterial chlorophyll-specific exponential growth rate (μ) of
31 4.5 d^{-1} . Two PE-rich strains demonstrated wider ability to modulate light capture capacity,
32 whereas two PC-rich strains showed less change in light capture across increasing cumulative
33 diel photon dose. All four coastal strains showed a decrease of effective absorption cross section
34 for PSII photochemistry, versus increasing cumulative diel PAR doses. Within each strain, μ
35 showed consistent, saturating responses to increasing cumulative diel PSII electron flux, with
36 more variations in responses of μ to cumulative Photosynthetically Usable Radiation. As
37 photoperiod opportunists, coastal picocyanobacteria show potential to expand into longer photic
38 regimes as higher latitudes warm.

39

40 **Introduction**

41 The photic regime, comprised of Photosynthetically Active Radiation (PAR), spectral
42 quality, and photoperiod, is a pivotal influence on the growth and productivity of phytoplankton
43 within aquatic ecosystems. PAR refers to the spectral range of solar radiation, approximately
44 400-700 nm, that is capable of driving photosynthesis. The availability and distribution of PAR

45 in aquatic ecosystems is influenced by cloud cover, water depth, and light attenuation due to
46 water turbidity and suspended particles, including a feedback loop whereby phytoplankton cells
47 themselves contribute to light attenuation (Field et al. 1998; Torremorell et al. 2009).

48 Photosynthetically Usable Radiation (PUR), is, in turn, the fraction of PAR that can be absorbed
49 for photosynthesis by pigments of given cyanobacteria or algae (Morel 1978). PUR thus depends
50 upon the interaction of PAR, and the phytoplankton expression of genomic capacities for light
51 capture under a given condition (Moejes et al. 2017). Cyanobacteria and algae also respond to
52 changes in photoperiod, which serves as a key environmental cue for photosynthesis, growth,
53 reproduction, and nutrient assimilation (LaRoche and Robicheau 2022). Thus, in polar regions,
54 prolonged periods of wintertime darkness place a primary limitation on phytoplankton biomass
55 production, while extended daylight during summer boosts photosynthetic activity (Arrigo
56 2014). In temperate regions, seasonal variation in light-limitation is less pronounced, but
57 phytoplankton are still influenced by daily and seasonal fluctuations, with a contrast between
58 more favorable conditions for their growth in spring and summer, compared to fall and winter
59 (Huisman et al. 2002; Holtrop et al. 2021). In the tropics, daylight hours remain nearly constant
60 throughout the year (Behrenfeld et al. 2006), and phytoplankton productivity is primarily
61 controlled by nutrients resupplied into the euphotic zone (Li et al. 2015), and mortality through
62 viral lysis (Ortmann et al. 2002) or zooplankton grazing (Christaki et al. 1999).

63 The picocyanobacterial genus *Synechococcus*, one of the most abundant phytoplankton
64 primary producer in oceans, comprises a diversity of strains of differing pigmentations
65 (Śliwińska-Wilczewska et al. 2018b; a). *Synechococcus* collectively exhibits a distribution
66 spanning diverse geographical regions (Flombaum et al. 2013), with strains demonstrating a
67 remarkable range of adaptations to environmental conditions (Śliwińska-Wilczewska et al.

68 2018a; Aguilera et al. 2023). *Synechococcus* capacities to thrive across diverse marine and
69 freshwater habitats positions it as a pivotal agent in energy and nutrient transfer within food
70 webs, connecting the microbial loop with higher trophic levels, offering direct sustenance to
71 grazers, including zooplankton and small fish (Li 1995). As one of the two dominant
72 picocyanobacterial genera in oceanic waters, *Synechococcus* contribute significantly to light
73 attenuation and light availability for other photosynthetic marine organisms, thereby influencing
74 ocean colour and allowing satellite detection of *Synechococcus*-rich communities (Xi et al.
75 2020). General relations among optical absorption spectra and pigment compositions have been
76 used to determine diagnostic pigment indices of major phytoplankton functional types (Hirata et
77 al. 2011). Modeling suggests that *Synechococcus* abundance and ranges will increase due to
78 climate warming (Flombaum et al. 2013). The projected changes may vary geographically and
79 may include shifts in the spatial distribution of the main picocyanobacteria, as well as changes in
80 the proportions among *Synechococcus* lineages (Six et al. 2021), potentially pushing lineages
81 into new photic regimes. *Synechococcus* exhibits significant phenotypic diversity across
82 lineages, encompassing strains rich in phycobiliprotein pigments, phycoerythrin (PE-rich) or
83 phycocyanin (PC-rich) (Haverkamp et al. 2009; Aguilera et al. 2023). Phycobiliprotein pigments
84 are pivotal for light absorption during photosynthesis and confer distinctive colours to the
85 picocyanobacteria (Stomp et al. 2007). The disparate light preferences between PC-rich and PE-
86 rich *Synechococcus* strains influence their ecological niches. PC-rich strains thrive in surface
87 waters and coastal regions. PE-rich strains exhibit adaptation to lower-light conditions, primarily
88 inhabiting the deeper layers of the water column. PC-rich and PE-rich *Synechococcus* strains
89 thus predominantly occupy complementary habitats (Six et al. 2007; Haverkamp et al. 2009; Six
90 et al. 2021), although differential responses of *Synechococcus* lineages to photoperiod, have not

91 been studied in detail, except for thermophilic PC-rich *Synechococcus* PCC 6715 (Klepacz-
92 Smołka et al. 2020).

93 Picocyanobacteria are the most abundant phytoplankters in aquatic ecosystems and are
94 crucial to the optical properties of ocean water, by influencing its colour and transparency. PC-
95 rich and PE-rich *Synechococcus* may have different costs and physiological strategies for growth
96 under different photic regimes, which could drive spatial and temporal variability of
97 picocyanobacteria biomass and community composition, in current and potential future aquatic
98 habitats. Therefore, our aim was to determine whether photoperiod and light differentially affect
99 growth and light-capture, between representative PC-rich and PE-rich *Synechococcus*. This study
100 emphasizes the potential importance of photoperiod as a factor influencing poleward expansions
101 of marine picocyanobacteria in the face of climate change.

102

103 **Materials and Methods**

104 **Experimental setup**

105 Two xenic PhycoCyanin(PC)-rich (CCBA_056 or CCBA_077) strains and two
106 PhycoErythrin(PE)-rich (CCBA_048 or CCBA_127) strains of *Synechococcus* were obtained
107 from the Culture Collection of Baltic Algae (CCBA; <https://ccba.ug.edu.pl/pages/en/home.php>).
108 The phylogenetic placement of CCBA strains (Fig. S1 in Supporting Information) within cluster
109 5 picocyanobacteria was explored by amplifying and sequencing a fragment of the 16S rRNA
110 gene using universal primers 27F and 1492R (Lane 1991). 16S rRNA gene sequences were
111 aligned with MAFFT v. 7.5 using the G-INS-I algorithm (Katoh et al. 2019).

112 Picocyanobacteria strains were maintained in Tissue Culture Flasks (VWR International,
113 Cat. No. 10062-872, PA, USA) and were transferred to fresh f/2 media (Guillard 1975) at

114 salinity of 8 PSU (which corresponds to their natural habitat) every two weeks, under a
115 photoperiod of 12 h and Photosynthetically Active Radiation (PAR) of 10 $\mu\text{mol photons m}^{-2}\text{s}^{-1}$
116 supplied from cool white fluorescent tubes, at 22°C.

117 Experimental cultures of each strain were grown in 8 x 80 mL round bottom cylindrical
118 glass tubes in a Multi-Cultivator MC 1000-OD (Photon Systems Instruments, Drásov, Czech
119 Republic). Each culture tube contained 75 mL of f/2 medium inoculated with 5 mL of growing
120 pre-culture, to achieve exponential growth from the beginning of the experiment, with little to no
121 lag phase upon inoculation. Culture tubes were inoculated in the afternoon while the
122 photoregime of a sinuisoidal photoperiod commenced the following morning such that peak PAR
123 occurred at noon each day.

124 Cultures grew at 22°C, with photoperiods of 8, 12, 16, or 24 h, with peak PAR of 30, 90,
125 180, 300, 600, or 900 $\mu\text{mol photons m}^{-2}\text{s}^{-1}$ independently supplied to each culture tube from
126 white LED lamps. To approximate diel cycles, the photoperiods of 8 – 16 h were applied in a
127 sinuisoidal shape, while the 24-hour photoperiod was applied continuously. The area under the
128 sinuisoidal curve is 1/2 the area under a rectangle of equal 24-hour width, therefore at equivalent
129 peak PAR the 24 h square photoperiod cultures received 4 times the diel photon doses of the 12 h
130 sinuisoidal photoperiod cultures.

131 Culture tubes were closed with a silicone inert silicone stopper perforated by an aeration
132 input tube extending to the bottom of the culture tube, and a pressure outlet tube. Aeration with a
133 total air flow rate of around $\sim 140 \text{ mL min}^{-1} \text{ tube}^{-1}$ through a 0.2 μm filter ensured mixing and
134 provided air and CO₂ to cultures through the entire culture volume. The pH showed little
135 fluctuation and remained between $\sim 8 – 9$. Light, temperature, optical density, and aeration gas of

136 the Multi-Cultivator system were monitored and controlled via the Photobioreactor Control
137 Software (Photon Systems Instruments, Drásov, Czech Republic).

138

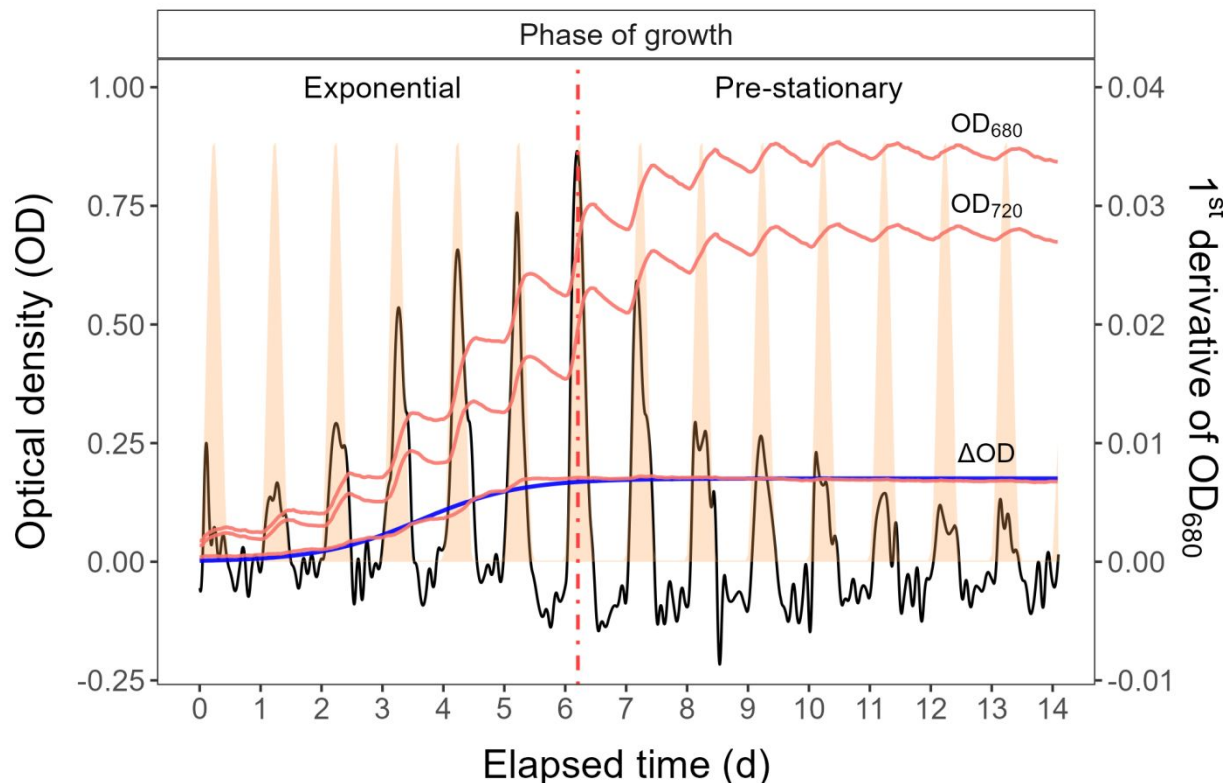
139 **Growth curves and chlorophyll-specific exponential growth rates**

140 Picocyanobacterial growth was monitored every 5 minutes for 14 days, independently for
141 each culture tube, by automatically recording OD₆₈₀, a proxy for chlorophyll *a* content; OD₇₂₀; a
142 proxy for cell scatter; and ΔOD (ΔOD = OD₆₈₀ – OD₇₂₀), a proxy for chlorophyll *a* content
143 (Nedbal et al. 2008). The exceptions were experiments conducted with a photoperiod of 24 h and
144 light of 600 or 900 μmol photons m⁻²s⁻¹, which lasted 7 days (Fig. S2). The chlorophyll-specific
145 exponential growth rates (μ) were determined by fitting logistic growth curves using a modified
146 Levenberg-Marquardt fitting algorithm (Elzhov et al. 2023) to plots of the chlorophyll *a* proxy of
147 ΔOD vs. elapsed time for each combination of strain, photoperiod, and peak PAR (Fig. S3).

148 To summarize the growth responses of the four picocyanobacterial strains we used a
149 Generalized Additive Model (GAM) (Wood 2017) applied to the relation of chlorophyll-specific
150 μ , d⁻¹ to photoperiod and PAR level. The R package *mgcv* (Wood 2017) was used to model the
151 growth rate with smoothing terms and indicate the 90, 50 and 10% quantiles for growth rate
152 across the levels of factors. Only growth rate estimates for which the amplitude of standard error
153 was smaller than 50% of the fitted growth rate were included in the GAM. We visually
154 compared the GAM contours to isolines of equal cumulative diel PAR (μmol photons m⁻²d⁻¹).

155 The 1st derivative of OD₆₈₀ taken over 1 h increments was computed using *xts*: eXtensible
156 Time Series (Ryan et al. 2024) and *signal*: Signal Processing (Ligges et al. 2024) R packages.
157 The time when the cultures reached their maximum absolute hourly growth (tMaxAHG), at the
158 maximum 1st derivative of OD₆₈₀, was taken as the time of transition from exponential to pre-

159 stationary growth phases (Fig. 1), which then progresses to the stationary growth phase. In this
 160 work, all measurements obtained after transition time were termed the pre-stationary phase of
 161 growth, according to Schuurmans et al. (2017).



162

163 **Fig. 1.** Example of a growth curve (tracked as OD_{720} , OD_{680} , or ΔOD ; red solid lines, left y-axis) of PE-rich culture
 164 of *Synechococcus* (048; grown at 180 peak PAR $\mu\text{mol photons m}^{-2}\text{s}^{-1}$; and photoperiods of 12 h vs. elapsed time
 165 (d, x-axis). 1st derivative of OD_{680} taken over 1 h increments (black solid line, right y-axis); solid blue line shows
 166 logistic fits of chlorophyll proxy $OD_{680} - OD_{720}$ (ΔOD) vs. elapsed time. The vertical red dot dash line represents the
 167 time when the culture reached the maximum of the 1st derivative of OD_{680} , or maximum absolute hourly growth
 168 (tMaxAHG), taken as the time of transition from exponential to pre-stationary growth phases.

169

170 Whole-cell absorbance spectra

171 Absorbance measurements on intact cells in suspension were conducted in an integrating
 172 cavity upgrade spectrophotometer (CLARiT^Y 17 UV/Vis/NIR, On-Line Instrument Systems,

173 Inc., Bogart, GA, USA). 8 mL of f/2 medium were added to both the sample and reference
174 observation cavities of the spectrophotometer. After recording a baseline from 375 to 710 nm, 1
175 mL was withdrawn from the sample cavity and replaced with 1 mL of picocyanobacteria cell
176 suspension. The pathlength corrected absorbance per cm was performed by determining the
177 Javorfi coefficients (Jávorfi et al. 2006) as described in the equipment manual.

178

179 Photosynthetically Usable Radiation (PUR)

180 Using whole-cell absorbance spectra of *Synechococcus* cultures, we estimated
181 Photosynthetically Usable Radiation (PUR; $\mu E = \mu\text{mol photons m}^{-2}\text{s}^{-1}$) according to Morel
182 (1978). Representative absorbance spectra for one growth light treatment (300 $\mu\text{mol photons}$
183 $\text{m}^{-2}\text{s}^{-1}$), for one PE and one PC rich strain, are shown in Fig. S4. The other 476 spectra used to
184 estimate PUR are available at <https://github.com/FundyPhytoPhys/BalticPhotoperiod>. We
185 normalized the obtained whole-cell Absorbances (A) and the Emission spectra of the white LED
186 lamps (Em) from 400 nm to 700 nm to a reference wavelength of 440 nm. PUR is then the ratio
187 of the sum of Absorbance Normalized to 440 nm (NormA₄₄₀) multiplied by the sum of Emission
188 spectra Normalized to 440 nm (NormEm₄₄₀) to the sum of the Emission spectra Normalized to
189 440 nm (NormEm₄₄₀), multiplied by the PAR (Eq. (1)).

$$190 PUR (\mu E) = \frac{\sum(NormA_{440} \times NormEm_{440})}{\sum(NormEm_{440})} \times PAR (\mu E) \quad (1)$$

191

192 Cumulative diel PAR and PUR

193 Based on the length and shape of the photoperiod (sinuisoidal wave for photoperiods of 8,
194 12, 16 h; square for photoperiod of 24 h) and the peak PAR ($\mu E = \mu\text{mol photons m}^{-2}\text{s}^{-1}$), we
195 estimated the value of the cumulative diel PAR ($\mu\text{mol photons m}^{-2}\text{d}^{-1}$). For sinuisoidal

196 photoperiods we used Eq. (2); for the continuous 24 h photoperiod we used Eq. (3). Cumulative
197 diel PUR was estimated similarly after estimation of peak PUR from peak PAR.

198
$$\frac{PAR (\mu E) \times 60 (s min^{-1}) \times 60 (min h^{-1}) \times photoperiod (h d^{-1})}{2} = Cumulative\ diel\ PAR (\mu mol\ photons\ m^{-2}\ d^{-1}) \quad (2)$$

199
$$PAR (\mu E) \times 60 (s min^{-1}) \times 60 (min h^{-1}) \times photoperiod (h d^{-1}) = Cumulative\ diel\ PAR (\mu mol\ photons\ m^{-2}\ d^{-1}) \quad (3)$$

200

201 **Pigment content**

202 Chlorophyll *a* (Chl *a*) ($\mu\text{g mL}^{-1}$) was measured using Trilogy Laboratory Fluorometer
203 (Turner Designs, Inc., CA, USA) equipped with Chlorophyll In-Vivo Module, previously
204 calibrated using 20 mL ampoules with known Chl *a* concentrations in 3:2 90% acetone:DMSO
205 solution. Quantitative analysis of Chl *a* was obtained after adding 50 μL of culture and 2 mL of a
206 90% acetone:DMSO solution in a 3:2 ratio.

207 We also estimated the pigment content ($\mu\text{g mL}^{-1}$): chlorophyll *a* (Chl *a*), carotenoids (Car),
208 phycoerythrin (PE), phycocyanin (PC), and allophycocyanin (APC) in *Synechococcus* cultures
209 over time using previously determined linear correlations between pigment content obtained by
210 extraction (Strickland and Parsons 1972; Bennett and Bogorad 1973) and absorbance values of
211 individual pigment peaks (Car; 480, PE; 565, PC; 620, APC; 650, and Chl *a*; 665 nm) obtained
212 from the whole-cell absorbance spectra using integrating cavity upgrade spectrophotometer
213 (CLARiTY 17 UV/Vis/NIR, On-Line Instrument Systems, Inc., Bogart, GA, USA) (Tab. S1 in
214 Supporting Information). The sum of phycobiliproteins (PE, PC, APC protein) to Chl *a* ratio
215 ($\mu\text{g}:\mu\text{g}$) for individual strains was also calculated.

216

217 The effective absorption cross section of PSII and electron flux

218 We harvested 2 mL of cultures for photophysiological characterizations repeatedly across
219 the growth trajectories. We used Fast Repetition Rate fluorometry (Kolber et al. 1998) (FRRf,
220 Solisense, USA), with a lab built temperature control jacket (22°C), to apply series of flashlets to
221 drive saturation induction/relaxation trajectories, fit using the onboard Solisense LIFT software
222 (Falkowski and Kolber 1993; Kolber et al. 1998). From the model fits we took the initial
223 fluorescence before induction (F_O , F_O' , or F_S , depending upon the level of actinic light and step
224 in the light response curve); the maximum fluorescence (F_M or F_M') once Photosystem II (PSII)
225 was driven to closure by the saturation induction flashlet train; and the effective absorption cross
226 section for PSII photochemistry (σ_{PSII} or σ_{PSII}' ; $\text{nm}^2 \text{ quanta}^{-1}$) (Tortell and Suggett 2021). We
227 used a double tap protocol (Xu et al. 2017), where FRRf induction/relaxation trajectories were
228 collected during a rapid light curve sequence increasing in steps of 10 s at 0, 20, 40, 80, 160, and
229 320 $\mu\text{mol photons m}^{-2}\text{s}^{-1}$ PAR, delivered from LED emitters centred at 445, preferentially
230 exciting chlorophyll, or 590 nm, preferentially exciting phycobiliproteins. Flash Power for 445
231 nm excitation was 60000 $\mu\text{mol photons m}^{-2}\text{s}^{-1}$ PAR, while for 590 nm excitation power was
232 14000 $\mu\text{mol photons m}^{-2}\text{s}^{-1}$, calibrated using a quantum sensor (LI-250, LI-COR, Inc.). We
233 applied 1 s darkness between sequential light steps, to allow re-opening of PSII. FRRf excitation
234 flashlets were applied at the same wavebands, 445 or 590 nm, as the actinic light steps (Fig.
235 S5A).

236 We calculated (Eq. (4)) an uncalibrated fluorescence based estimator for volumetric
237 electron transport, JV_{PSII} , ($\text{k} \times \text{e}^- \text{ L}^{-1} \text{ s}^{-1}$) under both 445 and 590 nm excitation bands
238 (Oxborough et al. 2012; Boatman et al. 2019; Tortell and Suggett 2021).

$$239 JV_{PSII} = \frac{\sigma_{PSII}' \times qP \times I \times F_O}{\sigma_{PSII}} \quad (4)$$

240 where σ_{PSII}' is effective absorption cross section for PSII photochemistry under the relevant
241 actinic PAR step ($\text{nm}^2 \text{ quanta}^{-1}$); qP is the fraction of PSII open for photochemistry estimated
242 according to Oxborough and Baker (1997); I is the applied PAR ($\mu\text{mol photons m}^{-2}\text{s}^{-1}$); F_O is the
243 minimum fluorescence from a given sample and excitation bandwidth (relative fluorescence) and
244 σ_{PSII} is the maximum effective absorption cross section for PSII photochemistry from a given
245 sample and excitation bandwidth ($\text{nm}^2 \text{ quanta}^{-1}$). We compared several other algorithms for
246 JV_{PSII} (Tortell and Suggett 2021) and found similar results.

247 We calibrated the JV_{PSII} estimator to absolute rates of electron transport (Eq. (5)) using
248 parallel measures of oxygen evolution ($\mu\text{mol O}_2 \text{ L}^{-1} \text{ s}^{-1}$), captured simultaneously with the FRRf
249 measures, below light saturation of electron transport, using a FireSting robust oxygen probe
250 (PyroScience, Germany) inserted in the cuvette for select Rapid Light Curve (RLC) runs (Fig.
251 S5B-C). For the blue LED ($\text{Ex}_{445\text{nm}}$) excitation we used a calibration slope of 108832, while for
252 orange LED ($\text{Ex}_{590\text{nm}}$) excitation we used a calibration slope of 254327

$$253 JV_{PSII}(e^{-} \text{ L}^{-1} \text{ s}^{-1}) = \frac{\text{Uncalibrated } JV_{PSII}(e^{-} \text{ L}^{-1} \text{ s}^{-1})}{\text{Calibration slope}} \quad (5)$$

254

255 Statistical analysis

256 We used R version 4.3.0 (R Core Team 2023) running under RStudio (Posit team 2022).
257 We performed three-way factorial ANOVA (*aov()* function; R Base package) to determine
258 whether peak PAR, photoperiod, strain, and their interactions, significantly influence the
259 chlorophyll-specific exponential growth rate (μ ; d^{-1}), estimated from logistic fits (*nlsLM()*
260 function; Elzhov et al. (2023)) of chlorophyll proxy $\text{OD}_{680} - \text{OD}_{720}$ vs. cumulative diel PUR
261 (Table S2). We also used the *nlsLM()* function to fit a three parameter light response model

262 (Harrison and Platt 1986) of growth rates (α , initial slope of curve; β , reflecting the
263 photoinhibition process; P_{\max} , the maximum rate of growth curve).

264 To examine statistical differences between fits of light responses, we performed one-way
265 ANOVA (*aov()* function) of the three parameter model (Harrison and Platt 1986) fit to pooled
266 data for each taxa, compared to separate fits for each different photoperiod (8, 12, 16, or 24); or
267 to separate fits for each different peak PAR (30, 90, 180, 300, 600 together with 900). These
268 comparisons were run for chlorophyll-specific exponential growth rate vs. cumulative diel PUR
269 (Table S3, S4); vs. cumulative diel PAR (Table S5, S6) or vs. PSII electron flux (JV_{PSII} ; $\mu\text{mol e}^{-}$
270 $\mu\text{mol Chl } \alpha^{-1} \text{ d}^{-1}$; Table S7, S8). One-way ANOVA was also used to examine statistical
271 differences between single phase exponential decay fits (*SSasymp()* function; Serway et al.
272 (2004)) of pooled data across different strains for a given phase of growth and across different
273 phase of growth for a given strain for PUR/PAR ratio (Table S9); Phycobiliprotein to Chl α ratio
274 (Table S10); or effective absorption cross section of PSII (σ_{PSII}' ; $\text{nm}^2 \text{ quanta}^{-1}$) measured under
275 diel peak PAR growth light under Ex_{590nm} (orange) excitation in relation to the cumulative diel
276 PAR ($\mu\text{mol photons m}^{-2}\text{d}^{-1}$) (Table S11).

277 We used *t*-tests (*t.test()* function; R Base package) of linear fits (*lm()* function) to compare
278 pooled data across different strains for a given phase of growth, and across different phases of
279 growth, for a given strain, for effective absorption cross section of PSII (σ_{PSII}' ; $\text{nm}^2 \text{ quanta}^{-1}$)
280 measured under diel peak PAR growth light under Ex_{445nm} (blue) excitation vs. the cumulative
281 diel PAR ($\mu\text{mol photons m}^{-2}\text{d}^{-1}$; Table S12); or vs. the Phycobiliprotein to Chl α ratio (Table
282 S13). The same *t*-test analyses were performed for effective absorption cross section of PSII
283 (σ_{PSII}' or σ_{PSII} ; $\text{nm}^2 \text{ quanta}^{-1}$) measured under Ex_{590nm} (orange) excitation vs. the Phycobiliprotein
284 to Chl α ratio (Table S14, S15).

285 Statistical differences for all analyses were determined at significance level $\alpha = 0.05$. The
286 manuscript was prepared as a Rmarkdown document (Handel 2020) with figures prepared using
287 the ggplot2 (Wickham 2016) and patchwork (Pedersen 2024) packages. All metadata, data and
288 code is available on GitHub (<https://github.com/FundyPhytoPhys/BalticPhotoperiod>).

289

290 **Results**

291 **Chlorophyll-specific exponential growth rates**

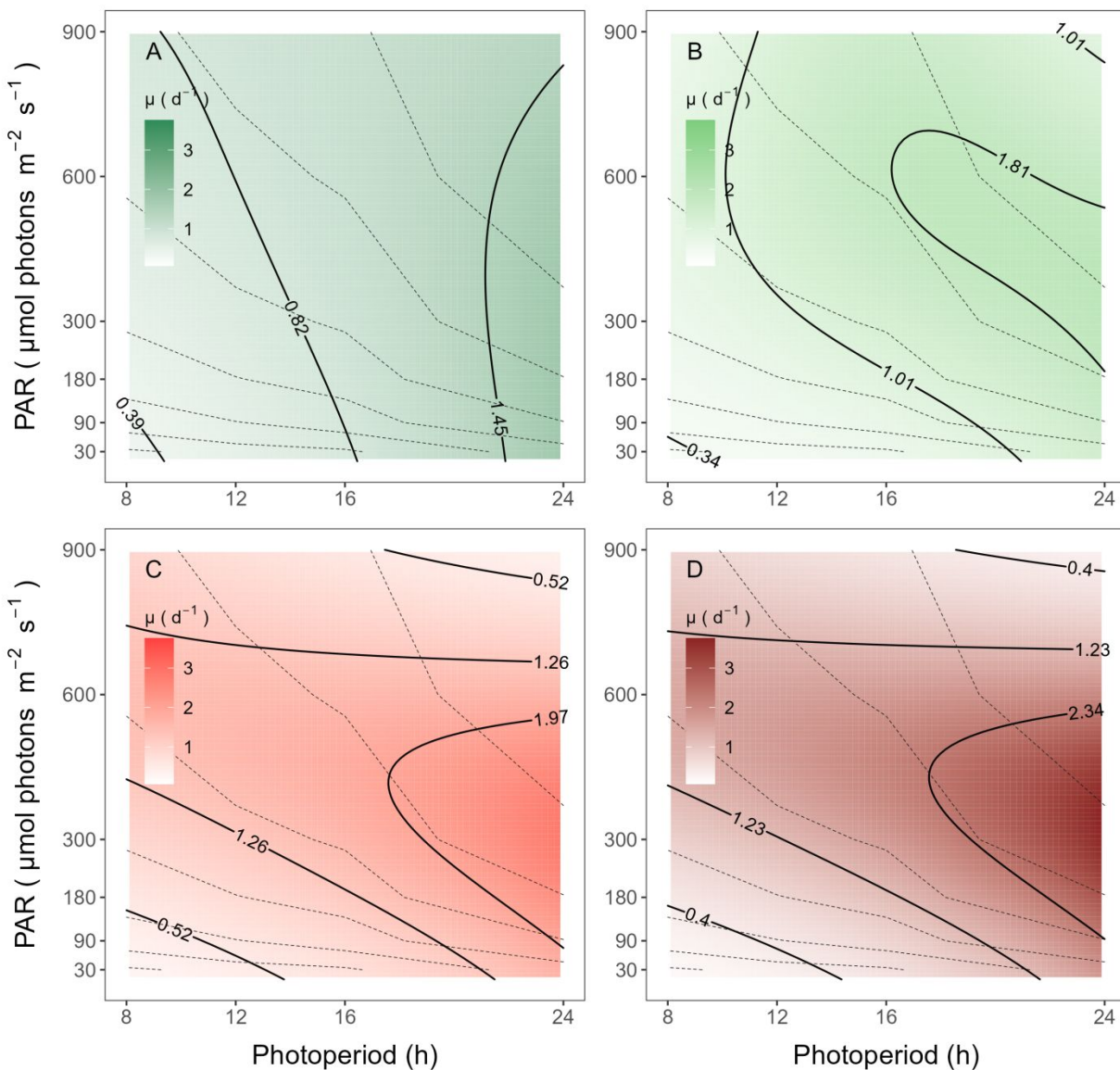
292 Not all cultures were grown long enough to reach full stationary phase, but onset of
293 stationary phase, when determined, occurred fairly consistently when cultures reached ~ 0.5
294 OD₇₂₀ (PC-rich) or ~ 0.65 OD₇₂₀ (PE-rich), no matter the level of culture PAR. It is therefore
295 unlikely that an onset of light limitation imposed stationary phase on the cultures, which
296 remained optically fairly thin, with even illumination to each tube from the PSI MultiCultivator
297 array of LED. Based upon parallel studies re-launching growth after stationary phase by dilution
298 with fresh media, with the same strains, under the same growth conditions (unpub.), we
299 hypothesize that nutrient limitation imposes the transition to stationary phase.

300 We used logistic curve fits (Fig. S3B) to determine chlorophyll-specific exponential
301 growth rates (μ ; d^{-1}), for two PhycoCyanin(PC)-rich cultures (056, 077) and two
302 PhycoErythrin(PE)-rich cultures (048, 127) of *Synechococcus* grown at 30, 90, 180, 300, 600, or
303 900 peak PAR $\mu\text{mol photons m}^{-2}\text{s}^{-1}$ (μE); and photoperiods of 8, 12, 16, or 24 h. There were
304 significant effects of all three independent variables on μ as well as significant interactions
305 between variables (ANOVA, $F_{2,88} > 1000$; $p < 0.05$ for all; Table S2). All tested strains, except
306 PE-rich_048, grew even under peak PAR 900 $\mu\text{mol photons m}^{-2}\text{s}^{-1}$ and 24 h photoperiod. The
307 highest growth rate was recorded for *Synechococcus* PE-rich_127 ($\mu = 4.5 d^{-1}$; 3.7 h doubling

308 time) and PC-rich_056 ($\mu = 3.4 \text{ d}^{-1}$; 4.9 h doubling time) at 180 $\mu\text{mol photons m}^{-2}\text{s}^{-1}$ peak PAR
309 and photoperiod of 24 h.

310 The GAM model in Fig. 2 summarizes the growth responses of the PC-rich and PE-rich
311 picocyanobacteria to peak PAR and photoperiod. PC-rich_056 *Synechococcus* showed highest
312 growth rates under a photoperiod of 24 h, across a wide range of peak PAR indicated by the
313 contour line labeled 1.45 d^{-1} , representing the 90th percentile of achieved growth rates for the
314 strain. On the other hand, the other tested PC-rich strain (077) showed highest growth rates in the
315 range of photoperiod 16-24 h and peak PAR between 300 – 700 $\mu\text{mol photons m}^{-2}\text{s}^{-1}$, indicated
316 by the 1.81 d^{-1} contour line again representing the 90th percentile of maximum achieved growth
317 rates for the strain. For both PC-rich strains, growth was slowest under 30 $\mu\text{mol photons m}^{-2}\text{s}^{-1}$
318 and a photoperiod of 8 h.

319 Both PE-rich strains achieved fastest growth rates above peak PAR of $\sim 300 \mu\text{mol photons}$
320 $\text{m}^{-2}\text{s}^{-1}$, under the longest photoperiod of 24 h, indicated by the 1.97 d^{-1} for PE-rich_048, and
321 2.34 d^{-1} for PE-rich_127, contour lines. For the PE-rich strains growth decreased with decreasing
322 photoperiod and decreasing peak PAR. Moreover, PE-rich strains showed photoinhibition of
323 growth at peak PAR of 900 $\mu\text{mol photons m}^{-2}\text{s}^{-1}$ and photoperiods of 16- 24 h. The growth rate
324 contours for PC-rich and PE-rich *Synechococcus* did not generally follow the isoclines of
325 cumulative diel photon dose ($\mu\text{mol photons m}^{-2}\text{d}^{-1}$, dashed lines), showing that photoperiod, and
326 peak PAR, influenced growth rates beyond cumulative diel photon dose.



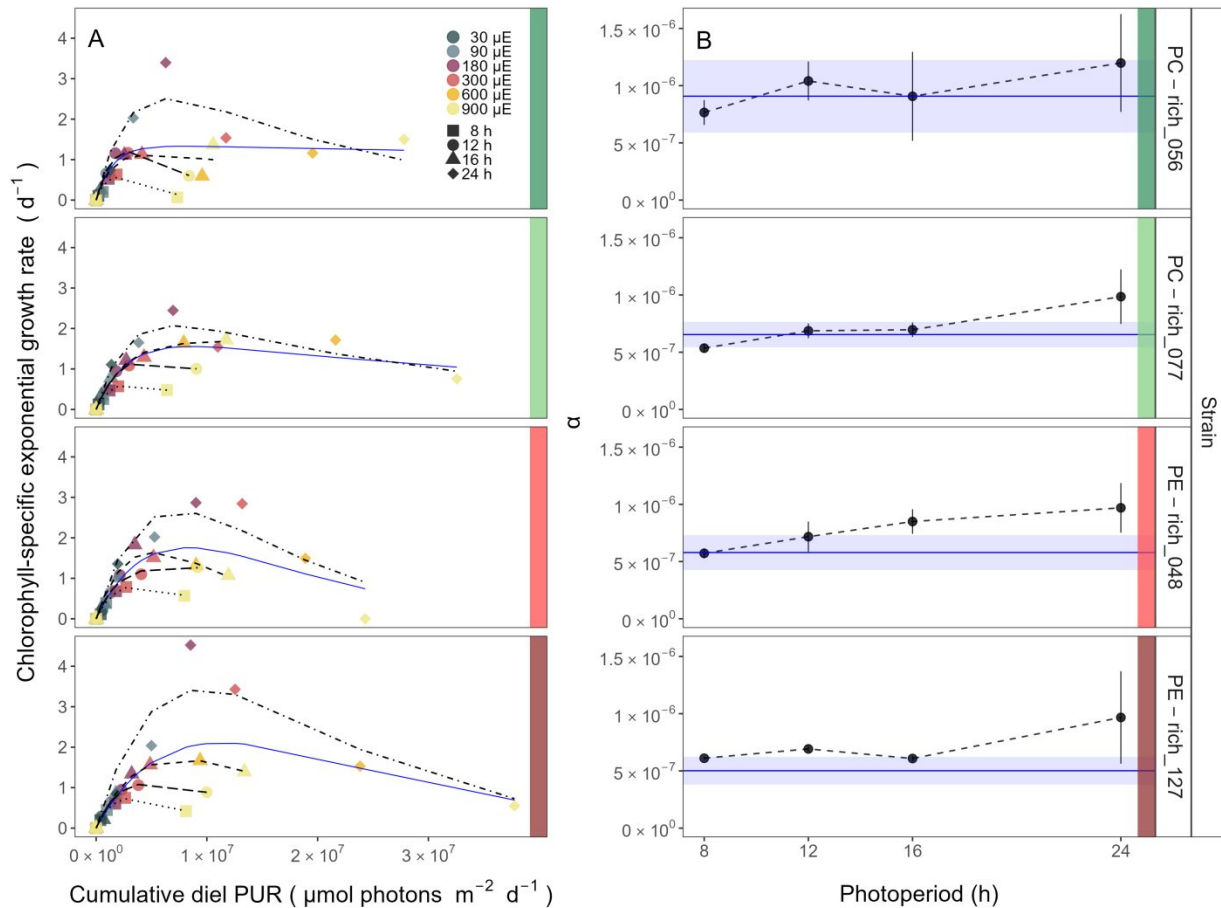
327

328 **Fig. 2.** A contour plot of a Generalized Additive Model (GAM) of chlorophyll-specific growth rates (d^{-1}) for two
 329 PC-rich cultures: **(A)** 056, **(B)** 077 and two PE-rich cultures: **(C)** 048, **(D)** 127 of *Synechococcus* grown at 30, 90,
 330 180, 300, 600, or 900 peak PAR $\mu\text{mol photons m}^{-2}\text{s}^{-1}$; and photoperiods of 8, 12, 16, or 24 h. Legends show colour
 331 gradients of growth rate (μ ; d^{-1}) from no growth (white) to 3.0 d^{-1} (dark green for PC-rich_056, light green for PC-
 332 rich_077, light red for PE-rich_048 or dark red for PE-rich_127 strains). Labeled contour lines indicate the 90%,
 333 50%, and 10% quantiles for achieved growth rate. Dotted lines show isoclines of cumulative diel photon dose (μmol
 334 photons $\text{m}^{-2}d^{-1}$).

335

336 A three parameter light response model fit (Harrison and Platt 1986) of chlorophyll-
337 specific exponential growth rates vs. cumulative diel PUR dose for two PC-rich and two PE-rich
338 cultures of *Synechococcus* showed significant differences between model fits of the pooled data
339 vs. fits for all tested photoperiods (8, 12, 16, or 24 h; ANOVA, $F_{1,16} \geq 6.9$; $p < 0.05$ for all; Fig.
340 3A, Table S3). The alpha parameters of the initial rise of growth rate (α) vs. cumulative diel
341 PUR, estimated from data pooled for each photoperiod increased with increasing photoperiod for
342 all strains. The highest increase (>2-fold) of α with increasing photoperiod was recorded for PC-
343 rich_056 (Fig. 3B). Strains also showed distinct growth rate responses to cumulative diel PUR,
344 depending upon peak PAR (Fig. S6A, Table S4), that differ from a single light response model
345 fit to the pooled data across all peak PAR from a strain. Exceptions were observed in the strains
346 PC-rich_077 and PE-rich_048 with the peak PAR of 600 or 900 $\mu\text{mol photons m}^{-2}\text{s}^{-1}$, which
347 were not significantly different from the pooled data model. A caveat to these findings is that
348 cumulative diel photon dose is a product of photoperiod and PAR, so the highest levels of
349 cumulative PUR dose are only achieved under the 600 or 900 $\mu\text{mol photons m}^{-2}\text{s}^{-1}$. The alpha
350 parameters of the initial rise of growth rate (α) vs. cumulative diel PUR, estimated from data
351 pooled for each peak PAR decreased across peak PAR for all tested strains (Fig. S6B).

352 Growth rate saturated under increasing cumulative diel PUR for all strains, however, the
353 achieved estimates of μ_{\max} varied depending upon photoperiod and peak diel PAR. Growth rates
354 vs. cumulative diel PAR relationships, estimated for exponential phase cultures, followed similar
355 patterns (Fig. S7, Fig. S8 and Table S5, S6 in Supporting Information).



356

357 **Fig. 3.** (A) Chlorophyll-specific exponential growth rates (d^{-1}) vs. cumulative diel Photosynthetically Usable
 358 Radiation (PUR, $\mu\text{mol photons m}^{-2}\text{d}^{-1}$). Growth rates (\pm SE falling within symbols) were estimated from logistic fits
 359 of chlorophyll proxy $\text{OD}_{680} - \text{OD}_{720}$ (ΔOD) vs. elapsed time (Fig. 1, Fig. S3B), for two PC-rich cultures (056; dark
 360 green, 077; light green) and two PE-rich cultures (048; light red, 127; dark red) of *Synechococcus* grown at 30 (dark
 361 gray), 90 (light gray), 180 (purple), 300 (red), 600 (orange), or 900 (yellow) peak PAR $\mu\text{mol photons m}^{-2}\text{s}^{-1}$ (μE);
 362 and photoperiods of 8 (square), 12 (circle), 16 (triangle), or 24 (diamond) h. Solid blue line shows a fit of the pooled
 363 growth rates through photoperiods for each strain, with a three parameter model (Harrison and Platt 1986). We also
 364 fit the same model separately for 8 (dotted line), 12 (long dash line), 16 (dashed line), or 24 (two dash line) h
 365 photoperiods, since for all strains they were each significantly different (ANOVA, $p < 0.05$) from the fit of pooled
 366 data. (B) Alpha parameters of the initial rise of growth rate (α) vs. cumulative diel Photosynthetically Usable
 367 Radiation (PUR), estimated from data pooled for each photoperiod (points (\pm SE) connected by dashed lines), and
 368 estimated for all data across photoperiods (solid blue horizontal line \pm SE), for each strain.

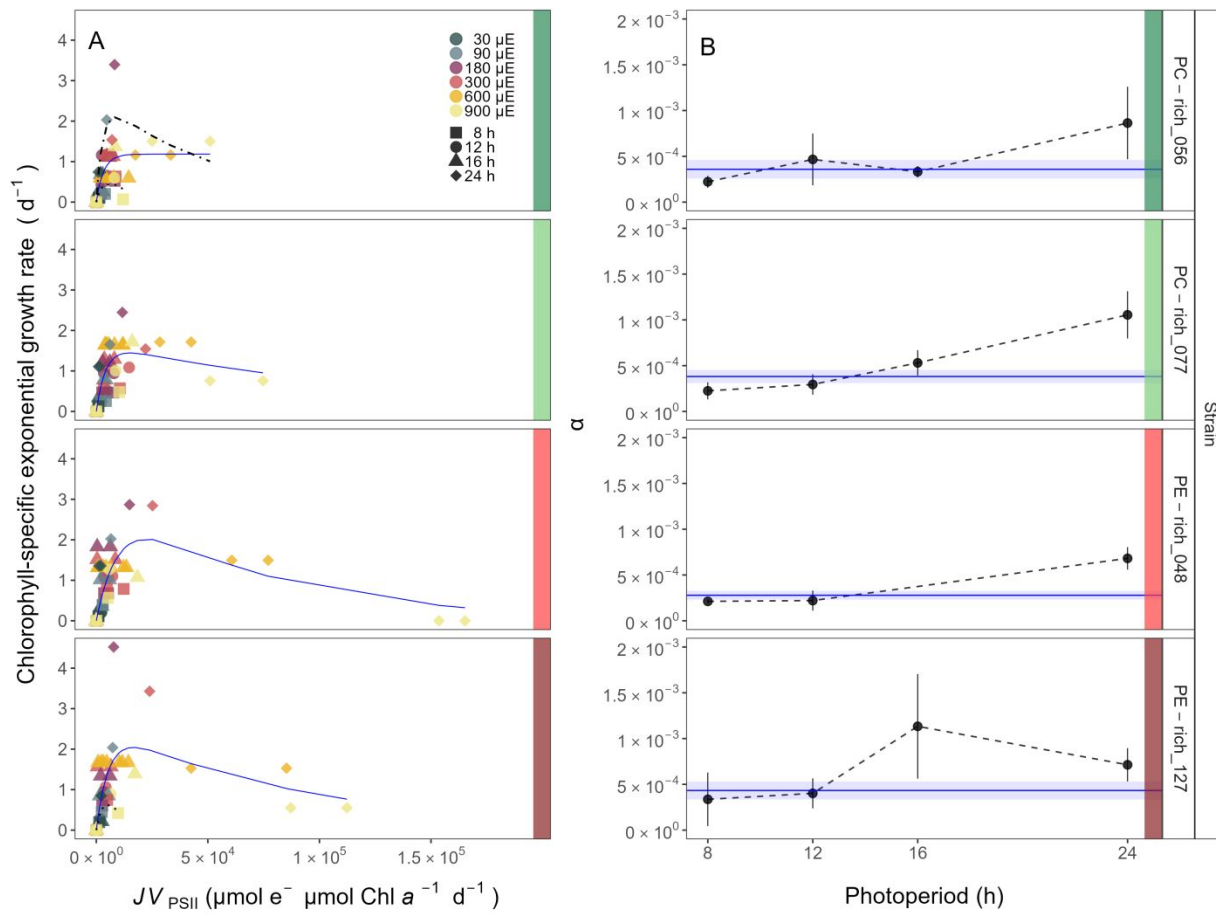
369

370 **Growth rates vs. cumulative diel PSII electron flux**

371 Chlorophyll-specific exponential growth rates (d^{-1}), within each strain, show fairly
372 consistent saturating responses to increasing cumulative diel PSII electron flux (JV_{PSII} ; $\mu\text{mol e}^-$
373 $\mu\text{mol Chl } \alpha^{-1} d^{-1}$) estimated under diel peak PAR growth light, and estimated using FRRf
374 induction curves with excitation of chlorophyll ($Ex_{445\text{nm}}$, blue), although photoperiod (Fig. 4A,
375 Table S7) and peak PAR (Fig. S14, Table S8) retained a secondary influence on achieved growth
376 responses for some growth conditions.

377 A three parameter model fit of (Harrison and Platt 1986) vs. cumulative diel PSII electron
378 flux (JV_{PSII} ; $\mu\text{mol e}^- \mu\text{mol Chl } \alpha^{-1} d^{-1}$) for two PC-rich and two PE-rich cultures of
379 *Synechococcus* showed no significant differences between fits of the pooled data vs. fits for
380 different photoperiods (8, 12, 16, or 24 h; ANOVA, $F_{1,16} \leq 4.1$; $p > 0.05$), with exception of 8
381 and 24 h photoperiod for PC-rich_056 and 8 h photoperiod for PE-rich_127 strains (ANOVA,
382 $F_{1,16} \geq 3.3$; $p < 0.05$; Table S7).

383 Alpha parameters of the initial rise of growth rate (α) vs. cumulative diel JV_{PSII} reflect the
384 yield of growth from electron transport. Alpha data pooled for each photoperiod showed an
385 increase across increasing photoperiods for each strain except for PE-rich_0127. The highest
386 increase (>2-fold) of α from the lowest to the highest photoperiod was recorded for PC-rich_077
387 (Fig. 4B).



388

389 **Fig. 4.** (A) Chlorophyll-specific exponential growth rates (d^{-1}) vs. cumulative diel PSII electron flux (JV_{PSII} ; $\mu\text{mol e}^-$
 390 $\mu\text{mol Chl } a^{-1} d^{-1}$) measured under diel peak PAR growth light. Growth rates (\pm SE falling within symbols) were
 391 estimated from logistic fits of chlorophyll proxy $OD_{680} - OD_{720}$ (ΔOD) vs. elapsed time (Fig. S3B). JV_{PSII} was
 392 estimated using FRRf induction curves with excitation of chlorophyll ($Ex_{445\text{nm}}$, blue), for two PC-rich cultures (056;
 393 dark green, 077; light green) and two PE-rich cultures (048; light red, 127; dark red) of *Synechococcus* grown at 30
 394 (μE), 90 (light gray), 180 (purple), 300 (red), 600 (orange), or 900 (yellow) peak PAR $\mu\text{mol photons m}^{-2}\text{s}^{-1}$
 395 (μE); and photoperiods of 8 (square), 12 (circle), 16 (triangle), or 24 (diamond) h. Solid blue line shows a fit of the
 396 pooled growth rates for each strain, with a three parameter model (Harrison and Platt 1986). We also fit the same
 397 model separately for 8 (dotted line) and 24 (two dash line) h photoperiods, when they were significantly different
 398 (ANOVA, $p < 0.05$) from the fit of pooled data. (B) Alpha parameters of the initial rise of growth rate (α)
 399 vs. cumulative diel JV_{PSII} , estimated from data pooled for each photoperiod (points (\pm SE) connected by dashed
 400 lines), and estimated for all data across photoperiods (horizontal line \pm SE), for each strain.

401

402 **Discussion**403 **Photic regimes - implications for picocyanobacteria growth and distribution**

404 Light regimes, including photoperiod, and peak PAR, are major factors affecting the
405 distribution and seasonality of phytoplankters (Erga and Heimdal 1984). Changes in photoperiod
406 trigger acclimation responses, shaping the temporal dynamics and community structure of
407 phytoplankton (Theus et al. 2022; Longobardi et al. 2022). Each tested picocyanobacterial strain
408 showed influences of photoperiod upon the responses of growth rate to cumulative diel PUR
409 (Fig. 3) and PAR (Fig. S6). To our surprise, increasing photoperiod increased the ranges of
410 responses to PAR and PUR. Both the PC-rich and the PE-rich strains of *Synechococcus* exhibited
411 their highest initial responses of growth to increasing PUR and PAR (alpha, Fig. 3B, Fig. S6B),
412 and their fastest growth rates under continuous light (24 h photoperiod), consistent with some
413 other strains (Jacob-Lopes et al. 2009; Klepacz-Smólka et al. 2020). Yet, 24 h photoperiod also
414 exacerbated eventual photoinhibition under excess cumulative diel PUR and PAR. Our four
415 temperate strains do not currently experience direct selective pressures to exploit a continuous 24
416 photoperiod (Brand and Guillard 1981), so achieving maximum growth under a 24 h photoperiod
417 rather suggests lack of a requirement for a dark period, and lack of requirement for a regular
418 photoperiod. Coastal phytoplankton strains are selected to exploit instantaneous light (Brand and
419 Guillard 1981), of whatever duration, to cope with fluctuating light and nutrients in coastal
420 environments (MacIntyre et al. 2000; Litchman et al. 2009), leading to a pleiotropic capacity for
421 exploiting continuous light. *Synechococcus* assemblages in coastal areas would tend to be
422 dominated by PC-rich strains by virtue of the higher turbidity of these areas relative to the open
423 ocean, perhaps regardless of photoperiod. However, the ability of both PC-rich and PE-rich

424 coastal picocyanobacteria to exploit continuous light means they could, potentially, grow rapidly
425 at higher latitudes, in future warmer polar summer water.

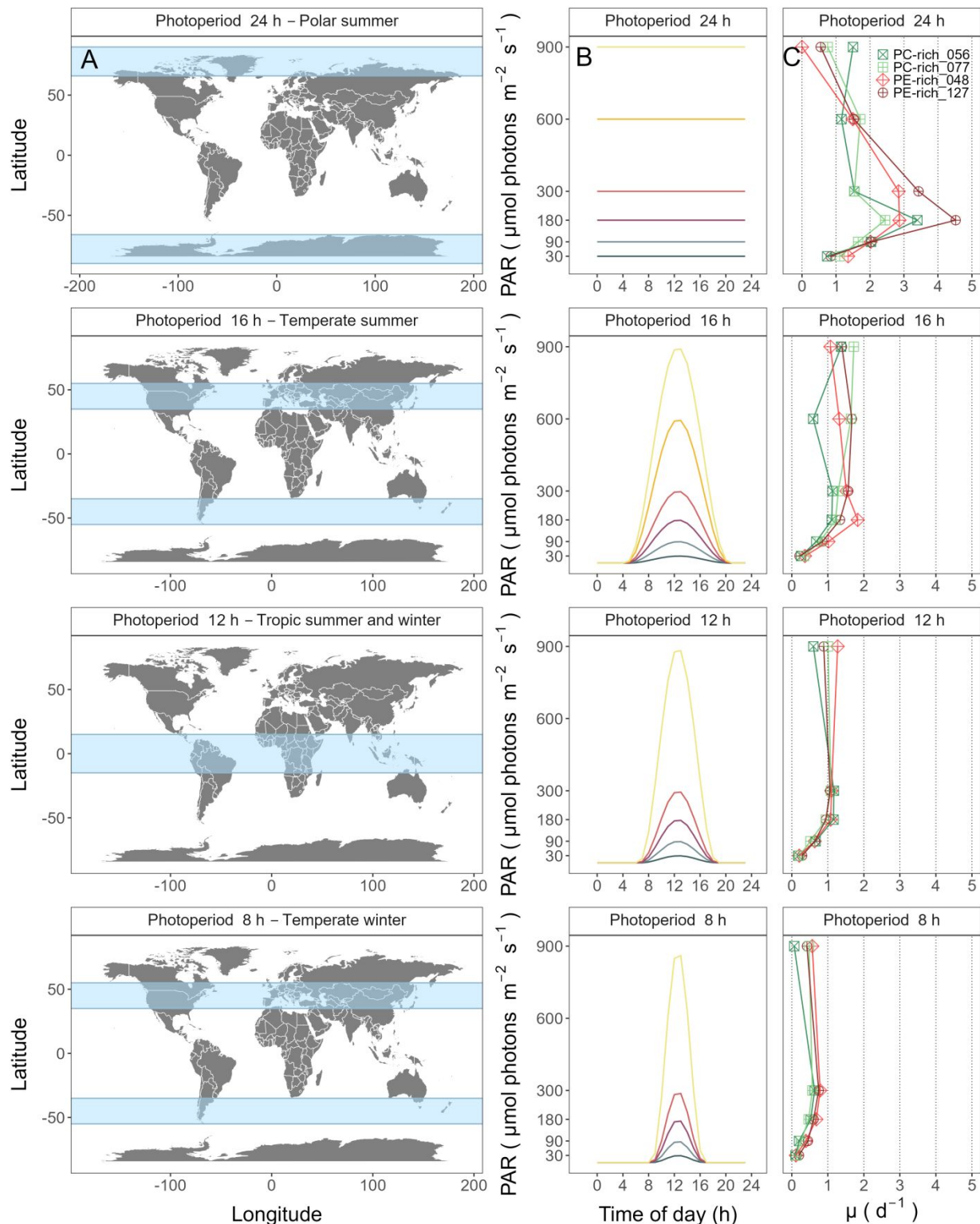
426 Light level is another key driver of picocyanobacteria productivity (Pick 1991; Six et al.
427 2007; Aguilera et al. 2023). The spatial and temporal distribution of PAR within aquatic
428 ecosystems is influenced by solar angle, water depth, water clarity, and the presence of light-
429 absorbing substances such as dissolved organic matter (Morel 1978, 1988) and phytoplankton
430 cells themselves. PUR then represents the light potentially available for phytoplankton to
431 photosynthesize. PUR is always smaller than PAR ($\text{PUR} < \text{PAR}$), and depends on the spectral
432 composition of the PAR, versus the phytoplankton pigment composition, determining cellular
433 spectral absorption (Morel 1978), which changes depending upon taxa, growth conditions and
434 the phase of growth.

435 PE-rich and PC-rich *Synechococcus* strains show distinct growth responses to cumulative
436 diel photon dose, depending upon the peak PAR or PUR of the applied photoregime (Fig. 3).
437 Chlorophyll-specific exponential growth rates of the PE-rich and PC-rich *Synechococcus* strains
438 increased with increasing light levels, to a plateau in the range of 180 – 300 μmol photons
439 $\text{m}^{-2}\text{s}^{-1}$. Growth above 600 μmol photons $\text{m}^{-2}\text{s}^{-1}$ occurred with a growth yield per cumulative diel
440 photon lower than under moderate light, particularly when combined with short 8 h or long 24 h
441 photoperiods. Even though PE-rich *Synechococcus* are more adapted to lower-light conditions
442 deeper in the water column (Stomp et al. 2007), our findings show that PE-rich strains will grow
443 under higher irradiance, which is generally contradictory to previous literature reports (Vörös et
444 al. 1998; Moser et al. 2009). Observations that PE-rich picocyanobacteria may be better adapted
445 for lower light may be more a consequence of light quality, rather than the light quantity
446 (Hauschild et al. 1991; Pick 1991).

447 The maximum growth rate of *Synechococcus* PE-rich_127 strain under 22°C, 24 h
448 photoperiod and peak PAR of 180 $\mu\text{mol photons m}^{-2}\text{s}^{-1}$ was 4.5 d^{-1} ($\mu = 0.187 \text{ h}^{-1}$),
449 corresponding to a doubling time of 3.7 h (Fig. 3); faster than previously reported for marine
450 picocyanobacteria, and indeed faster than for the model freshwater cyanobacteria *Synechococcus*
451 PCC6301 (doubling time of 4.5-5 h under 38°C, constant illumination and 250 $\mu\text{mol photons}$
452 $\text{m}^{-2}\text{s}^{-1}$) (Sakamoto and Bryant 1999), or *Synechocystis* PCC 6803 (doubling time of 4.3 h under
453 30°C and 120 $\mu\text{mol photons m}^{-2}\text{s}^{-1}$) (van Alphen et al. 2018). The fastest growth rate as yet
454 achieved for any phytoplankton was in a genetically modified green algae *Picochlorum celeri*,
455 with a maximum of about 6.7 d^{-1} and ~2.5 h doubling time (under 30°C, constant illumination,
456 and 900 $\mu\text{mol photons m}^{-2}\text{s}^{-1}$) (Weissman et al. 2018). The Baltic *Synechococcus* strains, not
457 genetically modified, preferred 24 h photoperiod and moderate peak PAR of 180 $\mu\text{mol photons}$
458 $\text{m}^{-2}\text{s}^{-1}$, suggesting they could, potentially, thrive in warming polar latitude waters.
459 *Synechococcus* strains indeed already occur across geographical regions (Śliwińska-Wilczewska
460 et al. 2018b) with different photic regimes, including polar regions (reviewed by Velichko et al.
461 (2021)), exceeding latitude 80°S and 80°N. The prolonged daylight hours of polar summers,
462 coupled with nutrient-rich waters, promote growth of genetically diverse *Synechococcus*
463 populations (Vincent et al. 2000), contributing significantly to primary productivity. Gradinger
464 and Lenz (1989) suggested that *Synechococcus*-type picocyanobacteria may serve as indicator
465 organisms for the advection of warm water masses into polar regions, important in the context of
466 monitoring upcoming climate changes.

467 The coastal PC-rich and PE-rich strains of *Synechococcus* showed saturation, and then
468 photoinhibition of growth rates under increasing cumulative diel PUR, although the achieved
469 estimates of μ_{\max} , and the onset of photoinhibition of growth, varied depending upon strain,

470 photoperiod and peak PAR (Fig. 2). The tested strains were generally opportunistic in exploiting
471 longer photoperiods to achieve faster μ , although PE-rich strains suffered strong photoinhibition
472 of growth under peak PAR above 600 $\mu\text{mol photons m}^{-2}\text{s}^{-1}$ and 24 h photoperiod (Fig. 3),
473 consistent with the PE-rich strains being better adapted to lower light and deeper parts of the
474 water column. The least favorable growth conditions for both PE-rich and PC-rich strains of
475 *Synechococcus* were under high light ($> 600 \mu\text{mol photons m}^{-2}\text{s}^{-1}$) and the shortest photoperiod
476 (8 h), even though the cumulative diel PUR dose was equivalent to conditions where the light
477 intensity was lower, and the photoperiod was longer. Thus, these Baltic picocyanobacteria are
478 prone to photoinhibition under both the longest, and the shortest, photoperiod regimes, with
479 flatter growth responses to light under intermediate photoperiods. In regions and periods with a
480 longer photoperiod, both PC-rich and PE-rich *Synechococcus* could become dominant species in
481 surface waters but could suffer under shorter photoperiods (Fig. 5).



482

483 **Fig. 5.** Latitudinal bands, equivalent summer or winter photoperiods, and picocyanobacterial growth responses. **(A)**
484 Latitudinal bands corresponding to tested growth photoperiods. **(B)** Tested photoperiod and peak PAR regimes used

485 for growth experiments. (C) Chlorophyll specific exponential growth rates (\pm SE falling within symbols) for two
486 PhycoCyanin(PC)-rich cultures (056; dark green, 077; light green) and two PhycoErythrin(PE)-rich cultures (048;
487 light red, 127; dark red) of *Synechococcus* under tested photoperiod and peak PAR regimes.

488

489 **Photic regimes and growth phase both influence cellular absorbance and light
490 use**

491 Cyanobacteria growth includes lag, exponential growth, stationary, and death phases
492 (Reynolds 2006). During the lag phase, cyanobacteria acclimate to the environment and prepare
493 for active growth by synthesizing essential cellular components. Exponential growth phase is
494 marked by cell division and biomass accumulation, fueled by nutrient and light availability. If
495 growth is limited by declining nutrients, by light, or by accumulation of inhibitory factors, algae
496 enter stationary phase, characterized by a balance between cell division and death, leading to a
497 plateau in population. The death phase occurs when cyanobacteria cell death outruns division,
498 leading to net decomposition, contributing to nutrient recycling in aquatic ecosystems (Reynolds
499 2006). Moreover, Schuurmans et al. (2017) proposed an additional phase between the
500 exponential and stationary phases of picocyanobacteria growth, which is often neglected in
501 physiological studies. Herein, we summarize the results obtained both in the exponential phase
502 of growth and after the transition to the pre-stationary and stationary growth phases.

503 Under nutrient replete exponential growth the picocyanobacterial strains show an
504 exponential decline in PUR/PAR ratio versus cumulative diel photon doses. Thus, under nutrient
505 repletion the picocyanobacteria adjust pigment composition to match light conditions (Fig. S9).
506 In addition to chlorophyll *a*, picocyanobacteria use phycobilins, including phycocyanin
507 (harvesting red light at 620 nm) and phycoerythrin (harvesting yellow light at 570 nm), as
508 accessory pigments to enhance light harvesting efficiency. Picocyanobacteria enhance phycobilin

509 production to compensate for limited irradiance, thereby optimizing their photosynthetic
510 capabilities (Śliwińska-Wilczewska et al. 2018a) and increasing their PUR/PAR. During the pre-
511 stationary phase, the PE-rich strains lose these capabilities and the relative absorbance of PE
512 peak was much lower, which would not be expected if light was limiting, as cell density
513 increased, again suggesting that nitrogen could be the limiting factor leading to entry into pre-
514 stationary and stationary phase.

515 The effective absorption cross section for photochemistry of PSII in the light (σ_{PSII}')
516 comprises the probability of light capture by PSII and the quantum yield for subsequent
517 photochemistry. PC-rich and PE-rich strains of *Synechococcus* again show consistent patterns of
518 an exponential decay to a plateau with increasing cumulative diel PAR doses, for σ_{PSII}' (nm^2
519 quanta $^{-1}$, measured under diel peak PAR growth light under $\text{Ex}_{590\text{nm}}$ (orange) excitation), without
520 detectable influences of photoperiod, nor of peak PAR (Fig. S11A). σ_{PSII}' excited through
521 chlorophyll absorbance at 445 nm was, in contrast, consistently small across strains and growth
522 conditions (Fig. S12, Fig. S13), since in cyanobacteria the number of chlorophyll serving each
523 PSII is nearly fixed (Xu et al. 2018). σ_{PSII}' excited through phycobilisome absorbance at 590 nm
524 shows, as expected, a positive correlation with Phycobiliprotein:Chl *a*. Growth under low
525 cumulative diel PAR results in an increased Phycobiliprotein:Chl *a*, as the picocyanobacteria
526 allocate protein resources towards phycobiliprotein-mediated light capture (Beale 1994;
527 Stadnichuk et al. 2015; Chakdar and Pabbi 2016). PC-rich and PE-rich strains of *Synechococcus*
528 in exponential growth nonetheless show significant scatter around this pattern, likely related to
529 regulatory control of σ_{PSII}' , beyond pigment composition. In pre-stationary phase σ_{PSII}'
530 vs. Phycobiliprotein:Chl *a* was better aligned, suggesting reliance upon fixed compositional

531 regulation of phycobiliprotein content to control light delivery to PSII, as opposed to shorter-
532 term regulation.

533 A 16S rRNA gene phylogeny (amplicon average 1385 bp) placed the tested strains in order
534 Synechococcales and family Synechoccaceae, within the cluster 5 picocyanobacterial lineage, in
535 sub-cluster 5.2 together with other freshwater, brackish and halotolerant strains, separate from
536 marine sub-clusters 5.1 and 5.3 (Fig. 1S). The 16S rRNA of the strains showed ~100% identity
537 with strains assigned to *Synechococcus* spp. or to *Cyanobium* spp. It is worth emphasizing that
538 light capture and light absorption abilities differed significantly among these tested strains (Six et
539 al. 2021). The PE-rich strains show a much higher PUR/PAR ratio under low cumulative diel
540 photon doses during exponential phase, but decay towards a plateau and reach a similar value to
541 the PC-rich strains as cumulative diel photon dose increases. Thus, the PE-rich strains in
542 exponential phase demonstrated higher ability to modulate light absorbance capacity, whereas
543 PC-rich strains retained a more stable PUR/PAR across cumulative diel photon doses. What is
544 more, during exponential phase, the PE-rich strains show a much higher σ_{PSII}' under low
545 cumulative diel photon dose, and their σ_{PSII}' remains higher than the PC-rich strains, even as
546 cumulative diel photon dose increases. Hence, PE-rich strains exhibit higher light harvesting
547 efficiency, at the expense of susceptibility to higher light levels, particularly under the shortest
548 (8h) and longest (24h) photoperiods.

549 *Synechococcus* exhibits remarkable acclimation even within a given strain to different
550 environmental conditions (Śliwińska-Wilczewska et al. 2018a, 2020; Aguilera et al. 2023).
551 Under high cumulative diel photon dose, *Synechococcus* employs photoprotective mechanisms
552 to prevent the harmful effects of excess light energy. These include the dissipation of excess
553 energy as heat via non-photochemical quenching (NPQ) and the regulation of phycobilisome

554 antenna pigments, to balance light absorption and energy transfer. In contrast, under conditions
555 of low cumulative diel PAR dose, *Synechococcus* increases the expression of light-harvesting
556 complexes to enhance light absorption (Fig. S9) and capture (Fig. S11).

557 Available photic regimes, combining photoperiod and peak PAR, may influence the
558 occurrences of PC-rich and PE-rich picocyanobacterial phenotypes. Nitrogen (N) is an essential
559 element for cyanobacteria, while the N costs to produce photosynthetic pigments varies. The
560 molecular weight of the two phycoerythrin (PE; phycoerythrobilin) subunits is about 20,000 and
561 18,300 g mol⁻¹, while the two phycocyanin (PC; phycocyanobilin) subunits are about 17,600 and
562 16,300 g mol⁻¹, and allophycocyanin (APC) is lower still, about 16,000 g mol⁻¹ (Bennett and
563 Bogorad 1971). It follows that N-cost of producing PE is higher than that of PC, even though
564 PE-rich picocyanobacteria capture light better than PC-rich phenotypes (Fig. S9; Fig. S11). Our
565 results confirm that PE-rich strains are stronger light-harvesting competitors, while the PC-rich
566 strains have lower N-quotients for their phycobilin light capture system.

567

568 **Photic regimes - implications for cumulative diel PSII electron flux**

569 Algal dynamics respond rapidly to changes in environmental conditions (Connor 2018).
570 We used Fast Repetition Rate fluorometry (FRRf; Fig. S5) (Kolber et al. 1998) to generate an
571 index of PSII electron transport rate per unit volume (JV_{PSII}) (Oxborough et al. 2012; Tortell and
572 Suggett 2021; Berman-Frank et al. 2023), calibrated to absolute rates of electron transport
573 through parallel measures of oxygen evolution. Across different photic regimes the growth rates,
574 μ , of PC-rich and PE-rich picocyanobacteria show fairly consistent saturating responses to
575 increasing cumulative diel PSII electron flux (JV_{PSII} ; $\mu\text{mol e}^- \mu\text{mol Chl } a^{-1} d^{-1}$; Fig. 4). As
576 previously found for diatoms (Li et al. 2017) cumulative diel reductant generation was indeed a

577 better predictor of μ than was cumulative diel PUR, although photoperiod and peak PAR retain
578 some influences on achieved growth responses of the picocyanobacteria to JV_{PSII} .

579

580 **Conclusions**

581 Coastal picocyanobacteria show differing growth responses to photoperiod and light level,
582 even under combinations giving equivalent cumulative diel PUR. Both PE-rich and PC-rich
583 strains of *Synechococcus*, grew fastest under moderate light and a 24 h photoperiod.
584 Consequently, these coastal strains from *Synechococcus* cluster 5.2 show potential to emerge as
585 components of the phytoplankton during the Arctic or Antarctic summer under future, warmed,
586 polar regions. In optimal conditions (24 h of photoperiod and a peak PAR of 180 $\mu\text{mol photons}$
587 $\text{m}^{-2}\text{s}^{-1}$ and only 22°C), one of the PE-rich *Synechococcus*, reached a chlorophyll-specific
588 exponential growth rate of 4.5 d^{-1} (3.7 h doubling time), a record for a cyanobacteria. PE-rich
589 strains in the exponential phase of growth also demonstrated high ability to modulate their
590 PUR/PAR ratio by adjusting pigment composition, giving an advantage in the competition for
591 light. However, based on the present study the PE-rich strains are more susceptible to
592 photoinhibition of growth. We determined that growth yields of PC-rich and PE-rich
593 picocyanobacteria are well predicted by a saturating response to cumulative diel PSII electron
594 fluxes, across different photic regimes. PE-rich phenotypes of picocyanobacteria currently
595 predominate in abundance and genetic diversity in the Baltic Sea (Aguilera et al. 2023). This
596 dominance may be the result of eutrophication in the Baltic Sea, providing higher nitrogen for
597 phycobiliprotein synthesis, and leading to lower light even in near-surface waters. Our results
598 suggest possible expansion of the range of picocyanobacteria to new photic regimes in a warmed

599 future and indicate that PE-rich *Synechococcus* may be a dominant component of
600 picophytoplankton in nutrient-rich environments.

601

602 **Additional Supporting Information may be found in the online version of this article.**

603

604 **Authors Contribution Statement:** S.S-W. designed the study with input from D.A.C.
605 M.K. estimated the transition point between exponential and pre-stationary phase of growth.
606 M.S. ensured the proper operation of the photobioreactors. A.A. conducted genetic analysis.
607 N.M.O. solved technical problems related to computer operation and software. S.S-W., M.S.,
608 N.M.O., D.A.C. contributed to R coding and data analysis. S.S-W. conducted the experiments,
609 created plots and wrote the manuscript, with support from D.A.C. All authors contributed to the
610 discussion of the results, supported manuscript preparation, and approved the final submitted
611 manuscript.

612

613 **Data availability statement**

614 Data supporting this study is available on:

615 <https://github.com/FundyPhytoPhys/BalticPhotoperiod> (public GitHub Repository) and
616 https://docs.google.com/spreadsheets/d/1ZXpwR7Gfto-uRzVdXzMpQF4frbrvMLH_IyLqonFZRSw/edit#gid=0 (URL for MetaDataCatalog).

618 Code to perform data processing and analyses is available at

619 <https://github.com/FundyPhytoPhys/BalticPhotoperiod>.

620 16S rRNA sequences used in this study are available in GenBank under the accession
621 numbers PP034393, PP034394, PP034396 and PP034403.

622

623 **Acknowledgements**

624 We would thank the two Editors, Ilana Berman-Frank and Elisa Schaum, and two
625 Reviewers for their efforts reviewing and improving this manuscript. We thank Maximilian
626 Berthold for the code for the GAM model; Miranda Corkum who maintained cultures and trained
627 personnel in culture handling; Laurel Genge, and Carlie Barnhill (Mount Allison students) who
628 assisted with R code. This work was supported by Canada Research Chair in Phytoplankton
629 Ecophysiology (D.A.C) and Latitude & Light; NSERC of Canada Discovery Grant (D.A.C).

630

631 **Conflict of Interest**

632 None declared.

633

634 **References**

- 635 Aguilera, A., J. Alegria Zufia, L. Bas Conn, and others. 2023. Ecophysiological analysis reveals
636 distinct environmental preferences in closely related Baltic Sea picocyanobacteria.
637 Environmental Microbiology **25**: 1674–1695. doi:10.1111/1462-2920.16384
- 638 Arrigo, K. R. 2014. Sea ice ecosystems. Annual Review of Marine Science **6**: 439–467.
639 doi:10.1146/annurev-marine-010213-135103
- 640 Beale, S. I. 1994. Biosynthesis of cyanobacterial tetrapyrrole pigments: Hemes, chlorophylls,
641 and phycobilins, p. 519–558. In D.A. Bryant [ed.], The Molecular Biology of Cyanobacteria.
642 Springer Netherlands.

- 643 Behrenfeld, M. J., R. T. O'Malley, D. A. Siegel, and others. 2006. Climate-driven trends in
644 contemporary ocean productivity. *Nature* **444**: 752–755. doi:10.1038/nature05317
- 645 Bennett, A., and L. Bogorad. 1971. Properties of subunits and aggregates of blue-green algal
646 biliproteins. *Biochemistry* **10**: 3625–3634. doi:10.1021/bi00795a022
- 647 Bennett, A., and L. Bogorad. 1973. Complementary Chromatic Adaptation in a filamentous blue-
648 green alga. *Journal of Cell Biology* **58**: 419–435. doi:10.1083/jcb.58.2.419
- 649 Berman-Frank, I., D. Campbell, A. Ciotti, and others. 2023. Application of Single Turnover
650 Active Chlorophyll Fluorescence for Phytoplankton Productivity Measurements. Version 2.0,
651 June, 26, 2023. Report Scientific Committee on Oceanic Research (SCOR) Working Group 156.
- 652 Boatman, T. G., R. J. Geider, and K. Oxborough. 2019. Improving the accuracy of Single
653 Turnover Active Fluorometry (STAF) for the estimation of Phytoplankton Primary Productivity
654 (PhytoPP). *Frontiers in Marine Science* **6**. doi:10.3389/fmars.2019.00319
- 655 Brand, L. E., and R. R. L. Guillard. 1981. The effects of continuous light and light intensity on
656 the reproduction rates of twenty-two species of marine phytoplankton. *Journal of Experimental
657 Marine Biology and Ecology* **50**: 119–132. doi:10.1016/0022-0981(81)90045-9
- 658 Chakdar, H., and S. Pabbi. 2016. Cyanobacterial phycobilins: Production, purification, and
659 regulation, p. 45–69. In P. Shukla [ed.], *Frontier Discoveries and Innovations in Interdisciplinary
660 Microbiology*. Springer India.
- 661 Christaki, U., S. Jacquet, J. R. Dolan, D. Vaulot, and F. Rassoulzadegan. 1999. Growth and
662 grazing on *Prochlorococcus* and *Synechococcus* by two marine ciliates. *Limnology and
663 Oceanography* **44**: 52–61. doi:10.4319/lo.1999.44.1.0052

- 664 Connor, D. 2018. Investigating the use of fast repetition rate fluorometry in understanding algal
665 physiology in optically complex oceans.
- 666 Elzhov, T. V., K. M. Mullen, A.-N. Spiess, and B. Bolker. 2023. Minpack.lm: R Interface to the
667 Levenberg-Marquardt Nonlinear Least-Squares Algorithm Found in MINPACK, Plus Support
668 for Bounds.
- 669 Erga, S. R., and B. R. Heimdal. 1984. Ecological studies on the phytoplankton of Korsfjorden,
670 western Norway. The dynamics of a spring bloom seen in relation to hydrographical conditions
671 and light regime. *Journal of Plankton Research* **6**: 67–90. doi:10.1093/plankt/6.1.67
- 672 Falkowski, P., and Z. Kolber. 1993. Estimation of phytoplankton photosynthesis by active
673 fluorescence. *ICES Marine Science Symposium* **197**: 92–103.
- 674 Field, C. B., M. J. Behrenfeld, J. T. Randerson, and P. Falkowski. 1998. Primary production of
675 the biosphere: Integrating terrestrial and oceanic components. *Science* **281**: 237–240.
676 doi:10.1126/science.281.5374.237
- 677 Flombaum, P., J. L. Gallegos, R. A. Gordillo, and others. 2013. Present and future global
678 distributions of the marine Cyanobacteria *Prochlorococcus* and *Synechococcus*. *Proceedings of*
679 *the National Academy of Sciences* **110**: 9824–9829. doi:10.1073/pnas.1307701110
- 680 Gradinger, R., and J. Lenz. 1989. Picocyanobacteria in the high Arctic. *Marine Ecology Progress Series*
681 **52**: 99–101. doi:10.3354/meps052099
- 682 Guillard, R. R. L. 1975. Culture of phytoplankton for feeding marine invertebrates, p. 29–60. *In*
683 W.L. Smith and M.H. Chanley [eds.], *Culture of Marine Invertebrate Animals: Proceedings —*
684 *1st Conference on Culture of Marine Invertebrate Animals* Greenport. Springer US.

- 685 Handel, A. 2020. Andreas Handel - Custom Word formatting using R Markdown.
- 686 Harrison, W. G., and T. Platt. 1986. Photosynthesis-irradiance relationships in polar and
687 temperate phytoplankton populations. *Polar biology* **5**: 153–164.
- 688 Hauschild, C. A., H. J. G. McMurter, and F. R. Pick. 1991. Effect of Spectral Quality on Growth
689 and Pigmentation of Picocyanobacteria1. *Journal of Phycology* **27**: 698–702. doi:10.1111/j.0022-
690 3646.1991.00698.x
- 691 Haverkamp, T. H. A., D. Schouten, M. Doeleman, U. Wollenzien, J. Huisman, and L. J. Stal.
692 2009. Colorful microdiversity of *Synechococcus* strains (picocyanobacteria) isolated from the
693 Baltic Sea. *The ISME Journal* **3**: 397–408. doi:10.1038/ismej.2008.118
- 694 Hirata, T., N. J. Hardman-Mountford, R. J. W. Brewin, and others. 2011. Synoptic relationships
695 between surface Chlorophyll-*a* and diagnostic pigments specific to phytoplankton functional
696 types. *Biogeosciences* **8**: 311–327. doi:10.5194/bg-8-311-2011
- 697 Holtrop, T., J. Huisman, M. Stomp, and others. 2021. Vibrational modes of water predict spectral
698 niches for photosynthesis in lakes and oceans. *Nature Ecology & Evolution* **5**: 55–66.
699 doi:10.1038/s41559-020-01330-x
- 700 Huisman, J., M. Arrayás, U. Ebert, and B. Sommeijer. 2002. How do sinking phytoplankton
701 species manage to persist? *The American Naturalist* **159**: 245–254. doi:10.1086/338511
- 702 Jacob-Lopes, E., C. H. G. Scoparo, L. M. C. F. Lacerda, and T. T. Franco. 2009. Effect of light
703 cycles (night/day) on CO₂ fixation and biomass production by microalgae in photobioreactors.
704 *Chemical Engineering and Processing: Process Intensification* **48**: 306–310.
705 doi:10.1016/j.cep.2008.04.007

- 706 Jávorfi, T., J. Erostyák, J. Gál, A. Buzády, L. Menczel, G. Garab, and K. Razi Naqvi. 2006.
- 707 Quantitative spectrophotometry using integrating cavities. Journal of Photochemistry and
- 708 Photobiology B: Biology **82**: 127–131. doi:10.1016/j.jphotobiol.2005.10.002
- 709 Katoh, K., J. Rozewicki, and K. D. Yamada. 2019. MAFFT online service: Multiple sequence
- 710 alignment, interactive sequence choice and visualization. Briefings in Bioinformatics **20**: 1160–
- 711 1166. doi:10.1093/bib/bbx108
- 712 Klepacz-Smólka, A., D. Pietrzyk, R. Szeląg, P. Głusczk, M. Daroch, J. Tang, and S. Ledakowicz.
- 713 2020. Effect of light colour and photoperiod on biomass growth and phycocyanin production by
- 714 *Synechococcus* PCC 6715. Bioresource Technology **313**: 123700.
- 715 doi:10.1016/j.biortech.2020.123700
- 716 Kolber, Z. S., O. Prášil, and P. G. Falkowski. 1998. Measurements of variable chlorophyll
- 717 fluorescence using fast repetition rate techniques: Defining methodology and experimental
- 718 protocols. Biochimica et Biophysica Acta (BBA) - Bioenergetics **1367**: 88–106.
- 719 doi:10.1016/S0005-2728(98)00135-2
- 720 Lane, D. J. 1991. 16S/23S rRNA sequencing. Nucleic acid techniques in bacterial systematics
- 721 115–175.
- 722 LaRoche, J., and B. M. Robicheau. 2022. The Pelagic Light-Dependent Microbiome, p. 395–
- 723 423. In L.J. Stal and M.S. Cretoiu [eds.], The Marine Microbiome. Springer International
- 724 Publishing.

- 725 Li, G., D. Talmy, and D. A. Campbell. 2017. Diatom growth responses to photoperiod and light
726 are predictable from diel reductant generation. *Journal of Phycology* **53**: 95–107.
727 doi:10.1111/jpy.12483
- 728 Li, Q., L. Legendre, and N. Jiao. 2015. Phytoplankton responses to nitrogen and iron limitation
729 in the tropical and subtropical Pacific Ocean. *Journal of Plankton Research* **37**: 306–319.
730 doi:10.1093/plankt/fbv008
- 731 Li, W. K. W. 1995. Composition of ultraphytoplankton in the central North Atlantic. *Marine
732 Ecology Progress Series* **122**: 1–8.
- 733 Ligges, U., T. Short, P. Kienzle, and others. 2024. Signal: Signal Processing.
734 Litchman, E., C. A. Klausmeier, and K. Yoshiyama. 2009. Contrasting size evolution in marine
735 and freshwater diatoms. *Proceedings of the National Academy of Sciences* **106**: 2665–2670.
736 doi:10.1073/pnas.0810891106
- 737 Longobardi, L., L. Dubroca, F. Margiotta, D. Sarno, and A. Zingone. 2022. Photoperiod-driven
738 rhythms reveal multi-decadal stability of phytoplankton communities in a highly fluctuating
739 coastal environment. *Scientific Reports* **12**: 3908. doi:10.1038/s41598-022-07009-6
- 740 MacIntyre, H. L., T. M. Kana, R. J. Geider, H. L. MacIntyre, T. M. Kana, and R. J. Geider. 2000.
741 The effect of water motion on short-term rates of photosynthesis by marine phytoplankton.
742 *Trends in Plant Science* **5**: 12–17. doi:10.1016/S1360-1385(99)01504-6
- 743 Moejes, F. W., A. Matuszyńska, K. Adhikari, and others. 2017. A systems-wide understanding
744 of photosynthetic acclimation in algae and higher plants. *Journal of Experimental Botany* **68**:
745 2667–2681. doi:10.1093/jxb/erx137

- 746 Morel, A. 1978. Available, usable, and stored radiant energy in relation to marine
747 photosynthesis. Deep Sea Research **25**: 673–688. doi:10.1016/0146-6291(78)90623-9
- 748 Morel, A. 1988. Optical modeling of the upper ocean in relation to its biogenous matter content
749 (case I waters). Journal of Geophysical Research: Oceans **93**: 10749–10768.
750 doi:10.1029/JC093iC09p10749
- 751 Moser, M., C. Callieri, and T. Weisse. 2009. Photosynthetic and growth response of freshwater
752 picocyanobacteria are strain-specific and sensitive to photoacclimation. Journal of Plankton
753 Research **31**: 349–357. doi:10.1093/plankt/fbn123
- 754 Nedbal, L., M. Trtílek, J. Červený, O. Komárek, and H. B. Pakrasi. 2008. A photobioreactor
755 system for precision cultivation of photoautotrophic microorganisms and for high-content
756 analysis of suspension dynamics. Biotechnology and Bioengineering **100**: 902–910.
757 doi:10.1002/bit.21833
- 758 Ortmann, A. C., J. E. Lawrence, and C. A. Suttle. 2002. Lysogeny and Lytic Viral Production
759 during a Bloom of the Cyanobacterium *Synechococcus* spp. Microbial Ecology **43**: 225–231.
- 760 Oxborough, K., and N. R. Baker. 1997. Resolving chlorophyll *a* fluorescence images of
761 photosynthetic efficiency into photochemical and non-photochemical components – calculation
762 of qP and Fv-/Fm-; without measuring Fo-; Photosynthesis Research **54**: 135–142.
763 doi:10.1023/A:1005936823310
- 764 Oxborough, K., C. M. Moore, D. J. Suggett, T. Lawson, H. G. Chan, and R. J. Geider. 2012.
765 Direct estimation of functional PSII reaction center concentration and PSII electron flux on a

- 766 volume basis: A new approach to the analysis of Fast Repetition Rate fluorometry (FRRf) data.
- 767 Limnology and Oceanography: Methods **10**: 142–154. doi:10.4319/lom.2012.10.142
- 768 Pedersen, T. L. 2024. Patchwork: The Composer of Plots.
- 769 Pick, F. R. 1991. The abundance and composition of freshwater picocyanobacteria in relation to
770 light penetration. Limnology and Oceanography **36**: 1457–1462. doi:10.4319/lo.1991.36.7.1457
- 771 Posit team. 2022. RStudio: Integrated development environment for r, Posit Software, PBC.
- 772 R Core Team. 2023. R: A language and environment for statistical computing, R Foundation for
773 Statistical Computing.
- 774 Reynolds, C. S. 2006. The Ecology of Phytoplankton, Cambridge University Press.
- 775 Ryan, J. A., J. M. Ulrich, R. Bennett, and C. Joy. 2024. Xts: eXtensible Time Series.
- 776 Sakamoto, T., and D. A. Bryant. 1999. Nitrate transport and not photoinhibition limits growth of
777 the freshwater cyanobacterium *Synechococcus* species PCC 6301 at low temperature. Plant
778 Physiology **119**: 785–794. doi:10.1104/pp.119.2.785
- 779 Schuurmans, R. M., J. C. P. Matthijs, and K. J. Hellingwerf. 2017. Transition from exponential
780 to linear photoautotrophic growth changes the physiology of *Synechocystis* sp. PCC 6803.
781 Photosynthesis Research **132**: 69–82. doi:10.1007/s11120-016-0329-8
- 782 Serway, R. A., C. J. Moses, and C. A. Moyer. 2004. Modern Physics, Cengage Learning.
- 783 Six, C., Z. V. Finkel, A. J. Irwin, and D. A. Campbell. 2007. Light variability illuminates niche-
784 partitioning among marine picocyanobacteria. PLOS ONE **2**: e1341.
785 doi:10.1371/journal.pone.0001341

- 786 Six, C., M. Ratin, D. Marie, and E. Corre. 2021. Marine *Synechococcus* picocyanobacteria: Light
787 utilization across latitudes. Proceedings of the National Academy of Sciences **118**: e2111300118.
788 doi:10.1073/pnas.2111300118
- 789 Śliwińska-Wilczewska, S., A. Cieszyńska, J. Maculewicz, and A. Latała. 2018a.
790 Ecophysiological characteristics of red, green, and brown strains of the Baltic
791 picocyanobacterium *Synechococcus* sp. – a laboratory study. Biogeosciences **15**: 6257–6276.
792 doi:10.5194/bg-15-6257-2018
- 793 Śliwińska-Wilczewska, S., Z. Konarzewska, K. Wiśniewska, and M. Konik. 2020.
794 Photosynthetic pigments changes of three phenotypes of picocyanobacteria *Synechococcus* sp.
795 Under different light and temperature conditions. Cells **9**: 2030. doi:10.3390/cells9092030
- 796 Śliwińska-Wilczewska, S., J. Maculewicz, A. Barreiro Felpeto, and A. Latała. 2018b.
797 Allelopathic and bloom-forming picocyanobacteria in a changing world. Toxins **10**: 48.
798 doi:10.3390/toxins10010048
- 799 Stadnichuk, I. N., P. M. Krasilnikov, and D. V. Zlenko. 2015. Cyanobacterial phycobilisomes
800 and phycobiliproteins. Microbiology **84**: 101–111. doi:10.1134/S0026261715020150
- 801 Stomp, M., J. Huisman, L. Vörös, F. R. Pick, M. Laamanen, T. Haverkamp, and L. J. Stal. 2007.
802 Colourful coexistence of red and green picocyanobacteria in lakes and seas. Ecology Letters **10**:
803 290–298. doi:10.1111/j.1461-0248.2007.01026.x
- 804 Strickland, J. D., and T. R. Parsons. 1972. Practical Hand Book of Seawater Analysis. Fisheries
805 Research Board of Canada **167 (2nd edition)**: 1–311. doi:DOI: <http://dx.doi.org/10.25607/OBP-1791>

- 807 Theus, M. E., T. J. Layden, N. McWilliams, S. Crafton-Tempel, C. T. Kremer, and S. B. Fey.
808 2022. Photoperiod influences the shape and scaling of freshwater phytoplankton responses to
809 light and temperature. *Oikos* **2022**: e08839. doi:10.1111/oik.08839
- 810 Torremorell, A., M. E. Llames, G. L. Pérez, R. Escaray, J. Bustingorry, and H. Zagarese. 2009.
811 Annual patterns of phytoplankton density and primary production in a large, shallow lake: The
812 central role of light. *Freshwater Biology* **54**: 437–449. doi:10.1111/j.1365-2427.2008.02119.x
- 813 Tortell, P., and D. J. Suggett. 2021. A user guide for the application of Single Turnover active
814 chlorophyll fluorescence for phytoplankton productivity measurements. Version 1. Report
815 Scientific Committee on Oceanic Research (SCOR) Working Group 156.
- 816 van Alphen, P., H. Abedini Najafabadi, F. Branco dos Santos, and K. J. Hellingwerf. 2018.
817 Increasing the photoautotrophic growth rate of *Synechocystis* sp. PCC 6803 by identifying the
818 limitations of its cultivation. *Biotechnology Journal* **13**: 1700764. doi:10.1002/biot.201700764
- 819 Velichko, N., S. Smirnova, S. Averina, and A. Pinevich. 2021. A survey of Antarctic
820 cyanobacteria. *Hydrobiologia* **848**: 2627–2653.
- 821 Vincent, W. F., J. P. Bowman, L. M. Rankin, and T. A. McMeekin. 2000. Phylogenetic diversity
822 of picocyanobacteria in Arctic and Antarctic ecosystems. *Microbial biosystems: new frontiers.*
823 Proceedings of the 8th International Symposium on Microbial Ecology 317–322.
- 824 Vörös, L., C. Callieri, K. V.-Balogh, and R. Bertoni. 1998. Freshwater picocyanobacteria along a
825 trophic gradient and light quality range. *Phytoplankton and Trophic Gradients*. Springer
826 Netherlands. 117–125.

- 827 Weissman, J. C., M. Likhogrud, D. C. Thomas, W. Fang, D. A. J. Karns, J. W. Chung, R.
828 Nielsen, and M. C. Posewitz. 2018. High-light selection produces a fast-growing *Picochlorum*
829 *Celeri*. Algal Research **36**: 17–28. doi:10.1016/j.algal.2018.09.024
- 830 Wickham, H. 2016. Data Analysis, p. 189–201. In H. Wickham [ed.], Ggplot2: Elegant Graphics
831 for Data Analysis. Springer International Publishing.
- 832 Wood, S. N. 2017. Generalized Additive Models: An Introduction with R, Second Edition, 2nd
833 ed. Chapman and Hall/CRC.
- 834 Xi, H., S. N. Losa, A. Mangin, and others. 2020. Global retrieval of phytoplankton functional
835 types based on empirical orthogonal functions using CMEMS GlobColour merged products and
836 further extension to OLCI data. Remote Sensing of Environment **240**: 111704.
837 doi:10.1016/j.rse.2020.111704
- 838 Xu, K., J. L. Grant-Burt, N. Donaher, and D. A. Campbell. 2017. Connectivity among
839 Photosystem II centers in phytoplankters: Patterns and responses. Biochimica et Biophysica Acta
840 (BBA) - Bioenergetics **1858**: 459–474. doi:10.1016/j.bbabi.2017.03.003
- 841 Xu, K., J. Lavaud, R. Perkins, E. Austen, M. Bonnanfant, and D. A. Campbell. 2018.
842 Phytoplankton σ PSII and excitation dissipation; implications for estimates of primary
843 productivity. Frontiers in Marine Science **5**. doi:10.3389/fmars.2018.00281

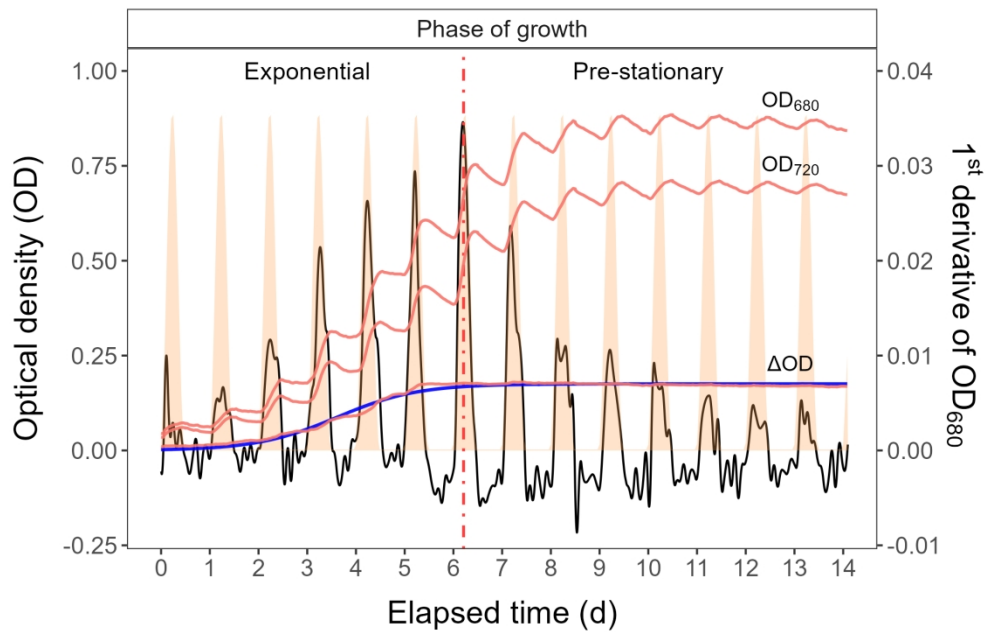


Fig. 1. Example of a growth curve (tracked as OD720, OD680, or Δ OD; red solid lines, left y-axis) of PE-rich culture of *Synechococcus* sp. (048; grown at 180 peak PAR $\mu\text{mol photons m}^{-2}\text{s}^{-1}$; and photoperiods of 12 h) vs. elapsed time (d, x-axis). 1st derivative of OD680 taken over 1 h increments (black solid line, right y-axis); solid blue line shows logistic fits of chlorophyll proxy $\text{OD}_{680} - \text{OD}_{720}$ (Δ OD) vs. elapsed time. The vertical red dot dash line represents the time when the culture reached the maximum of the 1st derivative of OD680, or maximum absolute hourly growth (tMaxAHG), taken as the time of transition from exponential to pre-stationary growth phases.

452x290mm (118 x 118 DPI)

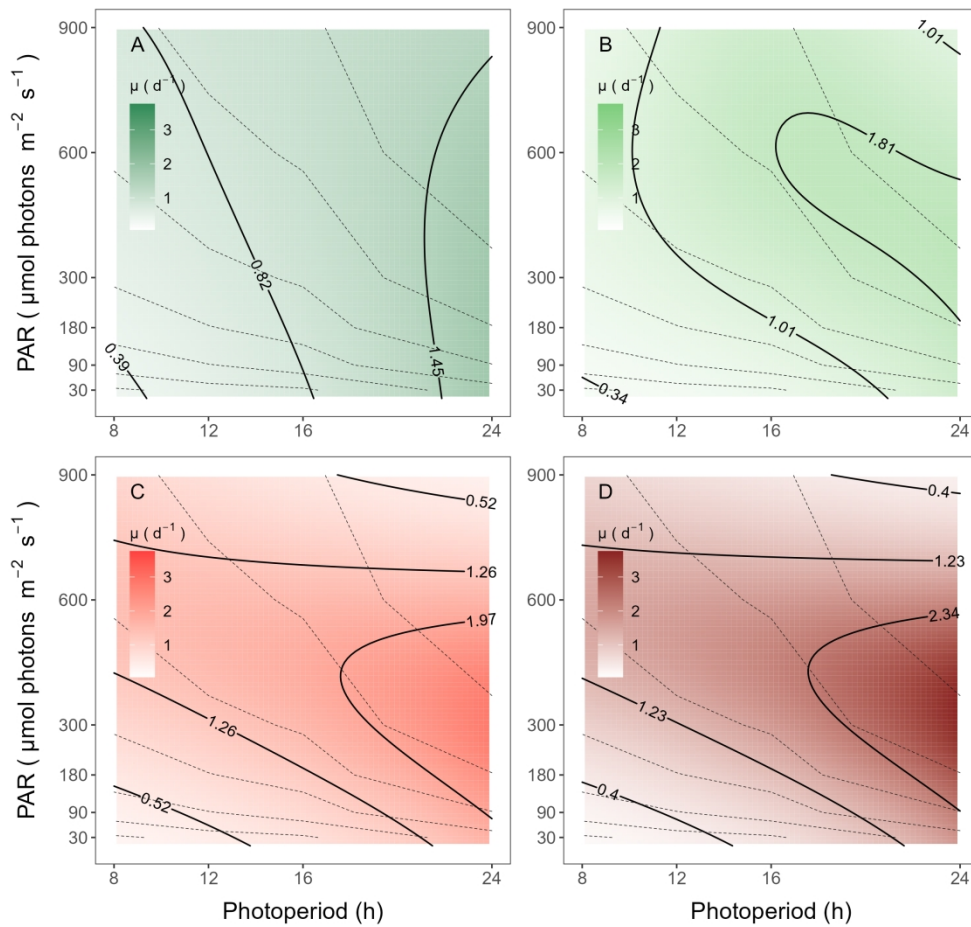


Fig. 4. A contour plot of a Generalized Additive Model (GAM) of chlorophyll-specific growth rates (d^{-1}) for two PC-rich cultures: (A) 056, (B) 077 and two PE-rich cultures: (C) 048, (D) 127 of *Synechococcus* sp. grown at 30, 90, 180, 300, 600, or 900 peak PAR $\mu\text{mol photons m}^{-2}\text{s}^{-1}$; and photoperiods of 8, 12, 16, or 24 h. Legends show colour gradients of growth rate ($\mu; d^{-1}$) from no growth (white) to 3.0 d^{-1} (dark green for PC-rich_056, light green for PC-rich_077, light red for PE-rich_048 or dark red for PE-rich_127 strains). Labeled contour lines indicate the 90%, 50%, and 10% quantiles for achieved growth rate. Dotted lines show isoclines of cumulative diel photon dose ($\mu\text{mol photons m}^{-2}\text{d}^{-1}$).

613x581mm (118 x 118 DPI)

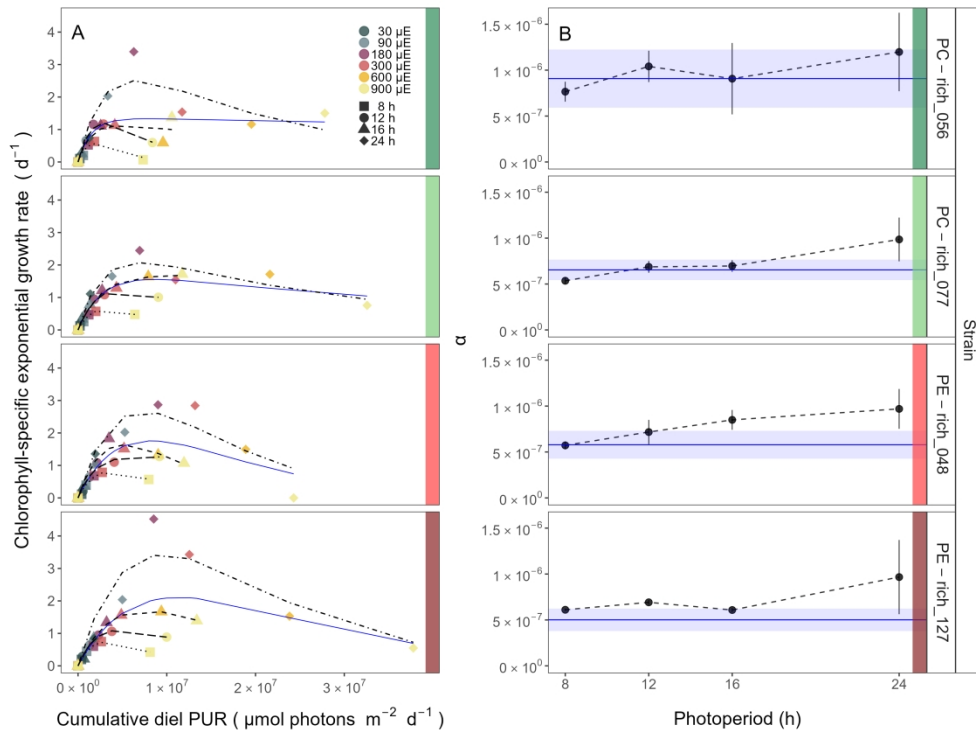


Fig. 5. (A) Chlorophyll-specific exponential growth rates (d^{-1}) vs. cumulative diel Photosynthetically Usable Radiation (PUR, $\mu\text{mol photons m}^{-2} \text{d}^{-1}$). Growth rates (\pm SE falling within symbols) were estimated from logistic fits of chlorophyll proxy OD₆₈₀ – OD₇₂₀ (Δ O_D) vs. elapsed time (Fig. 1, Fig. S3B), for two PC-rich cultures (056; dark green, 077; light green) and two PE-rich cultures (048; light red, 127; dark red) of *Synechococcus* sp. grown at 30 (dark gray), 90 (light gray), 180 (purple), 300 (red), 600 (orange), or 900 (yellow) peak PAR $\mu\text{mol photons m}^{-2}\text{s}^{-1}$ (μE); and photoperiods of 8 (square), 12 (circle), 16 (triangle), or 24 (diamond) h. Solid blue line shows a fit of the pooled growth rates through photoperiods for each strain, with a three parameter model (Harrison and Platt 1986). We also fit the same model separately for 8 (dotted line), 12 (long dash line), 16 (dashed line), or 24 (two dash line) h photoperiods, since for all strains they were each significantly different (ANOVA, $p < 0.05$) from the fit of pooled data. (B) Alpha parameters of the initial rise of growth rate (α) vs. cumulative diel Photosynthetically Usable Radiation (PUR), estimated from data pooled for each photoperiod (points (\pm SE) connected by dashed lines), and estimated for all data across photoperiods (solid blue horizontal line \pm SE), for each strain.

774x581mm (118 x 118 DPI)

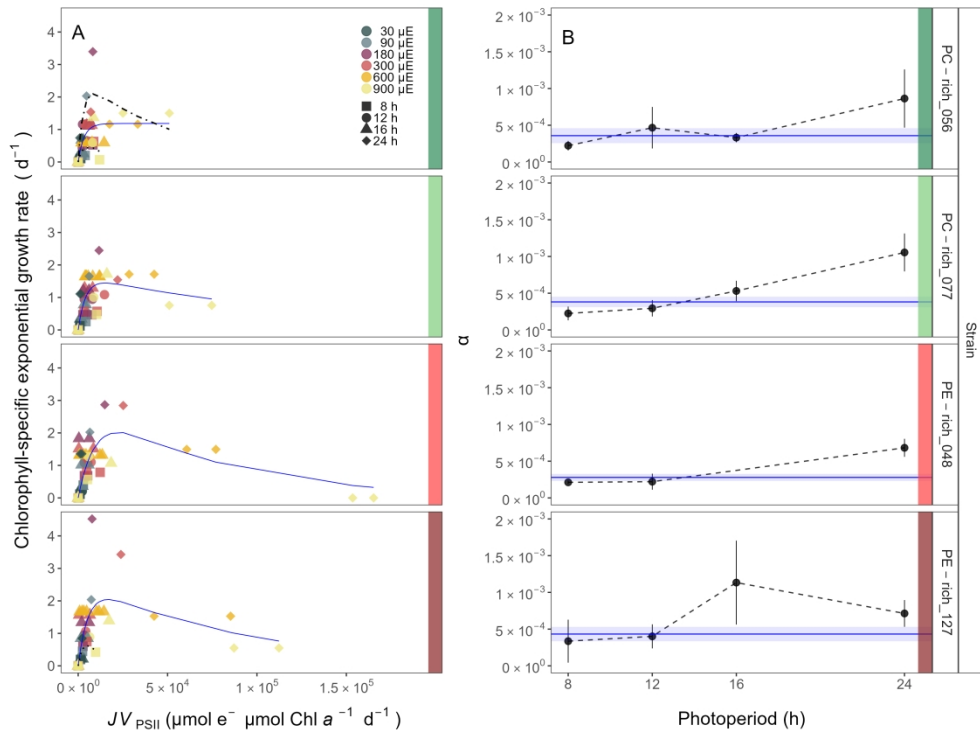


Fig. 8. (A) Chlorophyll-specific exponential growth rates (d^{-1}) vs. cumulative diel PSII electron flux (JV_{PSII} ; $\mu\text{mol e}^- \mu\text{mol Chl } a^{-1} d^{-1}$) measured under diel peak PAR growth light. Growth rates (\pm SE falling within symbols) were estimated from logistic fits of chlorophyll proxy OD₆₈₀ - OD₇₂₀ (Δ OD) vs. elapsed time (Fig. S3B). JV_{PSII} was estimated using FRRF induction curves with excitation of chlorophyll (Ex445nm, blue), for two PC-rich cultures (056; dark green, 077; light green) and two PE-rich cultures (048; light red, 127; dark red) of *Synechococcus* sp. grown at 30 (dark gray), 90 (light gray), 180 (purple), 300 (red), 600 (orange), or 900 (yellow) peak PAR $\mu\text{mol photons m}^{-2}\text{s}^{-1}$ (μE); and photoperiods of 8 (square), 12 (circle), 16 (triangle), or 24 (diamond) h. Solid blue line shows a fit of the pooled growth rates for each strain, with a three parameter model (Harrison and Platt 1986). We also fit the same model separately for 8 (dotted line) and 24 (two dash line) h photoperiods, when they were significantly different (ANOVA, $p < 0.05$) from the fit of pooled data. (B) Alpha parameters of the initial rise of growth rate (α) vs. cumulative diel JV_{PSII} , estimated from data pooled for each photoperiod (points (\pm SE) connected by dashed lines), and estimated for all data across photoperiods (horizontal line \pm SE), for each strain.

774x581mm (118 x 118 DPI)

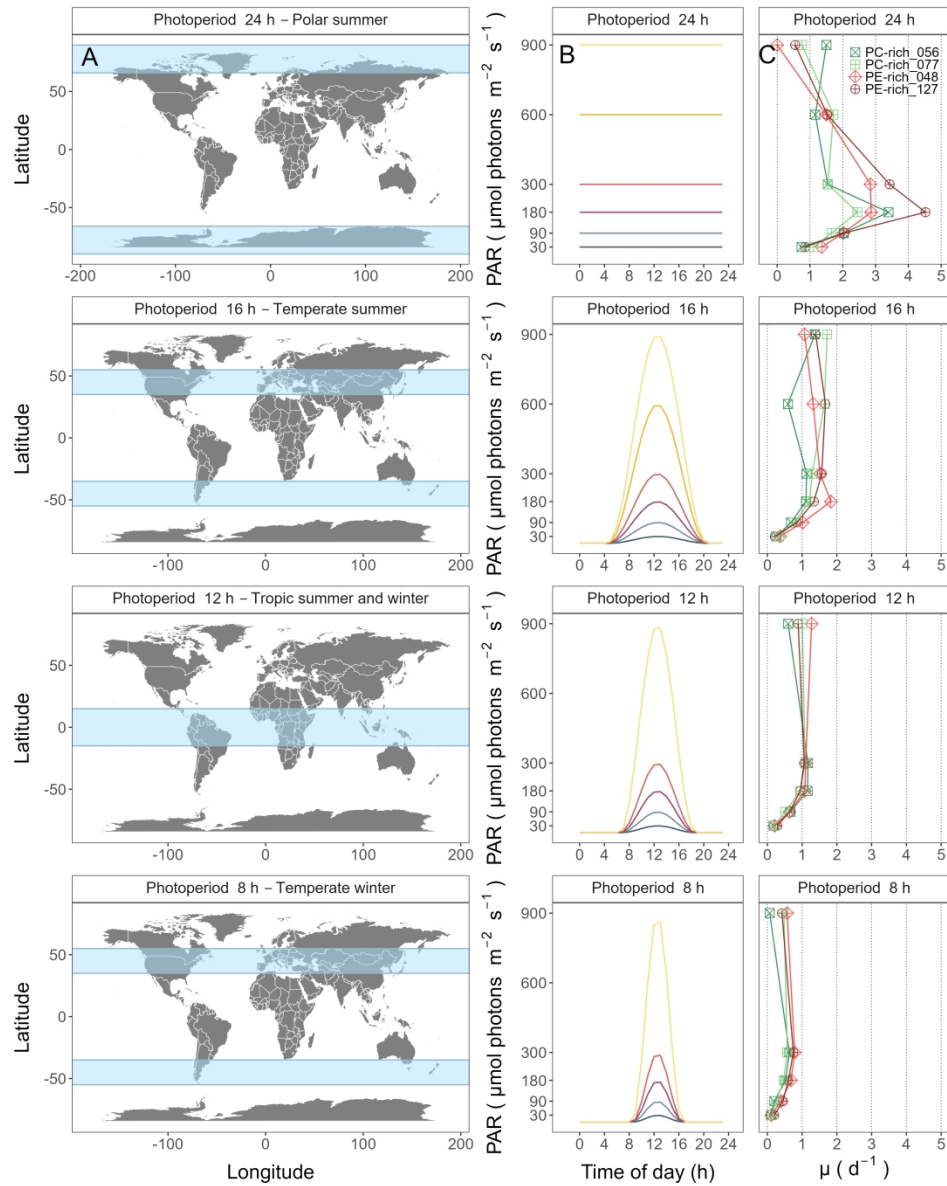


Fig. 9. Latitudinal bands, equivalent summer or winter photoperiods, and picocyanobacterial growth responses. (A) Latitudinal bands corresponding to tested growth photoperiods. (B) Tested photoperiod and peak PAR regimes used for growth experiments. (C) Chlorophyll specific exponential growth rates (\pm SE falling within symbols) for two PhycoCyanin(PC)-rich cultures (056; dark green, 077; light green) and two PhycoErythrin(PE)-rich cultures (048; light red, 127; dark red) of *Synechococcus* sp. under tested photoperiod and peak PAR regimes.

774x968mm (118 x 118 DPI)

1 **Long & low; or high & short; photoperiods and light**
2 **differential growth yields and light-capture capacities of**
3 **PhycoCyanin and PhycoErythrin-rich picocyanobacteria**

4

5 **Sylwia Śliwińska-Wilczewska^{1,2}, Marta Konik^{3,4}, Mireille Savoie¹, Anabella**
6 **Aguilera^{5,6}, Naaman M. Omar¹, and Douglas A. Campbell^{1,✉}**

7 ¹ Department of Biology, Mount Allison University, 53 York St., Sackville, NB, E4L 1C9,
8 Canada

9 ² Institute of Oceanography, University of Gdańsk, 46 Piłsudskiego St, 81-378, Gdynia, Poland

10 ³ Department of Geography, University of Victoria, Victoria, BC, V8P 5C2, Canada

11 ⁴ Institute of Oceanology, Polish Academy of Sciences, 81-712 Sopot, Poland

12 ⁵ Department of Biology and Environmental Science, Centre for Ecology and Evolution in
13 Microbial Model Systems (EEMiS), Linnaeus University, Kalmar, Sweden

14 ⁶ Department of Aquatic Sciences and Assessment, Swedish University of Agricultural Sciences,
15 Uppsala, Sweden (present address)

16 ✉ Correspondence: Douglas A. Campbell <dubhglascambeuil@gmail.com>

17

18

19 ***Supporting Information***

20

21 **Tab.1.** Linear regression, coefficient of determination (R square), Pearson correlation coefficients (R), and *p*-value
 22 used to calculate the pigment content ($\mu\text{g mL}^{-1}$) of two PhycoCyanin(PC)-rich cultures (056, 077) and two
 23 PhycoErythrin(PE)-rich cultures (048, 127) (Culture Collection of Baltic Algae) of *Synechococcus* sp. based on
 24 absorbance (A) measurements.

Pigment	Abs	Linear_regression	R_square	R	<i>p</i> _value
Chl <i>a</i>	665	Chla $\mu\text{g/mL} = (\text{Abs}665*13.411029)+0.154793$	0.865	0.930	0.000
Car	480	Car $\mu\text{g/mL} = (\text{Abs}480*5.469880)+0.089971$	0.791	0.890	0.000
PE	565	PE $\mu\text{g/mL} = (\text{Abs}565*26.760737)-0.143872$	0.698	0.840	0.000
PC	620	PC $\mu\text{g/mL} = (\text{Abs}620*29.979866)-0.182611$	0.807	0.900	0.000
APC	650	APC $\mu\text{g/mL} = (\text{Abs}650*3.873803)+0.021964$	0.087	0.300	0.000

25
 26 **Tab.2.** Three-way factorial ANOVA testing whether peak PAR, photoperiod, strain, and their interactions
 27 (Source_of_variation), significantly influence the chlorophyll specific exponential growth rate ($\mu; \text{d}^{-1}$), estimated
 28 from logistic fits of chlorophyll proxy OD680 – OD720 vs. cumulative diel PUR, for two PhycoCyanin(PC)-rich
 29 cultures (056, 077) and two PhycoErythrin(PE)-rich cultures (048, 127) (Culture Collection of Baltic Algae) of
 30 *Synechococcus* sp., grown at 30, 90, 180, 300, 600, or 900 peak PAR $\mu\text{mol photons m}^{-2}\text{s}^{-1}$; and photoperiods of 8,
 31 12, 16, or 24 h. Df – degrees of freedom; Sum Sq – sum of squares; Mean Sq – mean sum of squares; *F*_value –
 32 Fisher's F-test statistic; *p*_value - level of significance.

Source_of_variation	Df	Sum Sq	Mean Sq	<i>F</i> _value	<i>p</i> _value
Par_ue	5	0.049	0.010	3.276e+30	0.000
Photoperiod	3	0.076	0.025	8.367e+30	0.000
Strain	3	0.003	0.001	3.151e+29	0.000
Par_ue:Photoperiod	13	0.040	0.003	1.025e+30	0.000
Par_ue:Strain	15	0.007	0.000	1.593e+29	0.000
Photoperiod:Strain	9	0.004	0.000	1.306e+29	0.000
Par_ue:Photoperiod:Strain	39	0.017	0.000	1.434e+29	0.000
Residuals	88	0.000	0.000	NA	N/A

34 **Tab.3.** One-way ANOVA of a three parameter model (Harrison and Platt 1986) from pooled data (All) and data fit
 35 across different photoperiods (8, 12, 16, or 24) from chlorophyll specific exponential growth rate vs. cumulative diel
 36 PUR (Fit_model), for two PhycoCyanin(PC)-rich cultures (056, 077) and two PhycoErythrin(PE)-rich cultures (048,
 37 127) of *Synechococcus* sp., grown at 30, 90, 180, 300, 600, or 900 peak PAR $\mu\text{mol photons m}^{-2}\text{s}^{-1}$; and
 38 photoperiods of 8, 12, 16, or 24 h. Res.Df - residual degrees of freedom for each model; Res.Sum Sq - residual sum
 39 of squares for each model; F _value – Fisher's F-test statistic; p _value - level of significance.

Strain	Fit_model	Res.Df	Res.Sum Sq	F _value	p _value
PC-rich_056	8_All	41	8.063	1.807e+03	0.000
PC-rich_056	12_All	41	8.063	2.822e+01	0.001
PC-rich_056	16_All	41	8.063	8.566e+00	0.012
PC-rich_056	24_All	41	8.063	2.333e+01	0.001
PC-rich_077	8_All	41	3.015	6.193e+01	0.000
PC-rich_077	12_All	41	3.015	2.477e+01	0.001
PC-rich_077	16_All	41	3.015	1.855e+01	0.002
PC-rich_077	24_All	41	3.015	1.073e+01	0.007
PE-rich_048	8_All	41	6.731	1.443e+01	0.004
PE-rich_048	12_All	41	6.731	8.361e+01	0.000
PE-rich_048	16_All	41	6.731	8.403e+00	0.013
PE-rich_048	24_All	41	6.731	8.234e+01	0.000
PE-rich_127	8_All	41	13.016	1.453e+02	0.000
PE-rich_127	12_All	41	13.016	2.060e+03	0.000
PE-rich_127	16_All	41	13.016	6.908e+00	0.020
PE-rich_127	24_All	41	13.016	7.812e+01	0.000

40

41

42

43

44

45 **Tab.4.** One-way ANOVA of a three parameter model (Harrison and Platt 1986) from pooled data (All) and data fit
 46 across different peak PAR (30, 90, 180, 300, 600 together with 900) from chlorophyll specific exponential growth
 47 rate vs. cumulative diel PUR (Fit_model), for two PhycoCyanin(PC)-rich cultures (056, 077) and two
 48 PhycoErythrin(PE)-rich cultures (048, 127) of *Synechococcus* sp., grown at 30, 90, 180, 300, 600, or 900 peak PAR
 49 $\mu\text{mol photons m}^{-2}\text{s}^{-1}$; and photoperiods of 8, 12, 16, or 24 h. Res.Df - residual degrees of freedom for each model;
 50 Res.Sum Sq - residual sum of squares for each model; F_{value} – Fisher's F-test statistic; p_{value} - level of
 51 significance.

Strain	Fit_model	Res.Df	Res.Sum Sq	F_{value}	p_{value}
PC-rich_056	30_All	41	8.063	1.807e+03	0.000
PC-rich_056	90_All	41	8.063	2.822e+01	0.001
PC-rich_056	180_All	41	8.063	8.566e+00	0.012
PC-rich_056	300_All	41	8.063	2.333e+01	0.001
PC-rich_056	900_All	41	8.063	3.360e+00	0.030
PC-rich_077	30_All	41	3.015	6.193e+01	0.000
PC-rich_077	90_All	41	3.015	2.477e+01	0.001
PC-rich_077	180_All	41	3.015	1.855e+01	0.002
PC-rich_077	300_All	41	3.015	1.073e+01	0.007
PC-rich_077	900_All	41	3.015	6.508e-01	0.822
PE-rich_048	30_All	41	6.731	1.443e+01	0.004
PE-rich_048	90_All	41	6.731	8.361e+01	0.000
PE-rich_048	180_All	41	6.731	8.403e+00	0.013
PE-rich_048	300_All	41	6.731	8.234e+01	0.000
PE-rich_048	900_All	41	6.731	1.357e+00	0.328
PE-rich_127	30_All	41	13.016	1.453e+02	0.000
PE-rich_127	90_All	41	13.016	2.060e+03	0.000
PE-rich_127	180_All	41	13.016	6.908e+00	0.020
PE-rich_127	300_All	41	13.016	7.812e+01	0.000
PE-rich_127	900_All	41	13.016	3.523e+00	0.026

53 **Tab.5.** One-way ANOVA of a three parameter model (Harrison and Platt 1986) from pooled data (All) and data fit
 54 across different photoperiods (8, 12, 16, or 24) from chlorophyll specific exponential growth rate vs. cumulative diel
 55 PAR (Fit_model), for two PhycoCyanin(PC)-rich cultures (056, 077) and two PhycoErythrin(PE)-rich cultures (048,
 56 127) of *Synechococcus* sp., grown at 30, 90, 180, 300, 600, or 900 peak PAR $\mu\text{mol photons m}^{-2}\text{s}^{-1}$; and
 57 photoperiods of 8, 12, 16, or 24 h. Res.Df - residual degrees of freedom for each model; Res.Sum Sq - residual sum
 58 of squares for each model; F _value – Fisher's F-test statistic; p _value - level of significance.

Strain	Fit_model	Res.Df	Res.Sum Sq	F _value	p _value
PC-rich_056	8_All	135	18.854	1.089e+03	0.000
PC-rich_056	12_All	135	18.854	1.412e+01	0.000
PC-rich_056	16_All	135	18.854	7.420e+00	0.000
PC-rich_056	24_All	135	18.854	1.279e+01	0.000
PC-rich_077	8_All	131	5.672	2.749e+01	0.000
PC-rich_077	12_All	131	5.672	8.972e+00	0.000
PC-rich_077	16_All	131	5.672	5.640e+00	0.000
PC-rich_077	24_All	131	5.672	4.027e+00	0.000
PE-rich_048	8_All	133	16.660	2.122e+01	0.000
PE-rich_048	12_All	133	16.660	1.997e+01	0.000
PE-rich_048	16_All	133	16.660	3.576e+00	0.000
PE-rich_048	24_All	133	16.660	8.068e+01	0.000
PE-rich_127	8_All	133	26.508	6.568e+01	0.000
PE-rich_127	12_All	133	26.508	6.758e+03	0.000
PE-rich_127	16_All	133	26.508	1.515e+01	0.000
PE-rich_127	24_All	133	26.508	5.207e+01	0.000

59

60

61

62

63

64

65 **Tab.6.** One-way ANOVA of a three parameter model (Harrison and Platt 1986) from pooled data (All) and data fit
 66 across different peak PAR (30, 90, 180, 300, 600 together with 900) from chlorophyll specific exponential growth
 67 rate vs. cumulative diel PAR (Fit_model), for two PhycoCyanin(PC)-rich cultures (056, 077) and two
 68 PhycoErythrin(PE)-rich cultures (048, 127) of *Synechococcus* sp., grown at 30, 90, 180, 300, 600, or 900 peak PAR
 69 $\mu\text{mol photons m}^{-2}\text{s}^{-1}$; and photoperiods of 8, 12, 16, or 24 h. Res.Df - residual degrees of freedom for each model;
 70 Res.Sum Sq - residual sum of squares for each model; F_value – Fisher's F-test statistic; p_value - level of
 71 significance.

Strain	Fit_model	Res.Df	Res.Sum Sq	F_value	p_value
PC-rich_056	30_All	135	18.854	1.089e+03	0.000
PC-rich_056	90_All	135	18.854	1.412e+01	0.000
PC-rich_056	180_All	135	18.854	7.420e+00	0.000
PC-rich_056	300_All	135	18.854	1.279e+01	0.000
PC-rich_056	900_All	135	18.854	2.573e+00	0.003
PC-rich_077	30_All	131	5.672	2.749e+01	0.000
PC-rich_077	90_All	131	5.672	8.972e+00	0.000
PC-rich_077	180_All	131	5.672	5.640e+00	0.000
PC-rich_077	300_All	131	5.672	4.027e+00	0.000
PC-rich_077	900_All	131	5.672	7.428e-01	0.844
PE-rich_048	30_All	133	16.660	2.122e+01	0.000
PE-rich_048	90_All	133	16.660	1.997e+01	0.000
PE-rich_048	180_All	133	16.660	3.576e+00	0.000
PE-rich_048	300_All	133	16.660	8.068e+01	0.000
PE-rich_048	900_All	133	16.660	1.893e+00	0.034
PE-rich_127	30_All	133	26.508	6.568e+01	0.000
PE-rich_127	90_All	133	26.508	6.758e+03	0.000
PE-rich_127	180_All	133	26.508	1.515e+01	0.000
PE-rich_127	300_All	133	26.508	5.207e+01	0.000
PE-rich_127	900_All	133	26.508	2.800e+00	0.002

73 **Tab.7.** One-way ANOVA of a three parameter model (Harrison and Platt 1986) from pooled data (All) and data fit
 74 across different photoperiods (8, 12, 16, or 24) from chlorophyll specific exponential growth rate vs. PSII electron
 75 flux (JVPSII; $\mu\text{mol e} - \mu\text{mol Chl a}^{-1} \text{d}^{-1}$) (Fit_model), for two PhycoCyanin(PC)-rich cultures (056, 077) and two
 76 PhycoErythrin(PE)-rich cultures (048, 127) of *Synechococcus* sp., grown at 30, 90, 180, 300, 600, or 900 peak PAR
 77 $\mu\text{mol photons m}^{-2}\text{s}^{-1}$; and photoperiods of 8, 12, 16, or 24 h. Res.Df - residual degrees of freedom for each model;
 78 Res.Sum Sq - residual sum of squares for each model; F_{value} – Fisher's F-test statistic; p_{value} - level of
 79 significance.

Strain	Fit_model	Res.Df	Res.Sum Sq	F_{value}	p_{value}
PC-rich_056	8_All	61	11.802	3.972e+00	0.016
PC-rich_056	12_All	61	11.802	7.712e-01	0.730
PC-rich_056	16_All	61	11.802	2.287e-01	1.000
PC-rich_056	24_All	61	11.802	3.332e+00	0.037
PC-rich_077	8_All	61	9.014	1.125e+00	0.459
PC-rich_077	12_All	61	9.014	1.377e+00	0.350
PC-rich_077	16_All	61	9.014	6.146e-01	0.861
PC-rich_077	24_All	61	9.014	1.562e+00	0.260
PE-rich_048	8_All	61	16.583	1.332e+00	0.339
PE-rich_048	12_All	61	16.583	1.977e+00	0.174
PE-rich_048	16_All	61	16.583	5.540e-01	0.903
PE-rich_048	24_All	61	16.583	6.716e-01	0.817
PE-rich_127	8_All	53	21.117	7.994e+00	0.004
PE-rich_127	12_All	53	21.117	4.159e+00	0.057
PE-rich_127	16_All	53	21.117	5.525e-01	0.882
PE-rich_127	24_All	53	21.117	1.100e+00	0.504

80

81

82

83

84

85 **Tab.8.** One-way ANOVA of a three parameter model (Harrison and Platt 1986) from pooled data (All) and data fit
 86 across different peak PAR (30, 90, 180, 300, 600 together with 900) from chlorophyll specific exponential growth
 87 rate vs. PSII electron flux (JVPSII; $\mu\text{mol e}^- \mu\text{mol Chl a}^{-1} \text{d}^{-1}$) (Fit_model), for two PhycoCyanin(PC)-rich cultures
 88 (056, 077) and two PhycoErythrin(PE)-rich cultures (048, 127) of *Synechococcus* sp., grown at 30, 90, 180, 300,
 89 600, or 900 peak PAR $\mu\text{mol photons m}^{-2}\text{s}^{-1}$; and photoperiods of 8, 12, 16, or 24 h. Res.Df - residual degrees of
 90 freedom for each model; Res.Sum Sq - residual sum of squares for each model; F_{value} – Fisher's F-test statistic;
 91 p_{value} - level of significance.

Strain	Fit_model	Res.Df	Res.Sum Sq	F_{value}	p_{value}
PC-rich_056	30_All	61	11.802	3.972e+00	0.016
PC-rich_056	90_All	61	11.802	7.712e-01	0.730
PC-rich_056	180_All	61	11.802	2.287e-01	1.000
PC-rich_056	300_All	61	11.802	3.332e+00	0.037
PC-rich_056	900_All	61	11.802	2.156e+00	0.044
PC-rich_077	30_All	61	9.014	1.125e+00	0.459
PC-rich_077	90_All	61	9.014	1.377e+00	0.350
PC-rich_077	180_All	61	9.014	6.146e-01	0.861
PC-rich_077	300_All	61	9.014	1.562e+00	0.260
PC-rich_077	900_All	61	9.014	1.295e+00	0.287
PE-rich_048	30_All	61	16.583	1.332e+00	0.339
PE-rich_048	90_All	61	16.583	1.977e+00	0.174
PE-rich_048	180_All	61	16.583	5.540e-01	0.903
PE-rich_048	300_All	61	16.583	6.716e-01	0.817
PE-rich_048	900_All	61	16.583	3.125e+00	0.007
PE-rich_127	30_All	53	21.117	7.994e+00	0.004
PE-rich_127	90_All	53	21.117	4.159e+00	0.057
PE-rich_127	180_All	53	21.117	5.525e-01	0.882
PE-rich_127	300_All	53	21.117	1.100e+00	0.504
PE-rich_127	900_All	53	21.117	3.784e+00	0.002

93 **Tab.9.** One-way ANOVA of single phase exponential decay fit model (Fit_model) of pooled data across different
 94 strains for a given phase of growth (exponential; _Exp, pre-stationary; _St) and across different phase of growth for
 95 a given strain (_Exp_St) from PUR/PAR ratio in relation to the cumulative diel PAR ($\mu\text{mol photons m}^{-2}\text{d}^{-1}$), for two
 96 PhycoCyanin(PC)-rich cultures (056, 077) and two PhycoErythrin(PE)-rich cultures (048, 127) of *Synechococcus*
 97 sp., grown at 30, 90, 180, 300, 600, or 900 peak PAR $\mu\text{mol photons m}^{-2}\text{s}^{-1}$; and photoperiods of 8, 12, 16, or 24 h.
 98 Res.Df - residual degrees of freedom for each model; Res.Sum Sq - residual sum of squares for each model; F_value
 99 – Fisher's F-test statistic; p_value - level of significance.

Fit_model	Res.Df	Res.Sum Sq	F_value	p_value
056_077_Exp	43	0.025	2.813e+01	0.000
048_127_Exp	51	0.217	NA	N/A
056_048_Exp	51	0.307	2.762e+01	0.000
077_048_Exp	51	0.307	5.976e+01	0.000
056_127_Exp	51	0.217	1.607e+01	0.000
077_127_Exp	51	0.217	4.064e+01	0.000
056_077_St	20	0.006	-1.491e-01	1.000
048_127_St	2	0.000	5.386e+00	0.168
056_048_St	17	0.009	9.648e-02	0.999
077_048_St	17	0.009	-2.066e+00	1.000
056_127_St	2	0.000	1.415e+01	0.067
077_127_St	2	0.000	2.812e+00	0.294
056_Exp_St	7	0.008	1.882e+00	0.195
077_Exp_St	20	0.006	3.039e+00	0.007
048_Exp_St	17	0.009	1.681e+01	0.000
127_Exp_St	2	0.000	4.128e+01	0.024

100

101

102

103

104

105 **Tab.10.** One-way ANOVA of single phase exponential decay fit model (Fit_model) of pooled data across different
 106 strains for a given phase of growth (exponential; _Exp, pre-stationary; _St) and across different phase of growth for
 107 a given strain (_Exp_St) from Phycobiliprotein to Chl *a* ratio in relation to the cumulative diel PAR ($\mu\text{mol photons}$
 108 $\text{m}^{-2}\text{d}^{-1}$), for two PhycoCyanin(PC)-rich cultures (056, 077) and two PhycoErythrin(PE)-rich cultures (048, 127) of
 109 *Synechococcus* sp., grown at 30, 90, 180, 300, 600, or 900 peak PAR $\mu\text{mol photons m}^{-2}\text{s}^{-1}$; and photoperiods of 8,
 110 12, 16, or 24 h. Res.Df - residual degrees of freedom for each model; Res.Sum Sq - residual sum of squares for each
 111 model; *F*_value – Fisher's F-test statistic; *p*_value - level of significance.

Fit_model	Res.Df	Res.Sum Sq	<i>F</i> _value	<i>p</i> _value
056_077_Exp	49	38.089	1.531e+01	0.000
048_127_Exp	52	54.559	NA	N/A
056_048_Exp	52	39.302	4.333e+00	0.005
077_048_Exp	52	39.302	5.202e-01	0.670
056_127_Exp	52	54.559	1.067e+01	0.000
077_127_Exp	52	54.559	7.063e+00	0.000
056_077_St	24	3.580	-1.005e+01	1.000
048_127_St	19	3.343	NA	N/A
056_048_St	19	2.239	-2.229e-01	1.000
077_048_St	19	2.239	2.276e+00	0.088
056_127_St	19	3.343	-1.195e+00	1.000
077_127_St	19	3.343	2.686e-01	0.925
056_Exp_St	25	2.081	1.399e+01	0.000
077_Exp_St	24	3.580	9.255e+00	0.000
048_Exp_St	19	2.239	9.531e+00	0.000
127_Exp_St	19	3.343	8.820e+00	0.000

112

113

114

115

116

117 **Tab.11.** One-way ANOVA of single phase exponential decay fit model (Fit_model) of pooled data across different
 118 strains for a given phase of growth (exponential; _Exp, pre-stationary; _St) and across different phase of growth for
 119 a given strain (_Exp_St) from effective absorption cross section of PSII (σ_{PSII} ; nm² quanta⁻¹) measured under diel
 120 peak PAR growth light under Ex_{590nm} (orange) excitation in relation to the cumulative diel PAR ($\mu\text{mol photons}$
 121 m⁻²d⁻¹), for two PhycoCyanin(PC)-rich cultures (056, 077) and two PhycoErythrin(PE)-rich cultures (048, 127) of
 122 *Synechococcus* sp., grown at 30, 90, 180, 300, 600, or 900 peak PAR $\mu\text{mol photons m}^{-2}\text{s}^{-1}$; and photoperiods of 8,
 123 12, 16, or 24 h. Res.Df - residual degrees of freedom for each model; Res.Sum Sq - residual sum of squares for each
 124 model; F_value – Fisher's F-test statistic; p_value - level of significance.

Fit_model	Res.Df	Res.Sum Sq	F_value	p_value
056_077_Exp	97	116.359	9.926e-01	0.469
048_127_Exp	72	106.728	-1.652e+00	1.000
056_048_Exp	97	116.359	3.764e+01	0.000
077_048_Exp	112	134.219	8.037e+00	0.000
056_127_Exp	72	106.728	2.599e-01	1.000
077_127_Exp	72	106.728	4.636e-01	0.995
056_077_St	41	3.366	1.522e+01	0.000
048_127_St	45	38.775	3.762e+00	0.001
056_048_St	34	17.489	1.158e+02	0.000
077_048_St	34	17.489	-3.922e+00	1.000
056_127_St	45	38.775	1.566e+02	0.000
077_127_St	45	38.775	1.078e+02	0.000
056_Exp_St	17	0.150	1.650e+02	0.000
077_Exp_St	41	3.366	2.245e+01	0.000
048_Exp_St	34	17.489	1.146e+00	0.339
127_Exp_St	45	38.775	2.921e+00	0.001

125

126

127

128

129 **Tab.12.** T-test of linear fit model (Fit_model) of pooled data across different strains for a given phase of growth
 130 (exponential; _Exp, pre-stationary; _St) and across different phase of growth for a given strain (_Exp_St) from
 131 effective absorption cross section of PSII (σ_{PSII} ; nm² quanta⁻¹) measured under diel peak PAR growth light under
 132 Ex445nm (blue) excitation in relation to the cumulative diel PAR ($\mu\text{mol photons m}^{-2}\text{d}^{-1}$, for two PhycoCyanin(PC)-
 133 rich cultures (056, 077) and two PhycoErythrin(PE)-rich cultures (048, 127) of *Synechococcus* sp., grown at 30, 90,
 134 180, 300, 600, or 900 peak PAR $\mu\text{mol photons m}^{-2}\text{s}^{-1}$; and photoperiods of 8, 12, 16, or 24 h. Estimate - estimation
 135 statistics; Std.Error - standard error of the estimate; *t*_value – *t*-test statistic; *p*_value - level of significance.

Fit_model	Estimate	Std.Error	<i>t</i> _value	<i>p</i> _value
056_077_Exp	-1.451e-09	1.058e-09	-1.372	0.171
056_048_Exp	-2.188e-09	1.313e-09	-1.666	0.097
056_127_Exp	-8.236e-10	1.412e-09	-0.583	0.560
048_127_Exp	1.365e-09	1.603e-09	0.851	0.395
077_048_Exp	-7.373e-10	1.233e-09	-0.598	0.550
077_127_Exp	6.274e-10	1.336e-09	0.470	0.639
056_077_St	2.453e-09	1.349e-09	1.818	0.071
056_048_St	5.254e-09	2.098e-09	2.505	0.014
056_127_St	1.745e-09	1.862e-09	0.937	0.350
048_127_St	-3.509e-09	1.658e-09	-2.116	0.036
077_048_St	2.801e-09	1.263e-09	2.217	0.028
077_127_St	-7.077e-10	1.209e-09	-0.586	0.559
056_Exp_St	2.487e-09	1.643e-09	1.514	0.132
077_Exp_St	6.391e-09	9.166e-10	6.973	0.000
048_Exp_St	9.930e-09	1.695e-09	5.860	0.000
127_Exp_St	5.056e-09	1.621e-09	3.120	0.002

136

137

138

139

140

141 **Tab.13.** T-test of linear fit model (Fit_model) of pooled data across different strains for a given phase of growth
 142 (exponential; _Exp, pre-stationary; _St) and across different phase of growth for a given strain (_Exp_St) from
 143 effective absorption cross section of PSII (σ_{PSII} ; $\text{nm}^2 \text{ quanta}^{-1}$) measured under diel peak PAR growth light under
 144 Ex_{445nm} (blue) excitation in relation to Phycobiliprotein to Chl *a* ratio, for two PhycoCyanin(PC)-rich cultures (056,
 145 077) and two PhycoErythrin(PE)-rich cultures (048, 127) of *Synechococcus* sp., grown at 30, 90, 180, 300, 600, or
 146 900 peak PAR $\mu\text{mol photons m}^{-2}\text{s}^{-1}$; and photoperiods of 8, 12, 16, or 24 h. Estimate - estimation statistics;
 147 Std.Error - standard error of the estimate; t_value - *t*-test statistic; p_value - level of significance.

Fit_model	Estimate	Std.Error	t_value	p_value
056_077_Exp	0.003	0.008	0.424	0.672
056_048_Exp	0.078	0.009	9.082	0.000
056_127_Exp	0.039	0.009	4.382	0.000
048_127_Exp	-0.039	0.009	-4.416	0.000
077_048_Exp	0.075	0.008	8.954	0.000
077_127_Exp	0.036	0.009	4.117	0.000
056_077_St	-0.023	0.007	-3.495	0.000
056_048_St	-0.062	0.016	-3.788	0.000
056_127_St	-0.037	0.014	-2.606	0.009
048_127_St	0.026	0.023	1.143	0.253
077_048_St	-0.039	0.014	-2.823	0.005
077_127_St	-0.013	0.012	-1.117	0.264
056_Exp_St	0.083	0.013	6.327	0.000
077_Exp_St	0.057	0.009	6.590	0.000
048_Exp_St	-0.057	0.018	-3.217	0.001
127_Exp_St	0.008	0.020	0.389	0.698

148

149

150

151

152

153 **Tab.14.** T-test of linear fit model (Fit_model) of pooled data across different strains for a given phase of growth
 154 (exponential; _Exp, pre-stationary; _St) and across different phase of growth for a given strain (_Exp_St) from
 155 effective absorption cross section of PSII (σ_{PSII} ; $\text{nm}^2 \text{ quanta}^{-1}$) measured under $\text{Ex}_{590\text{nm}}$ (orange) excitation in
 156 relation to the Phycobiliprotein to Chl a ratio, for two PhycoCyanin(PC)-rich cultures (056, 077) and two
 157 PhycoErythrin(PE)-rich cultures (048, 127) of *Synechococcus* sp., grown at 30, 90, 180, 300, 600, or 900 peak PAR
 158 $\mu\text{mol photons m}^{-2}\text{s}^{-1}$; and photoperiods of 8, 12, 16, or 24 h. Estimate - estimation statistics; Std.Error - standard
 159 error of the estimate; t_value - t -test statistic; p_value - level of significance.

Fit_model	Estimate	Std.Error	t_value	p_value
056_077_Exp	-0.369	0.092	-4.000	0.000
056_048_Exp	0.149	0.082	1.812	0.070
056_127_Exp	0.606	0.099	6.122	0.000
048_127_Exp	0.457	0.090	5.084	0.000
077_048_Exp	0.518	0.083	6.267	0.000
077_127_Exp	0.976	0.097	10.089	0.000
056_077_St	0.077	0.029	2.669	0.008
056_048_St	-0.610	0.079	-7.751	0.000
056_127_St	-0.299	0.071	-4.191	0.000
048_127_St	0.311	0.177	1.759	0.080
077_048_St	-0.688	0.076	-9.099	0.000
077_127_St	-0.377	0.070	-5.371	0.000
056_Exp_St	0.440	0.117	3.761	0.000
077_Exp_St	0.887	0.091	9.780	0.000
048_Exp_St	-0.319	0.148	-2.164	0.031
127_Exp_St	-0.465	0.247	-1.882	0.060

160

161

162

163

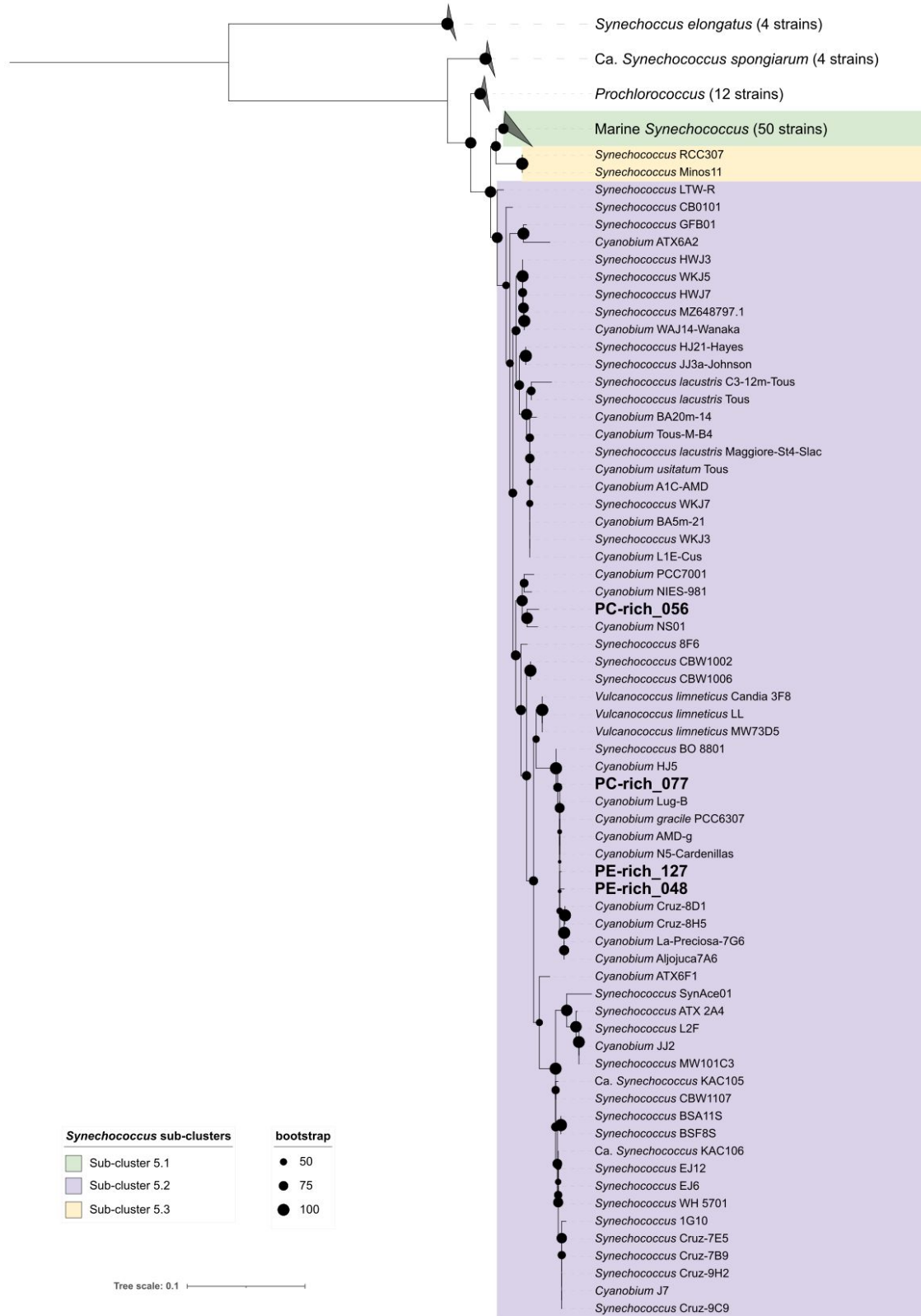
164

165 **Tab.15.** T-test of linear fit model (Fit_model) of pooled data across different strains for a given phase of growth
 166 (exponential; _Exp, pre-stationary; _St) and across different phase of growth for a given strain (_Exp_St) from
 167 effective absorption cross section of PSII (σ_{PSII} ; $\text{nm}^2 \text{ quanta}^{-1}$) measured under $\text{Ex}_{590\text{nm}}$ (orange) excitation in
 168 relation to the Phycobiliprotein to Chl *a* ratio, for two PhycoCyanin(PC)-rich cultures (056, 077) and two
 169 PhycoErythrin(PE)-rich cultures (048, 127) of *Synechococcus* sp., grown at 30, 90, 180, 300, 600, or 900 peak PAR
 170 $\mu\text{mol photons m}^{-2}\text{s}^{-1}$; and photoperiods of 8, 12, 16, or 24 h. Estimate - estimation statistics; Std.Error - standard
 171 error of the estimate; *t_value* - *t*-test statistic; *p_value* - level of significance.

Fit_model	Estimate	Std.Error	<i>t_value</i>	<i>p_value</i>
056_077_Exp	-0.118	0.060	-1.962	0.050
056_048_Exp	0.216	0.058	3.693	0.000
056_127_Exp	0.841	0.076	11.067	0.000
048_127_Exp	0.625	0.076	8.187	0.000
077_048_Exp	0.334	0.060	5.526	0.000
077_127_Exp	0.959	0.075	12.806	0.000
056_077_St	0.397	0.027	14.566	0.000
056_048_St	-0.120	0.064	-1.873	0.062
056_127_St	0.086	0.061	1.411	0.159
048_127_St	0.206	0.114	1.801	0.073
077_048_St	-0.516	0.048	-10.776	0.000
077_127_St	-0.310	0.044	-7.121	0.000
056_Exp_St	0.317	0.075	4.234	0.000
077_Exp_St	0.831	0.061	13.656	0.000
048_Exp_St	-0.019	0.122	-0.155	0.877
127_Exp_St	-0.438	0.209	-2.099	0.036

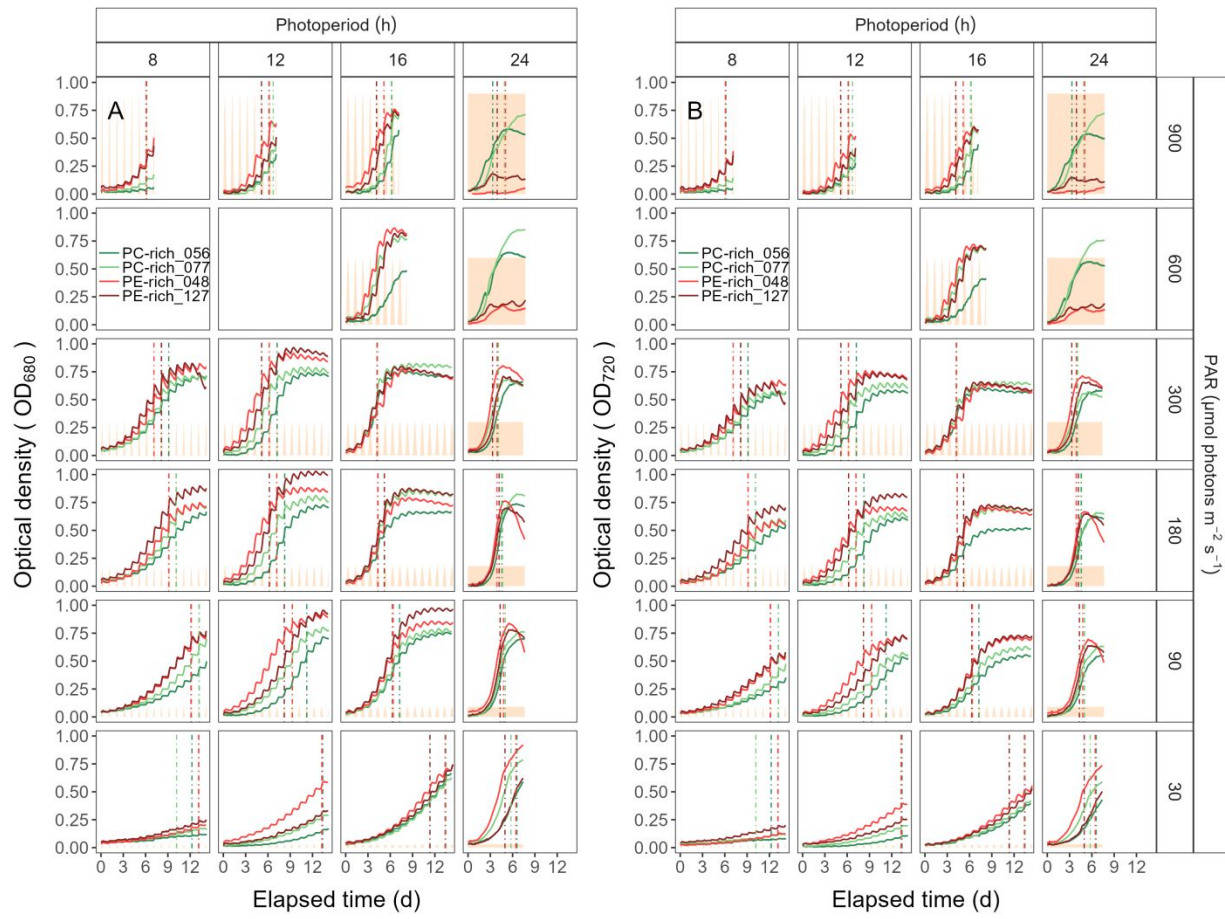
172

173



175 **Fig. S1.** Phylogenetic tree derived from partial 16S rRNA gene sequences using topology given by Maximum
176 Likelihood (1000 bootstraps). Support values are indicated by the size of internal nodes. Strains used in this study
177 are shown in bold. Phylogenetic trees were created using IQ-TREE v. 1.6.12 (Hoang et al. 2018), using
178 GTR+F+I+R3 model determined by ModelFinder (Kalyaanamoorthy et al. 2017). Bootstrap values were
179 calculated with 1000 replicates (Hoang et al. 2018). Samples for total genomic DNA were collected by harvesting
180 10 mL of each culture and centrifuging for 8 minutes at 8,000 x g. DNA was extracted using the FastDNATM SPIN
181 Kit for Soil (MP Biomedicals) with Matrix E columns following manufacturer instructions with the addition of an
182 incubation with proteinase-K (1% final concentration) at 55°C for one hour. DNA concentration was measured
183 using an Invitrogen Qubit 2.0 fluorometer (Thermo Fisher Scientific Inc.) and purity was assessed using a Thermo
184 ScientificTM NanoDrop 2000 spectrophotometer (Thermo Fisher Scientific Inc.).

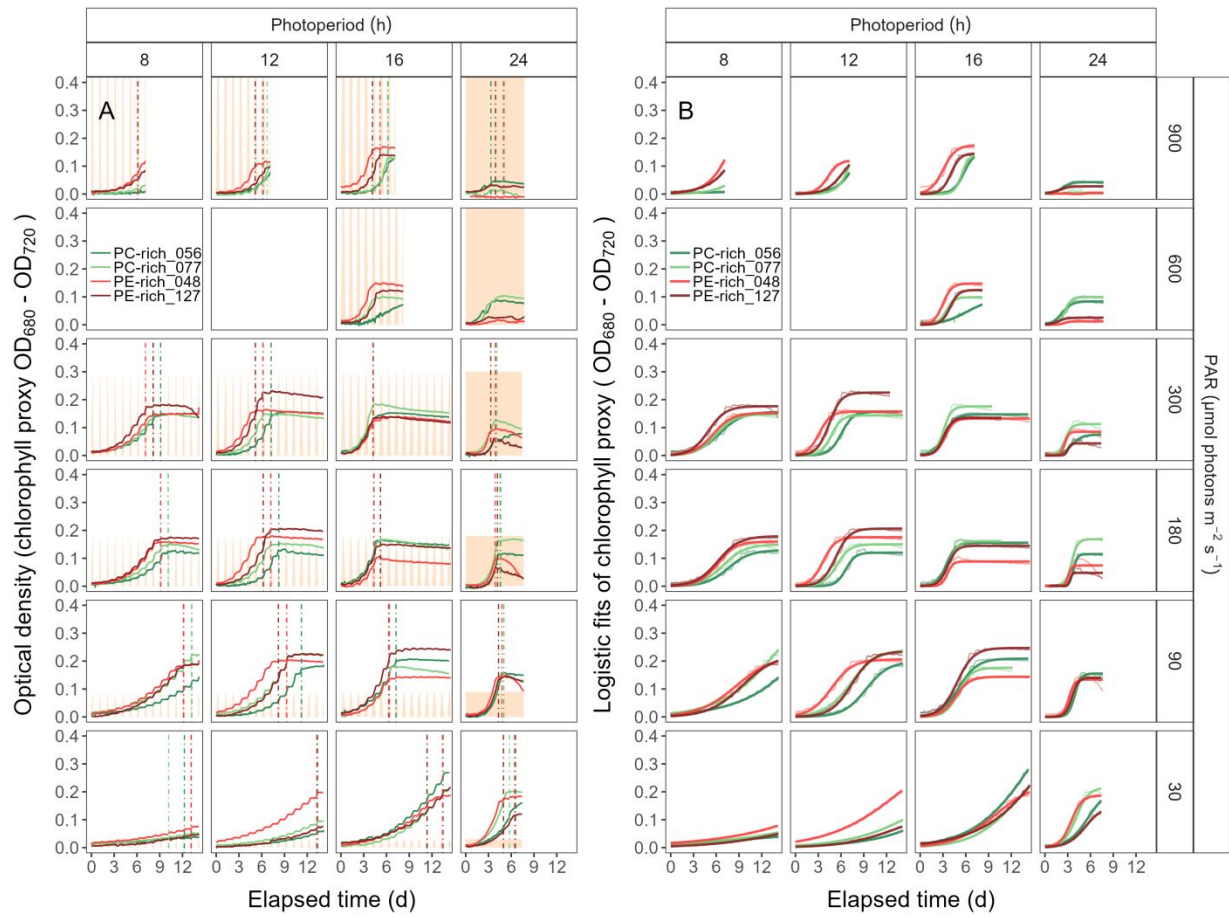
185



186

187 **Fig. S2.** Growth curves, tracked as OD₆₈₀ (**A**) and OD₇₂₀ (**B**) vs. elapsed time (d). Growth curves were estimated
 188 over 5-min intervals for two PC-rich cultures (056; dark green, 077; light green) and two PE-rich cultures (048; light
 189 red, 127; dark red) of *Synechococcus* sp. grown at 30, 90, 180, 300, 600, or 900 peak PAR $\mu\text{mol photons m}^{-2}\text{s}^{-1}$; and
 190 photoperiods of 8, 12, 16, or 24 h. The vertical lines represent the time when the cultures reached the maximum of
 191 the 1st derivative of OD₆₈₀, or maximum absolute hourly growth (tMaxAHG), taken as an index of transition from
 192 exponential to pre-stationary growth phases. The orange area represents the photoperiods, with peak PAR $\times 1/1000$
 193 to scale to the Y axis.

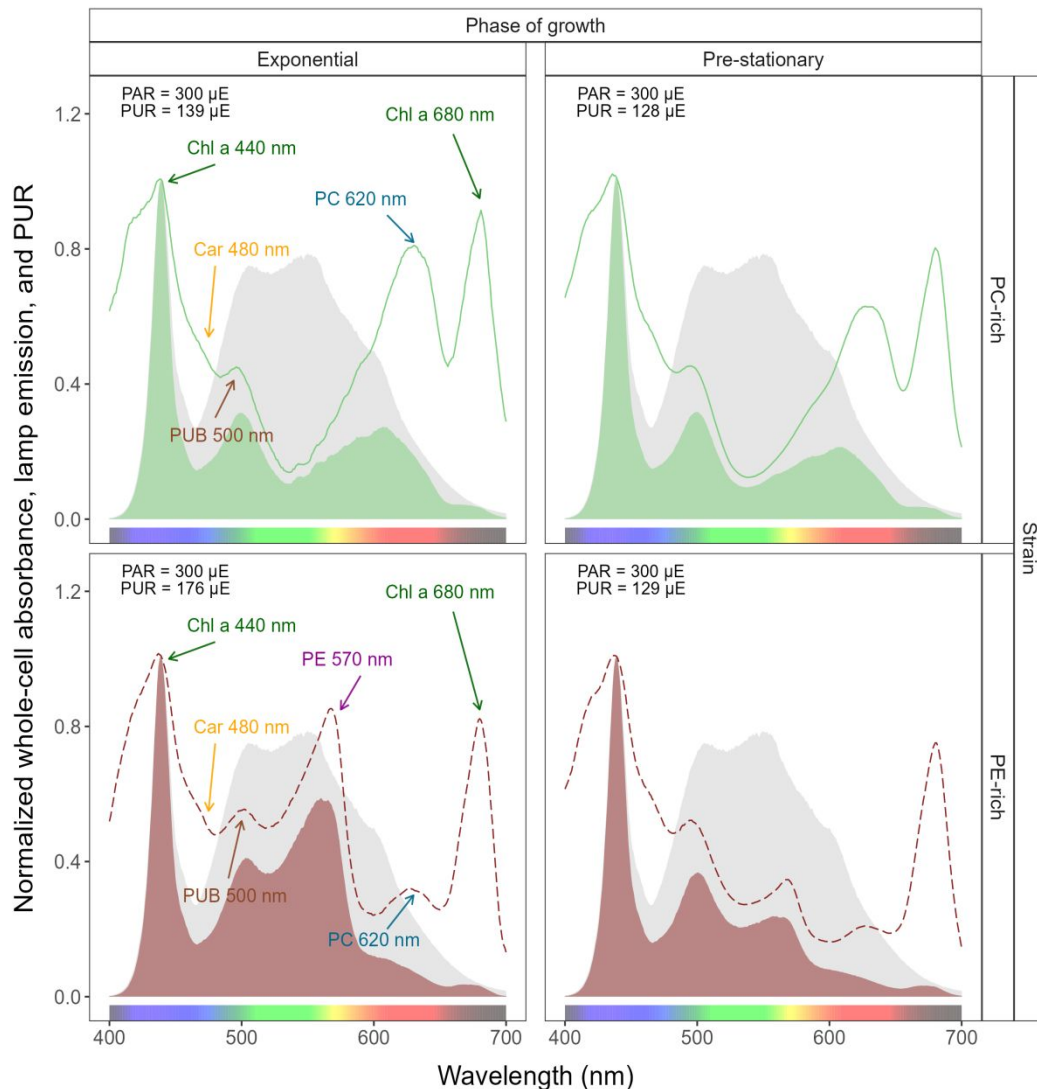
194



195

196 **Fig. S3.** (A) Growth curves (tracked as chlorophyll proxy $\text{OD}_{680} - \text{OD}_{720}$; Δ OD) vs. elapsed time (d). Growth curves
 197 were estimated over 5-min intervals for two PC-rich cultures (056; dark green, 077; light green) and two PE-rich
 198 cultures (048; light red, 127; dark red) of *Synechococcus* sp. grown at 30, 90, 180, 300, 600, or 900 peak PAR μmol
 199 photons $\text{m}^{-2}\text{s}^{-1}$; and photoperiods of 8, 12, 16, or 24 h. The vertical lines represent the time when the cultures
 200 reached the maximum of the 1st derivative of OD_{680} , or maximum absolute hourly growth (tMaxAHG), taken as an
 201 index of transition from exponential to pre-stationary growth phases. The orange area represents the photoperiods,
 202 with peak PAR $\times 1/2000$ to scale to the Y axis. (B) Logistic fits (thick lines) of chlorophyll proxy $\text{OD}_{680} - \text{OD}_{720}$ (Δ
 203 OD) vs. elapsed time (d). Growth curves (thin line) measured over 5-min intervals for each strain were also
 204 presented.

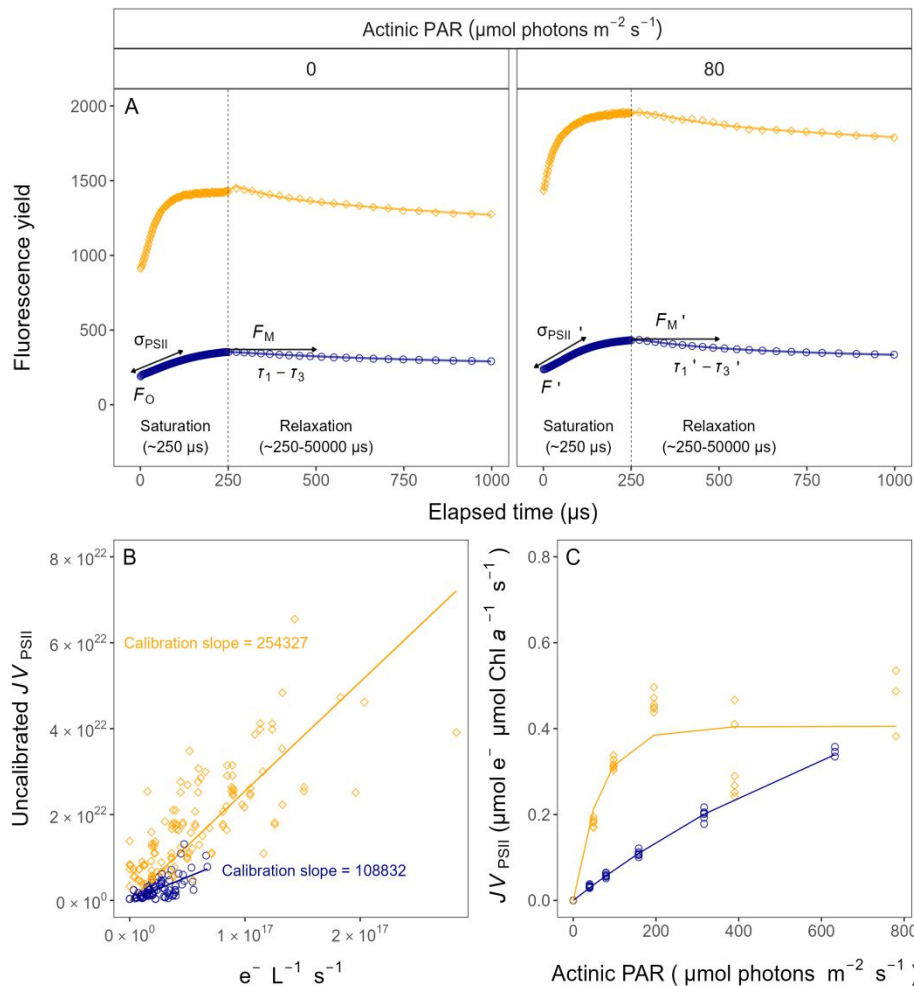
205



206

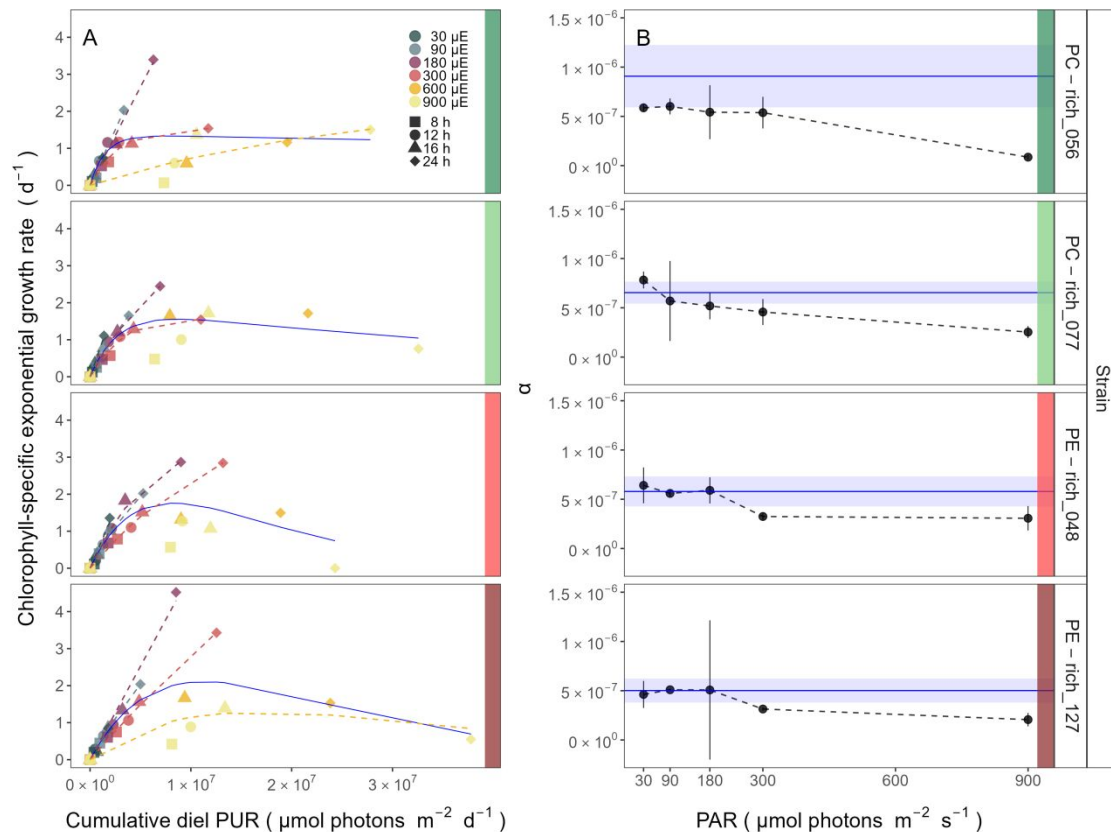
207 **Fig. S4.** Whole-cell absorbance spectra of PC-rich (077; solid light green lines) or PE-rich (127; dashed dark red
 208 lines) cultures of *Synechococcus* sp. Representative absorbance spectra, normalized to 440 nm (NormA_{440}), were
 209 measured from the exponential or pre-stationary phases of growth, together with emission spectra of the white LED
 210 lamp used for PAR, normalized to emission at 440 nm (NormEm_{440} , light gray area), in this example PAR was 300
 211 $\mu\text{mol photons m}^{-2}\text{s}^{-1}$. Estimated Photosynthetically Usable Radiation (PUR) is shown as a darker green area for the
 212 PC-rich strain and a darker red area for the PE-rich strain, with PUR given for each culture ($\mu\text{E} = \mu\text{mol photons}$
 213 $\text{m}^{-2}\text{s}^{-1}$). Peaks characteristic of known pigments are labeled; Chl *a*, chlorophyll *a*; PC, phycocyanin; PE,
 214 phycoerythrin; PUB, phycourobilin; Car, carotenoids.

215



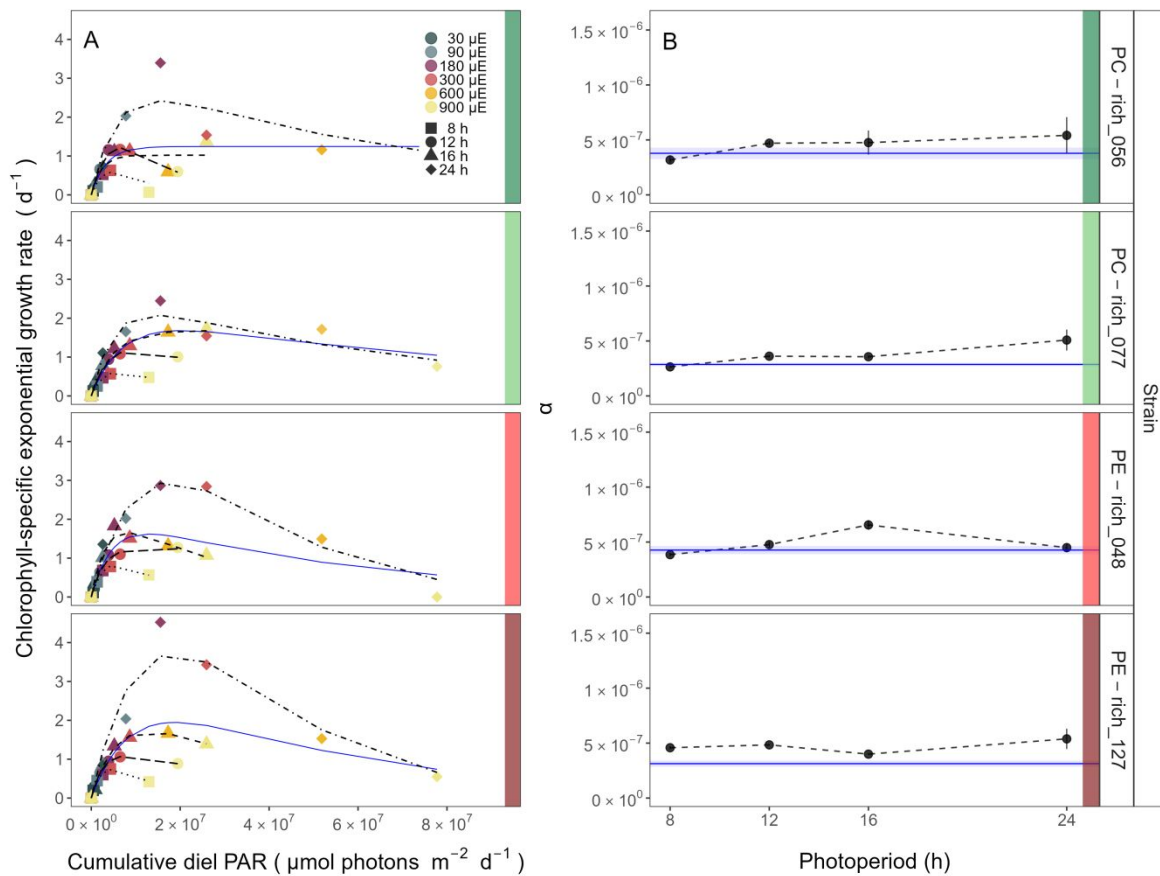
216

217 **Fig. S5.** Single turnover (ST) fluorescence induction by Fast Repetition Rate fluorometry (FRRf). **(A)** Examples of
 218 fluorescence yield vs. elapsed time (μs) for PE-rich culture of *Synechococcus* sp. (048) in the dark (dark-relaxed; 0
 219 $\mu\text{mol photons m}^{-2}\text{s}^{-1}$) and under actinic PAR (in this example 80 $\mu\text{mol photons m}^{-2}\text{s}^{-1}$) using blue LED (Ex_{445nm};
 220 open blue circles) or orange (Ex_{590nm}; open orange diamonds) excitation. The ST technique delivers a series of
 221 flashlets for non-intrusive, repeated monitoring of chlorophyll fluorescence parameters (including F_0 , F' , F_M , F'_M ,
 222 $\tau_1 - \tau_3$, $\tau'_1 - \tau'_3$, σ_{PSII} , and σ'_{PSII}). **(B)** Linear regressions of uncalibrated PSII electron flux (JV_{PSII}) vs. $e^{-} L^{-1} s^{-1}$ derived
 223 from simultaneously measured oxygen evolution Light Response Curves (LRC) under blue LED (Ex_{445nm}; open blue
 224 circles) or orange (Ex_{590nm}; open orange diamonds) excitation. **(C)** Rapid Light Curve (RLC), fit with a three
 225 parameter model (Harrison and Platt 1986), for PSII electron flux (JV_{PSII} ; $\mu\text{mol e}^{-} \mu\text{mol Chl } a^{-1} \text{s}^{-1}$) vs. actinic PAR
 226 measured under blue LED (Ex_{445nm}; open blue circles) or orange (Ex_{590nm}; open orange diamonds) excitation.



227

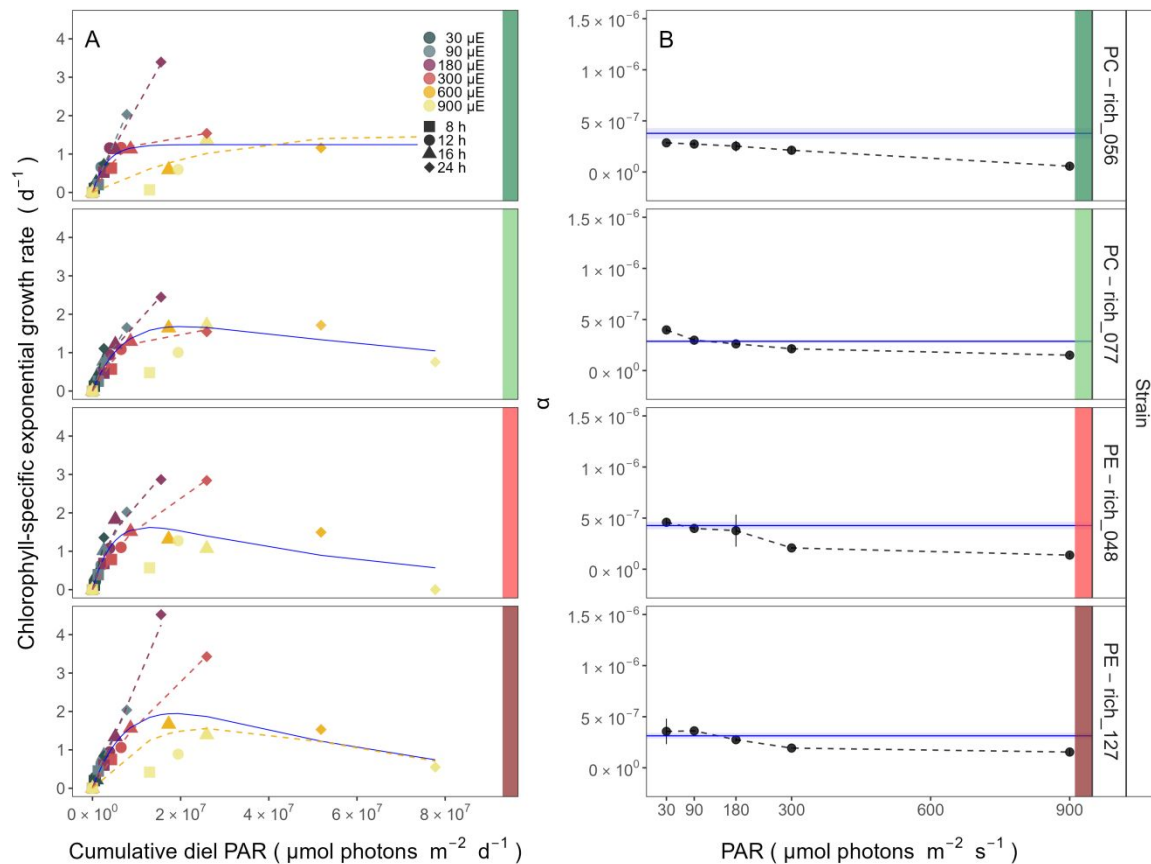
228 **Fig. S6.** (A) Chlorophyll-specific exponential growth rates (d^{-1}) vs. cumulative diel Photosynthetically Usable
 229 Radiation (PUR, $\mu\text{mol photons m}^{-2}\text{d}^{-1}$). Growth rates ($\pm \text{SE}$ falling within symbols) were estimated from logistic fits
 230 of chlorophyll proxy $\text{OD}_{680} - \text{OD}_{720}$ (ΔOD) vs. elapsed time (Fig. 1, Fig. S3B), for two PC-rich cultures (056; dark
 231 green, 077; light green) and two PE-rich cultures (048; light red, 127; dark red) of *Synechococcus* sp. grown at 30
 232 (dark gray), 90 (light gray), 180 (purple), 300 (red), 600 (orange), or 900 (yellow) peak PAR $\mu\text{mol photons m}^{-2}\text{s}^{-1}$
 233 (μE); and photoperiods of 8 (square), 12 (circle), 16 (triangle), or 24 (diamond) h. Solid blue line shows a fit of the
 234 pooled growth rates through peak PAR for each strain, with a three parameter model (Harrison and Platt, 1986). We
 235 also fit the same model separately for 30 (dark gray), 90 (light gray), 180 (purple), 300 (red), 600 together with 900
 236 (orange) peak PAR $\mu\text{mol photons m}^{-2}\text{s}^{-1}$, only when they were each significantly different (ANOVA, $p < 0.05$) from
 237 the fit of pooled data. (B) Alpha parameters of the initial rise of growth rate (α) vs. cumulative diel
 238 Photosynthetically Usable Radiation (PUR), estimated from data pooled for each peak PAR (points ($\pm \text{SE}$))
 239 connected by dashed lines), and estimated for all data across all peak PAR, for each strain (solid blue horizontal line
 240 $\pm \text{SE}$).



241

242 **Fig. S7.** **(A)** Chlorophyll-specific exponential growth rates (d^{-1}) vs. cumulative diel PAR ($\mu\text{mol photons m}^{-2}\text{d}^{-1}$).
243 Growth rates (\pm SE falling within symbols) were estimated from logistic fits of chlorophyll proxy OD₆₈₀ – OD₇₂₀
244 (ΔOD) vs. elapsed time (Fig. 1, Fig. S3B), for two PC-rich cultures (056; dark green, 077; light green) and two PE-
245 rich cultures (048; light red, 127; dark red) of *Synechococcus* sp. grown at 30 (dark gray), 90 (light gray), 180
246 (purple), 300 (red), 600 (orange), or 900 (yellow) peak PAR $\mu\text{mol photons m}^{-2}\text{s}^{-1}$ (μE); and photoperiods of 8
247 (square), 12 (circle), 16 (triangle), or 24 (diamond) h. Solid blue line shows a fit of the pooled growth rates through
248 photoperiod (h) for each strain, with a three parameter model (Harrison and Platt 1986). We also fit the same model
249 separately for 8 (dotted line), 12 (long dash line), 16 (dashed line), or 24 (two dash line) h photoperiods, since for all
250 strains they were each significantly different (ANOVA, $p < 0.05$) from the fit of pooled data. **(B)** Alpha parameters
251 of the initial rise of growth rate (α) vs. cumulative diel PAR, estimated from data pooled for each photoperiod
252 (points (\pm SE) connected by dashed lines), and estimated for all data across photoperiods (solid blue horizontal line
253 \pm SE), for each strain.

254



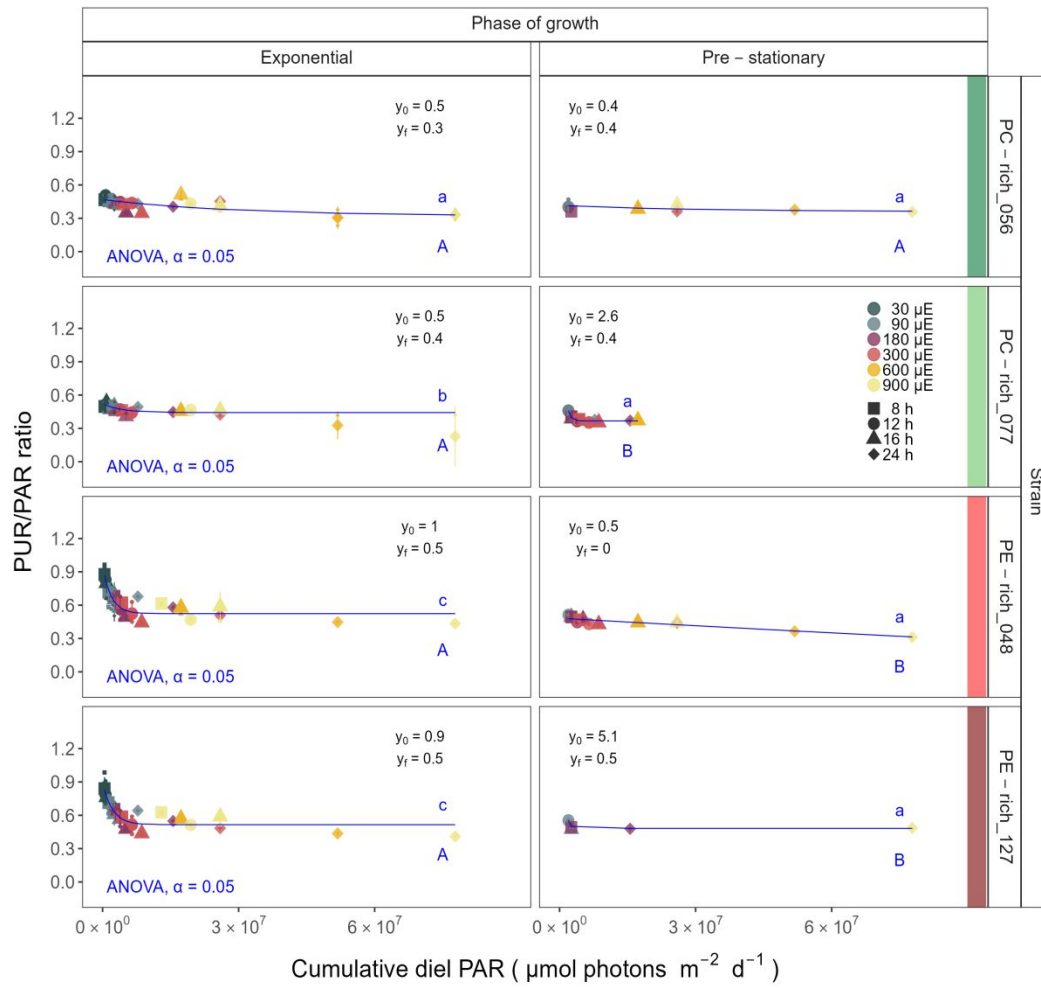
255

256 **Fig. S8. (A)** Chlorophyll-specific exponential growth rates (d^{-1}) vs. cumulative diel PAR ($\mu\text{mol photons m}^{-2}\text{d}^{-1}$).
 257 Growth rates ($\pm \text{SE}$ falling within symbols) were estimated from logistic fits of chlorophyll proxy $\text{OD}_{680} - \text{OD}_{720}$
 258 (ΔOD) vs. elapsed time (Fig. 1, Fig. S3B), for two PC-rich cultures (056; dark green, 077; light green) and two PE-
 259 rich cultures (048; light red, 127; dark red) of *Synechococcus* sp. grown at 30 (dark gray), 90 (light gray), 180
 260 (purple), 300 (red), 600 (orange), or 900 (yellow) peak PAR $\mu\text{mol photons m}^{-2}\text{s}^{-1}$ (μE); and photoperiods of 8
 261 (square), 12 (circle), 16 (triangle), or 24 (diamond) h. Solid blue line shows a fit of the pooled growth rates through
 262 peak PAR for each strain, with a three parameter model (Harrison and Platt, 1986). We also fit the same model
 263 separately for 30 (dark gray), 90 (light gray), 180 (purple), 300 (red), 600 together with 900 (orange) peak PAR
 264 $\mu\text{mol photons m}^{-2}\text{s}^{-1}$, only when they were each significantly different (ANOVA, $p < 0.05$) from the fit of pooled
 265 data. **(B)** Alpha parameters of the initial rise of growth rate (α) vs. cumulative diel PAR, estimated from data pooled
 266 for each peak PAR (points ($\pm \text{SE}$) connected by dashed lines), and estimated for all data across all peak PAR, for
 267 each strain (solid blue horizontal line $\pm \text{SE}$).

268

269 PUR/PAR ratio vs. cumulative diel PAR

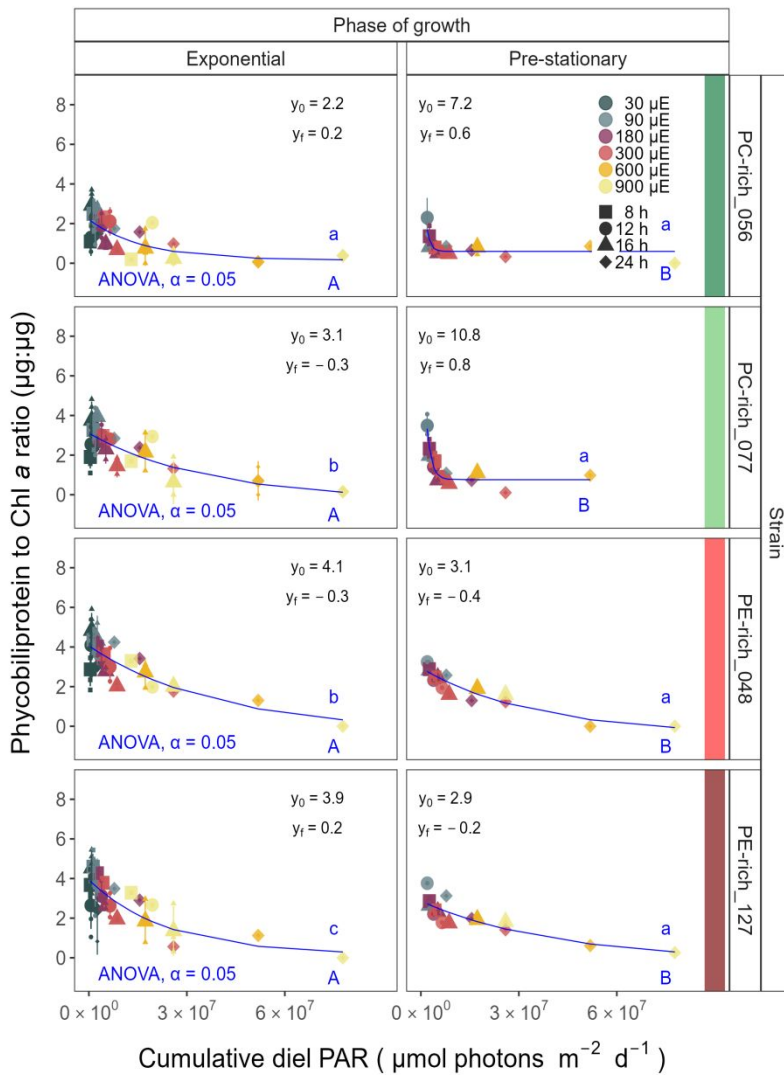
270 The PUR/PAR ratio is an index of the efficacy of light capture for a culture under a given
271 growth condition; showing the fraction of PAR that can be captured by the absorbance of the
272 cells (Fig. S9). For the two PC-rich and, particularly, for the two PE-rich cultures of
273 *Synechococcus* PUR/PAR decayed exponentially to a plateau, with increasing cumulative diel
274 PAR, when pooling PUR/PAR data across different combinations of photoperiod and peak PAR.
275 Although all strains followed a similar trend, the single phase exponential decay model fit
276 parameters varied significantly among strains, during their exponential phase of growth (Table
277 S9), except the model fits from PE-rich_048 and PE-rich_127, where no data was received.
278 Moreover, the PUR/PAR ratio was higher in the PE-rich strains under low cumulative diel
279 photon dose during their exponential phase of growth (y_0 greater or equal to 0.9), but decayed
280 towards a plateau close to the PC-rich strains as cumulative diel photon dose increases ($y_f = 0.5$).
281 On the other hand, the single phase exponential decay model fits did not differ significantly
282 among strains, during their pre-stationary phase of growth (Table S9). During this phase,
283 response of PUR/PAR ratio to increasing cumulative diel PAR exhibits damping, maintaining a
284 consistent trend across all strains within the y_f range of 0.4 to 0.5, with the exception of the PE-
285 rich_048 strain. We also find that model fits from different phases of growth differed within a
286 given strain, with the exception of PC-rich_056 (Table S9). A similar decay trend was observed
287 for Phycobiliprotein to Chl *a* ratio ($\mu\text{g}:\mu\text{g}$) across cumulative diel PAR (Fig. S10).



288

289 **Fig. S9.** Changes in PUR/PAR ratio vs. cumulative diel PAR ($\mu\text{mol photons m}^{-2}\text{d}^{-1}$). PUR/PAR ratio was estimated
 290 for two PC-rich cultures (056; dark green, 077; light green) and two PE-rich cultures (048; light red, 127; dark red)
 291 of *Synechococcus* sp. grown at 30 (dark gray), 90 (light gray), 180 (purple), 300 (red), 600 (orange), or 900 (yellow)
 292 peak PAR $\mu\text{mol photons m}^{-2}\text{s}^{-1}$ (μE); and photoperiods of 8 (square), 12 (circle), 16 (triangle), or 24 (diamond) h.
 293 Figure presents data (smaller symbols) and means (bigger symbols) from exponential or pre-stationary phase of
 294 growth. Blue solid line shows single phase exponential decay fit for data from each strain and growth phase, with fit
 295 parameters presented. Different lowercase letters indicate statistically significant differences between the fit models
 296 for different strains within a given phase of growth. Different uppercase letters indicate statistically significant
 297 differences between the fit models for different phases of growth within a given strain (ANOVA; $p < 0.05$).

298



299

300 **Fig. S10.** Changes of Phycobiliprotein to Chl *a* ratio ($\mu\text{g}:\mu\text{g}$) vs. cumulative diel PAR ($\mu\text{mol photons m}^{-2}\text{d}^{-1}$).

301 Phycobiliprotein to Chl *a* ratio was estimated for two PC-rich cultures (056; dark green, 077; light green) and two
 302 PE-rich cultures (048; light red, 127; dark red) of *Synechococcus* sp. grown at 30 (dark gray), 90 (light gray), 180
 303 (purple), 300 (red), 600 (orange), or 900 (yellow) peak PAR $\mu\text{mol photons m}^{-2}\text{s}^{-1}$ (μE); and photoperiods of 8
 304 (square), 12 (circle), 16 (triangle), or 24 (diamond) h. Figure presents data (smaller symbols) and means (bigger
 305 symbols) from exponential or pre-stationary phase of growth. Blue solid line shows single phase exponential decay
 306 fit for data from each strain and growth phase, fit parameters are presented. Different lowercase letters indicate
 307 statistically significant differences between the fit models for different strains within a given phase of growth.
 308 Different uppercase letters indicate statistically significant differences between the fit models for different phases of
 309 growth within a given strain (ANOVA; $p < 0.05$).

310 Effective absorption cross section of PSII of picocyanobacteria

311 The effective absorption cross section of PSII (σ_{PSII}' , $\text{nm}^2 \text{ quanta}^{-1}$), was estimated using
312 FRRf induction curves using $\text{Ex}_{590\text{nm}}$ (orange) excitation, for two PC-rich (056, 077) and two PE-
313 rich (048, 127) cultures of *Synechococcus* grown at 30, 90, 180, 300, 600, or 900 peak PAR
314 $\mu\text{mol photons m}^{-2}\text{s}^{-1}$ (μE); and photoperiods of 8, 12, 16, or 24 h (Fig. S11). The σ_{PSII}' measured
315 under diel peak PAR growth light under $\text{Ex}_{445\text{nm}}$ (blue) excitation vs. cumulative diel photon
316 dose is shown in Fig. S12, Table S12.

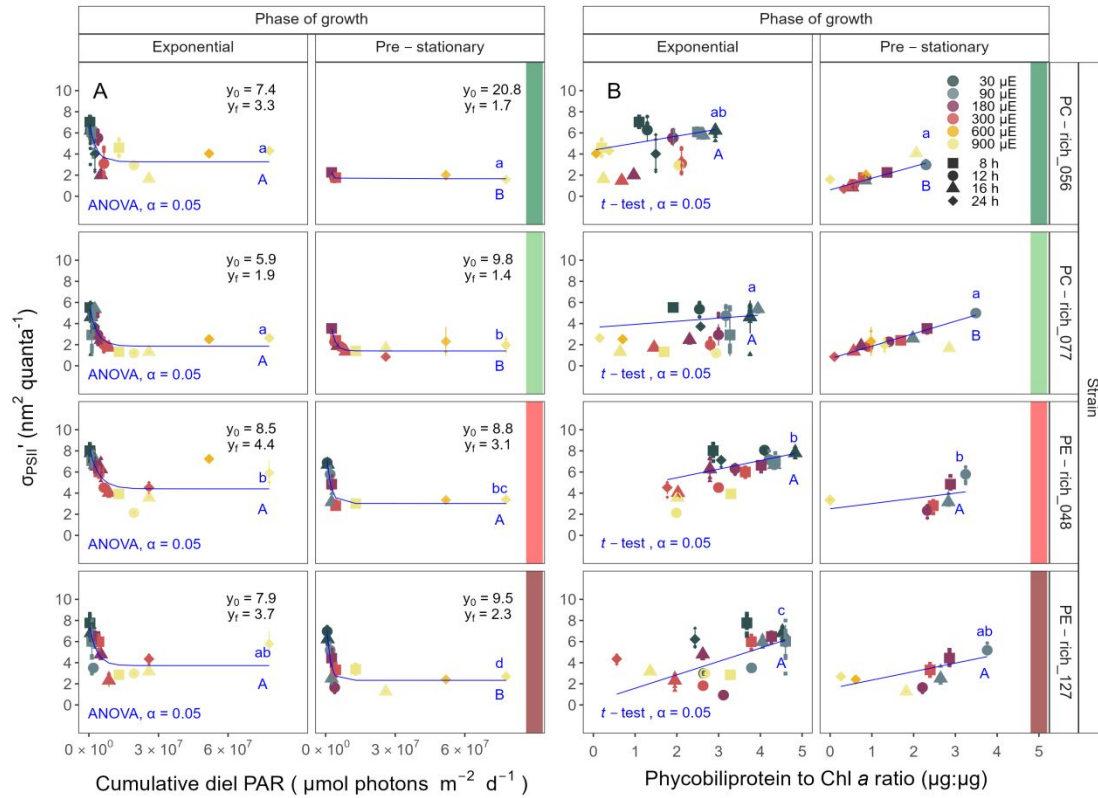
317 All strains showed consistent patterns of sharp, exponential decay of effective absorption
318 cross section for PSII photochemistry vs. cumulative diel photon doses, across different
319 combinations of photoperiod and peak PAR (Fig. S11 A). Although all strains showed this
320 response pattern, the exponential decay fits differed significantly among two PC-rich strains and
321 PE-rich_048 strains during their exponential phase of growth (Table S11). PE-rich strains
322 showed higher σ_{PSII}' under low cumulative diel photon dose (y_0 about 0.8 and y_f about 4) than did
323 PC-rich strains. During pre-stationary phase this response dampens in the PC-rich strains but
324 persists in the PE-rich strains (Table S11). σ_{PSII}' for the PE-rich strains during pre-stationary
325 phase of growth still remain higher (y_f between 2.3 – 3.0) than in the PC-rich strains (y_f between
326 1.4 – 1.7) even as cumulative diel photon dose increases. Model fits from different phases of
327 growth differed within a given strain, with the exception of PE-rich_048 (Table S11).

328 Effective absorption cross section of PSII (σ_{PSII}' ; $\text{nm}^2 \text{ quanta}^{-1}$), measured under diel peak
329 PAR growth light with $\text{Ex}_{590\text{nm}}$ (orange) excitation through phycobilisome absorbance PAR (Fig.
330 S11 B) shows positive linear correlations with the Phycobiliprotein to Chl *a* ratio, although
331 strains in exponential growth show significant scatter around this positive relation, likely related
332 to regulatory control of σ_{PSII}' under different measurement PAR, beyond pigment composition.

333 Under pre-stationary phase the relationship between σ_{PSII}' and Phycobiliprotein to Chl *a* ratio
334 was more consistent, suggesting increased reliance upon compositional regulation to control light
335 delivery to PSII, as opposed to shorter-term physiological regulation under changing light. The
336 linear fits of σ_{PSII}' vs. Phycobiliprotein to Chl *a* ratio also vary significantly between PC-
337 rich_077 and two PE-rich strains during their exponential phase of growth. During pre-stationary
338 phase we noted significant differences between two PC-rich strains and PE-rich_048. Moreover,
339 significant differences between the fit models for varying phases of growth were noted for PC-
340 rich strains 056 and 077 (*t*-test; $p < 0.05$, Table S14).

341 Changes in effective absorption cross section of PSII (σ_{PSII} ; nm² quanta⁻¹) measured in the
342 dark with Ex_{590nm} (orange) excitation vs. Phycobiliprotein to Chl *a* ratio (Fig. S13 A, Table S15)
343 and σ_{PSII}' measured under diel peak PAR growth light under Ex_{445nm} (blue) excitation
344 vs. Phycobiliprotein to Chl *a* ratio (Fig. S13 B and Table S13) are also shown.

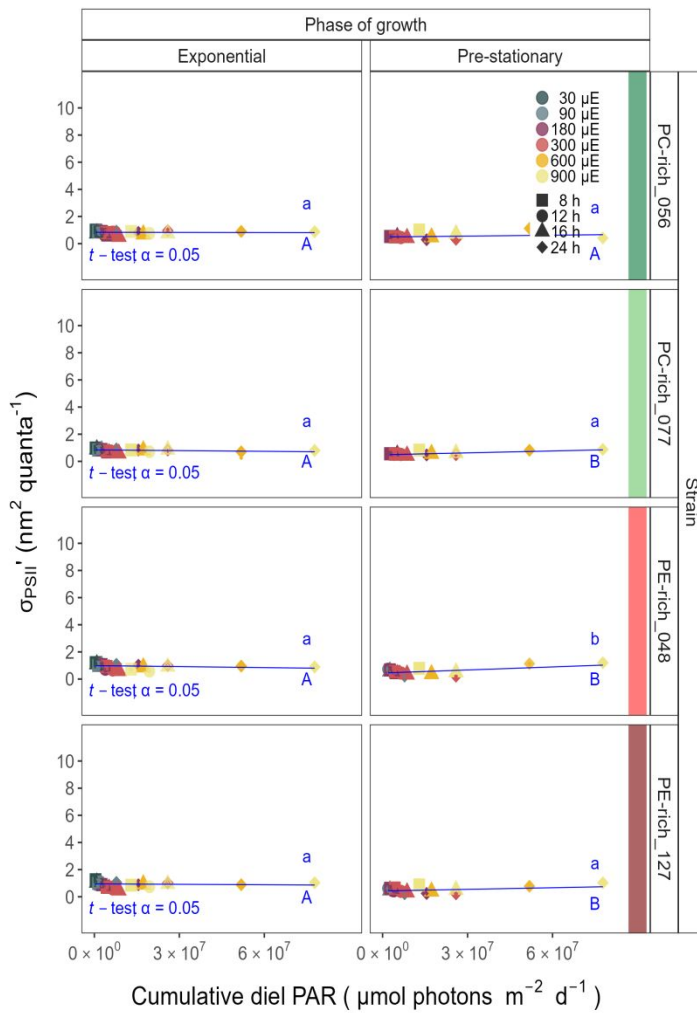
345



346

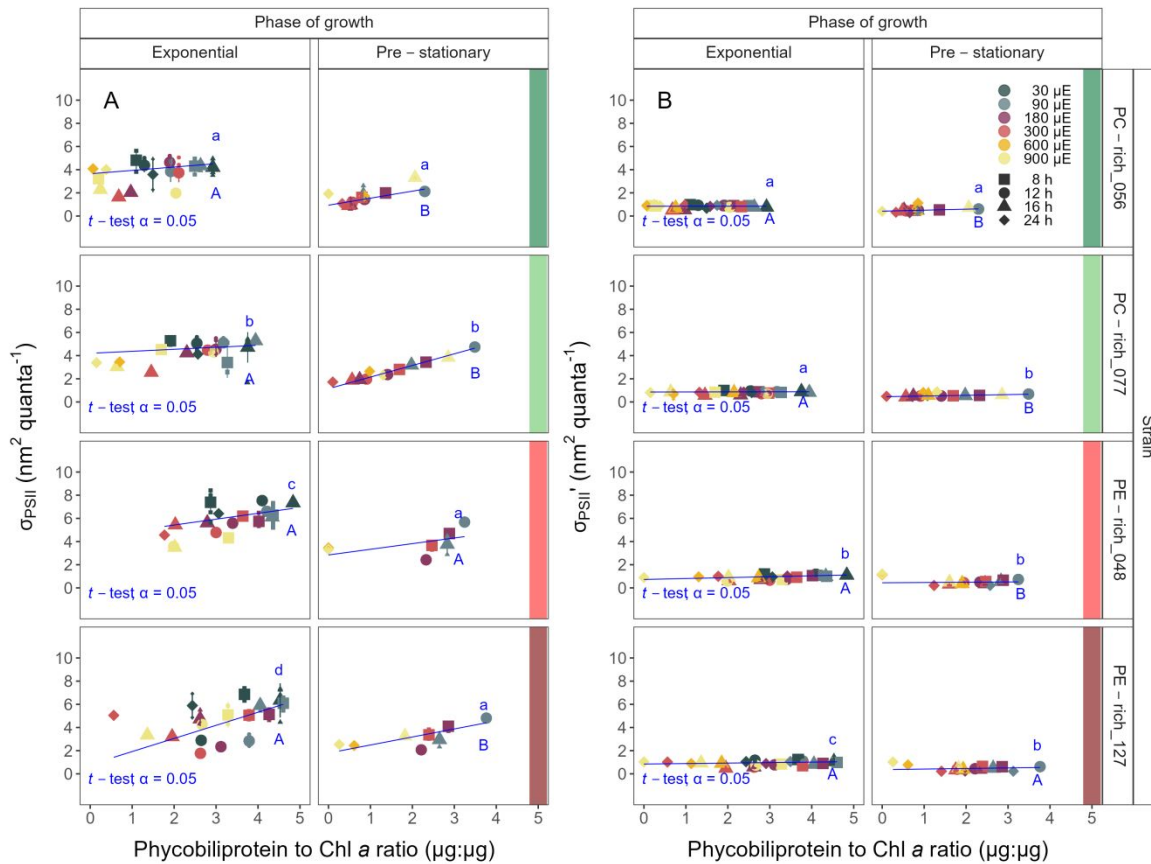
347 **Fig. S11. (A)** Effective absorption cross section of PSII (σ_{PSII}' ; $\text{nm}^2 \text{ quanta}^{-1}$) measured under diel peak PAR growth
 348 light vs. cumulative diel PAR ($\mu\text{mol photons m}^{-2} \text{ d}^{-1}$); blue solid line shows single phase exponential decay fit for
 349 data from each strain and growth phase. **(B)** Changes of σ_{PSII}' measured under diel peak PAR growth light vs. the
 350 ratio of sum of μg phycobilins (PE, PC, APC protein, Phycobiliprotein) to μg Chl *a*; blue solid line shows linear
 351 model fit for data from each strain and growth phase. σ_{PSII}' was estimated using FRRf induction curves with
 352 excitation of phycobilisomes (Ex_{590nm}, orange), for two PC-rich cultures (056; dark green, 077; light green) and two
 353 PE-rich cultures (048; light red, 127; dark red) of *Synechococcus* sp. grown at 30 (dark gray), 90 (light gray), 180
 354 (purple), 300 (red), 600 (orange), or 900 (yellow) peak PAR $\mu\text{mol photons m}^{-2} \text{ s}^{-1}$ (μE); and photoperiods of 8
 355 (square), 12 (circle), 16 (triangle), or 24 (diamond) h. Figure presents data (smaller symbols) and means (bigger
 356 symbols) from exponential or pre-stationary phase of growth. Different lowercase letters indicate statistically
 357 significant differences between the fit models for different strains within a given phase of growth. Different
 358 uppercase letters indicate statistically significant differences between the fit models for different phases of growth
 359 within a given strain ($p < 0.05$).

360



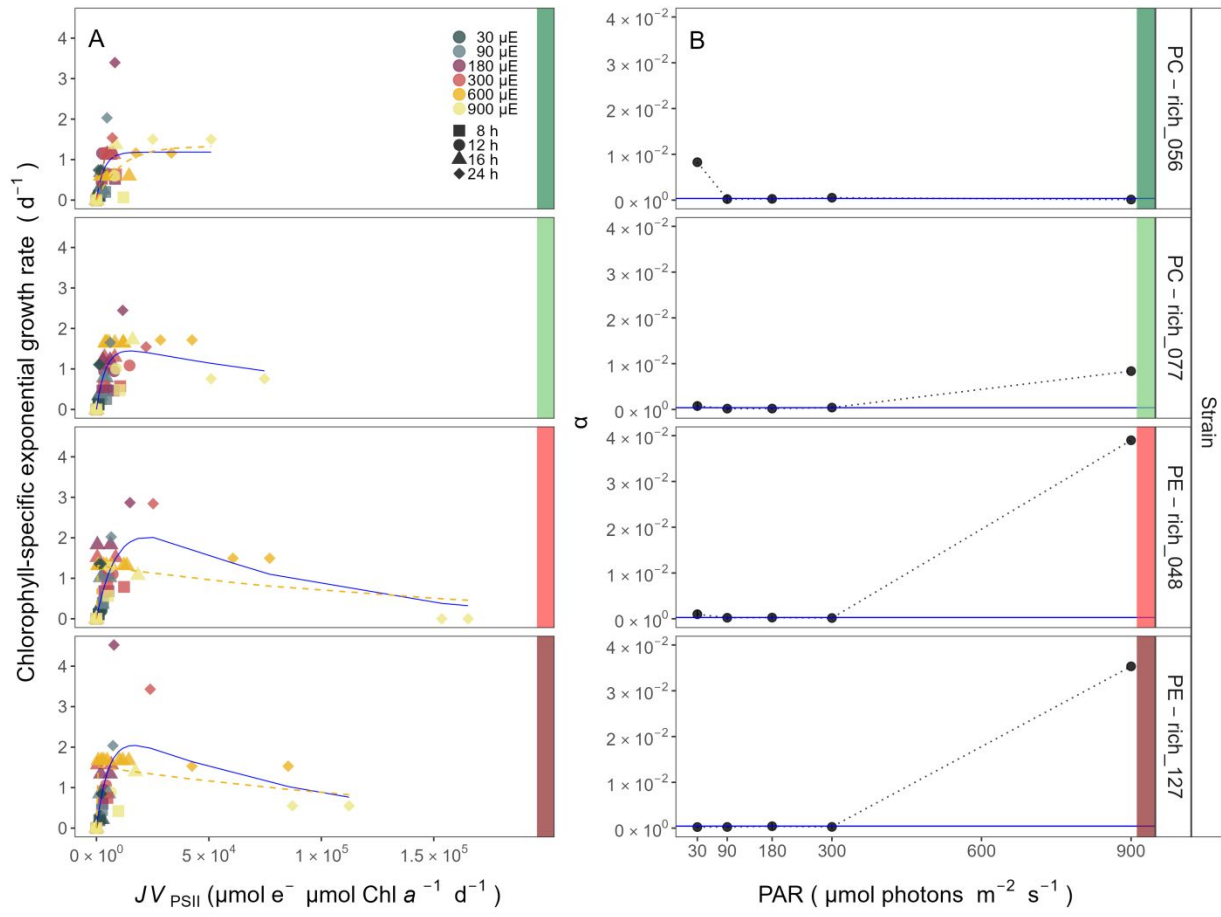
361

362 **Fig. S12.** Effective absorption cross section of PSII ($\sigma_{\text{PSII}'}$; $\text{nm}^2 \text{ quanta}^{-1}$) measured under diel peak PAR growth
 363 light under blue ($\text{Ex}_{445\text{nm}}$) excitation vs. cumulative diel PAR ($\mu\text{mol photons m}^{-2}\text{d}^{-1}$). $\sigma_{\text{PSII}'}$ was estimated for two
 364 PC-rich cultures (056; dark green, 077; light green) and two PE-rich cultures (048; light red, 127; dark red) of
 365 *Synechococcus* sp. grown at 30 (dark gray), 90 (light gray), 180 (purple), 300 (red), 600 (orange), or 900 (yellow)
 366 peak PAR $\mu\text{mol photons m}^{-2}\text{s}^{-1}$ (μE); and photoperiods of 8 (square), 12 (circle), 16 (triangle), or 24 (diamond) h.
 367 Figure presents data (smaller symbols) and means (bigger symbols) from exponential or pre-stationary phase of
 368 growth. Blue solid line shows linear model fit for data from each strain and growth phase. Different lowercase
 369 letters indicate statistically significant differences between the fit models for different strains within a given phase of
 370 growth. Different uppercase letters indicate statistically significant differences between the fit models for different
 371 phases of growth within a given strain (t -test; $p < 0.05$).



372

373 **Fig. S13.** **(A)** Changes of effective absorption cross section of PSII (σ_{PSII} ; $\text{nm}^2 \text{ quanta}^{-1}$) measured at the dark period
 374 under orange ($\text{Ex}_{590\text{nm}}$) excitation vs. the ratio of sum of μg phycobilins (PE, PC, APC protein, Phycobiliprotein) to
 375 μg Chl *a*. **(B)** Changes of effective absorption cross section of PSII ($\sigma_{\text{PSII}'}$; $\text{nm}^2 \text{ quanta}^{-1}$) measured under diel peak
 376 PAR growth light under blue ($\text{Ex}_{445\text{nm}}$) excitation vs. the ratio of sum of μg phycobilins (PE, PC, APC protein,
 377 Phycobiliprotein) to μg Chl *a*. $\sigma_{\text{PSII}'}$ was estimated for two PC-rich cultures (056; dark green, 077; light green) and
 378 two PE-rich cultures (048; light red, 127; dark red) of *Synechococcus* sp. grown at 30 (dark gray), 90 (light gray),
 379 180 (purple), 300 (red), 600 (orange), or 900 (yellow) peak PAR $\mu\text{mol photons m}^{-2}\text{s}^{-1}$ (μE); and photoperiods of 8
 380 (square), 12 (circle), 16 (triangle), or 24 (diamond) h. Figure presents data (smaller symbols) and means (bigger
 381 symbols) from exponential or pre-stationary phase of growth. Blue solid line shows linear model fit for data from
 382 each strain and growth phase. Different lowercase letters indicate statistically significant differences between the fit
 383 models for different strains within a given phase of growth. Different uppercase letters indicate statistically
 384 significant differences between the fit models for different phases of growth within a given strain (*t*-test; $p < 0.05$).
 385



386

387 **Fig. S14.** (A) Chlorophyll specific exponential growth rates (d^{-1}) vs. cumulative diel PSII electron flux (JV_{PSII} ; μmol
 388 $e^- \mu\text{mol Chl } a^{-1} d^{-1}$) measured under diel peak PAR growth light. Growth rates (\pm SE falling within symbols) were
 389 estimated from logistic fits of chlorophyll proxy $OD_{680} - OD_{720}$ (ΔOD) vs. elapsed time (Fig. S3). PSII flux was
 390 estimated using FRRf induction curves with excitation of chlorophyll ($Ex_{445\text{nm}}$, blue), for two PC-rich cultures (056;
 391 dark green, 077; light green) and two PE-rich cultures (048; light red, 127; dark red) of *Synechococcus* sp. grown at
 392 30 (dark gray), 90 (light gray), 180 (purple), 300 (red), 600 (orange), or 900 (yellow) peak PAR $\mu\text{mol photons}$
 393 $\text{m}^{-2}\text{s}^{-1}$ (μE); and photoperiods of 8 (square), 12 (circle), 16 (triangle), or 24 (diamond) h. Solid blue line shows a fit
 394 of the pooled growth rates for each strain, with a three parameter model (Harrison and Platt 1986). We also fit the
 395 same model separately for 600 together with 900 (orange) peak PAR $\mu\text{mol photons m}^{-2}\text{s}^{-1}$, when they were
 396 significantly different (ANOVA, $p < 0.05$) from the fit of pooled data. (B) Alpha parameters of the initial rise of
 397 growth rate (α) vs. cumulative diel JV_{PSII} , estimated from data pooled for each peak PAR (points (\pm SE) connected
 398 by dashed lines), and estimated for all data across all peak PAR, for each strain (solid blue horizontal line \pm SE).

399 **References**

- 400 Harrison, W. G., and T. Platt. 1986. Photosynthesis-irradiance relationships in polar and
401 temperate phytoplankton populations. *Polar biology* **5**: 153–164.
- 402 Hoang, D. T., O. Chernomor, A. von Haeseler, B. Q. Minh, and L. S. Vinh. 2018. UFBoot2:
403 Improving the Ultrafast Bootstrap Approximation. *Molecular Biology and Evolution* **35**: 518–
404 522. doi:10.1093/molbev/msx281
- 405 Kalyaanamoorthy, S., B. Q. Minh, T. K. F. Wong, A. von Haeseler, and L. S. Jermiin. 2017.
406 ModelFinder: Fast model selection for accurate phylogenetic estimates. *Nature Methods* **14**:
407 587–589. doi:10.1038/nmeth.4285